Calcium Phosphate Polymer hybrid materials

Inauguraldissertation

zur
Erlangung der Würde eines Doktors der Philosophie
vorgelegt der
Philosophisch-Naturwissenschaftlichen Fakultät
der Universität Basel

von

Sylvia Schweizer

aus Bretzwil, BL

St.Gallen, 2011

Genehmigt von der Philosophisch-Naturwissenschaftlichen Fakultät auf Auftrag von

Prof. Dr. Wolfgang Meier

und

Prof. Dr. Andreas Taubert

Basel, den 22.06.2010

Prof. Dr. Eberhard Parlow, Dekan

Abstract

Calcium phosphate (CaP) is of strong interest to the medical field because of its potential for bone repair, gene transfection, etc.[1-3] Nowadays, the majority of the commercially available materials are fabricated via "classical" materials science approaches, i.e. via high temperature or high pressure approaches, from rather poorly defined slurries, or from organic solvents.[3,4] Precipitation of inorganics with (polymeric) additives from aqueous solution on the other hand enables the synthesis of inorganic or organic/inorganic materials that are often much more closely related to biological structures, for example in bone.[5,6] Bone consists mainly of calcium phosphate, which is present in the form of hydroxyapatite (figure 1) in addition of proteins like collagen and other proteins such as growth factors.[7]

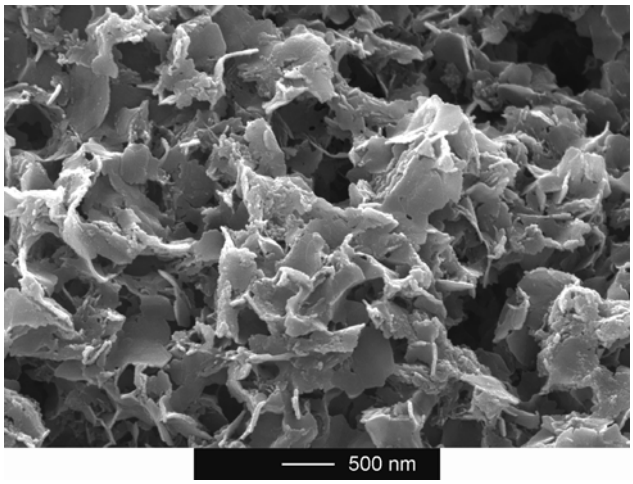

Figure 1: Hydroxyapatite mineralized from aqueous solution.[8]

This thesis combines the benefits of "classical" materials science approaches and inorganic precipitation from aqueous solutions by using biodegradable polyesters as scaffolds for calcium phosphate mineralization. The objective of this work was to design new polymeric scaffolds supporting calcium phosphate mineralization to obtain new bone substitute materials based on polyesters.

Polyesters are biodegradable polymers and can be synthesized by standard techniques such as polycondensation or ring opening polymerization. The polyester should be spun into fiber mats via electrospinning and calcium phosphate should mineralize on the mats to yield a biocompatible, biodegradable, and tunable hybrid material.

To ensure proper function of the home-built electrospinning-apparatus, polyesters like poly(caprolactone), poly(hydroxybutyrate) and poly(hydroxybutyrate-*co*-hydroxyvalerate) were initially chosen to compare the results with the literature.[9-11] All of these polyesters have already been electrospun.[12,13] The polymers were used, both in literature and in this work, as high molecular weight polymers such as poly(caprolactone) with a molecular mass of about 80000 g/mol. The molar mass influences the viscosity of the polymer solution, which is one important property for the electrospinning process.

For that reason, a further part of the thesis was concerned with the synthesis of high molecular weight polyesters with good solubility. Additionally, modifications at the polyester should be possible by simple "thiole-ene" click chemistry to afford polymers that can easily and rapidly be modified for different growth conditions. Modification of the polyester leads to various functional groups in the side-chain of the polymer. Different functional groups have an influence on calcium phosphate growth. Because the synthesis of α-allylpolyester is already known,[14] this polyester was chosen to achieve all the noted properties.

Besides, a coating for the "shape memory" material Nitinol was developed. This work was realised in collaboration with Admedes Schüssler GmbH. A shape memory alloy is a material that "remembers" its original shape and returns to that shape after being deformed. Among others, Nitinol is used as stent material. Stents are implants to keep hollow organs (such as arteries) open.

For the Nitinol coating, the layer-by-layer (LbL) technique was used.[15] For LbL, negatively and positively charged polyelectrolytes (charged polymers) are needed. Heparin and chitosan, two charged polysaccharides already used for medical applications, were selected.[16] Calcium phosphate was then grown on the coatings to vary the surface characteristics. The surface influences the cell adhesion. Therefore, the coating may assist or inhibit tissue formation and growth, which is an important parameter for the efficiency of an implant.

This thesis is structured as follows: The introduction discusses approaches for the fabrication of bioinspired calcium phosphate hybrid materials by precipitation from aqueous solution. The first part of the introduction focuses on polymers and self-assembling structures for the design of CaP/organic hybrids and pure CaP with crystal structures and morphologies regulated by the respective additive. The influence of polymers in calcium phosphate

composites with focus on the used polyesters is discussed subsequently. A summary of the most commonly used techniques and methods completes the introduction.

Chapter 2 introduces the electrospinning process and setup. The influence of different experimental parameters on fiber mat formation is discussed. The synthesis of the α-allylpolyester is described in Chapter 3, including synthesis problems. The Nitinol coating is the subject of Chapter 4. Also further developments of the layer-by-layer technique and its use for this project are discussed.

Abstract (deutsch)

Kalziumphosphate sind für medizinische Anwendungen sehr interessant. Als Knochenersatzmaterialien oder für die Gentransfektion besitzen sie grosses Potential.[1,2] Die meisten kommerziell verfügbaren Kalziumphosphate werden heutzutage immer noch unter hohem Druck und hohen Temperaturen hergestellt.[1-3] Zudem ist die Zusammensetzung der Ausgangsmasse oft nicht gut definiert oder die Reaktionskomponenten und -mischungen enthalten organische Lösungsmittel.[3,4]

Hauptbestandteil der menschlichen Knochen ist Kalziumphosphat in Form von Hydroxyapatit (Abbildung 1). Zusätzlich besteht der Knochen aus Wasser und organischen Materialien wie Kollagen oder anderen Proteinen.[7] Knochen ist eines der härtsten Materialien im menschlichen Körper und er kann sich bei Defekten und Beschädigungen regenerieren. Um die in der Natur vorkommenden Strukturen so identisch wie möglich simulieren zu können, ist es erstrebenswert, anorganische Materialien aus wässrigen Lösungen zu fällen. Dabei können auch (organische) Zusätze eingebracht werden, um der biologischen Vielfalt noch näher zu kommen.[5,6]

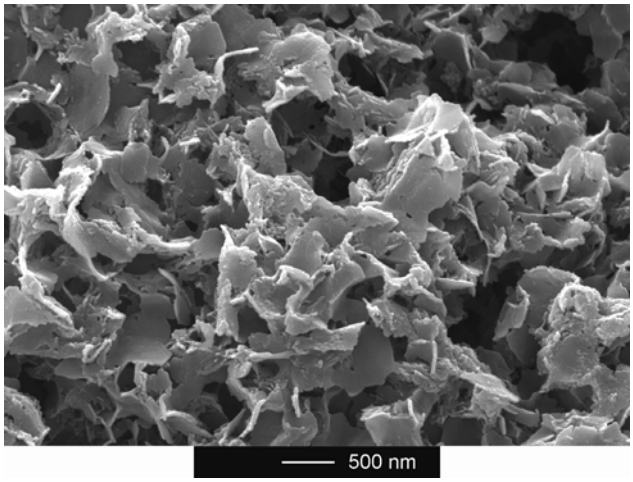

Abbildung 1: Aus wässriger Lösung mineralisierter Hydroxyapatit.[8]

Als Ausgangslage dieser Doktorarbeit dient die Mineralbildung von Kalziumphosphaten aus wässrigen Lösungen. Synthetische, chemisch leicht zu modifizierende Polyesterfasern dienen dabei als Gerüst für die Fällung des Kalziumphosphats. Die Doktorarbeit hat unter anderem zum Ziel, ein neues Polymer zu entwickeln, auf welchem Kalziumphosphat mineralisiert werden kann.

Um die mit Kalziumphosphat mineralisierten Polymere als Knochenersatzmaterial verwenden zu können und daraus einen Mehrwert für den Patienten und damit auch für die Industrie erzielen zu können, fiel die Wahl des Polymers auf einen Polyester. Polyester sind biologisch abbaubare Polymere, welche synthetisch recht einfach zugänglich sind. Der erhaltene Polyester sollte dann mittels der Elektrospinning-Technik zu einer Fasermatte verarbeitet werden, bevor er als Unterlage für das Kalziumphosphatwachstum genutzt wird.

Um herauszufinden ob die selbst aufgebaute Elektrospinning-Apparatur wie gewünscht funktioniert, sollten zuerst Polyester wie Poly(caprolakton), Poly(hydroxybutyrat) und Poly(hydroxybutyrat-*co*-hydroxyvalerat) mit dieser neuen Apparatur verarbeitet werden. Die genannten Polyester wurden bereits mehrfach mit dem Elektrospinning-Verfahren zu Fasern gesponnen und konnten daher mit den in der vorliegenden Arbeit erhaltenen Resultaten verglichen werden.[9-11] Grosse Polymerketten lassen sich besser und uniformer spinnen.[17] Daher wurden bisher und auch in der vorliegenden Arbeit, Polyester mit hohem Molekulargewicht eingesetzt. Es wurde z. B. Poly(caprolakton) mit einem Molekulargewicht von ca. 80000 g/mol verwendet.[12,13]

Ein Kernziel der Arbeit war es, einen neuen Polyester herzustellen, der ein hohes Molekulargewicht aufweist und trotzdem gut löslich ist. Ausserdem sollte das Polymer einfach zu modifizieren sein, um neue Funktionalitäten einführen zu können. Funktionelle Gruppen können das Kalziumphosphatwachstum und spätere Adhäsion der Zellen beeinflussen. Ein Polyester, der all diesen Anforderungen gerecht werden sollte, ist der α-Allylpolyester. Dieser Polyester wurde bereits erfolgreich mit hohem Molekulargewicht synthetisiert.[14]

Ein weiteres Projekt befasst sich mit der Entwicklung einer Beschichtung für Nitinol. Dies wurde in Zusammenarbeit mit der Firma Admedes Schüssler GmbH verwirklicht. Nitinol ist eine Legierung aus Nickel und Titan, die als Stentmaterial verwendet. Stents sind Implantate, die in Hohlorgane (z. B. Arterien) eingebracht werden, um diese offen zu halten. Das Material ist sehr interessant, da es aussergewöhnliche Eigenschaften aufweist. Wenn Nitinol mechanisch deformiert wird, bleibt es in dieser neuen Form. Wird es später erwärmt, nimmt das Nitinol wieder die Originalgestalt vor der Deformierung an. Zudem ist Nitinol weniger starr als Titan.

Um dieses Material zu beschichten, wurde die bekannte Layer-by-Layer-Technik[15] angewandt. Als Polyelektrolyte (geladene Polymere) wurden Heparin als negativ geladene und Chitosan als positiv geladene Komponente verwendet. Beides sind Polysaccharide, die

sich für medizinische Anwendungen bereits etabliert haben.[16] Anschliessend wurde Kalziumphosphat auf dieser Polyelektrolytschicht mineralisiert, um die Stentoberfläche zu variieren. Die Oberfläche beeinflusst die Adhäsion der Zellen und somit das An- und Einwachsen von Gewebe.

Die Doktorarbeit gliedert sich wie folgt: eine Literaturübersicht gibt zunaechst einen detaillierten Einblick in die Kalziumphosphatmineralisation aus wässrigen Lösungen. Dabei liegt der Fokus bei der Mineralisation in Anwesenheit von Polymeradditiven und deren Einfluss auf die Morphologie der anorganischen Strukturen. Im zweiten Teil der Einleitung werden die für das Elektrospinning verwendeten Polyester vorgestellt. Hier liegt der Fokus auf Verarbeitung und Gebrauch im Zusammenspiel mit Kalziumphosphat. Eine kurze Vorstellung der experimentellen Techniken und Charakterisierungsmethoden soll die Nachvollziehbarkeit der Arbeit erleichtern.

Im zweiten Kapitel wird das Elektrospinning beschrieben. Dabei wird auch der Aufbau der Apparatur erklärt und auf den Einfluss der Parameter für die resultierenden Fasermatten eingegangen. Die Synthese des α-Allylpolyesters und dessen Weiterverarbeitung ist Thema des dritten Kapitels. Die Probleme, die dabei aufgetaucht sind, werden intensiv diskutiert. Die Polyelektrolytbeschichtung des Nitinols wird im vierten Kapitel behandelt.

References

(1) Dagang, G.; Kewei, X.; Haoliang, S.; Yong, H. *Journal of Biomedical Materials Research, Part A* **2006**, *77A*, 313-323.

(2) Gauthier, O.; Khairoun, I.; Bosco, J.; Obadia, L.; Bourges, X.; Rau, C.; Magne, D.; Bouler, J. M.; Aguado, E.; Daculsi, G.; Weiss, P. *Journal of Biomedical Materials Research, Part A* **2003**, *66A*, 47-54.

(3) Pinchuk, N. D.; Ivanchenko, L. A. *Powder Metallurgy and Metal Ceramics (Translation of Poroshkovaya Metallurgiya (Kiev))* **2003**, *42*, 357-371.

(4) Thomas, M. E.; Richter, P. W.; Crooks, J.; Ripamonti, U. *Key Engineering Materials* **2001**, *192-195*, 441-444.

(5) Garcia-Ramos, J. V.; Carmona, P. *Journal of Crystal Growth* **1982**, *57*, 336-42.

(6) Schweizer, S.; Taubert, A. *Macromolecular Bioscience* **2007**, *7*, 1085-1099.

(7) Biltz, R. M.; Pellegrino, E. D. *J Bone Joint Surg Am* **1969**, *51*, 456-466.

(8) Taubert, A.; Furrer, E.; Meier, W. *Chemical Communications (Cambridge, United Kingdom)* **2004**, 2170-2171.

(9) Kim, H.-j.; Jung, Y.-h.; Khil, M.-s.; Kim, H.-y.; Bang, H.-J. *Journal of the Korean Fiber Society* **2004**, *41*, 424-432.

(10) Li, X.; Xie, J.; Yuan, X.; Xia, Y. *Langmuir* **2008**, *24*, 14145.

(11) Yang, F.; Wolke, J. G. C.; Jansen, J. A. *Chemical Engineering Journal (Amsterdam, Netherlands)* **2008**, *137*, 154-161.

(12) Sell, S.; Barnes, C.; Smith, M.; McClure, M.; Madurantakam, P.; Grant, J.; McManus, M.; Bowlin, G. *Polymer International* **2007**, *56*, 1349-1360.

(13) Lim, C. T.; Tan, E. P. S.; Ng, S. Y. *Applied Physics Letters* **2008**, *92*, 141908/1-141908/3.

(14) Parrish, B.; Quansah, J. K.; Emrick, T. *Journal of Polymer Science, Part A: Polymer Chemistry* **2002**, *40*, 1983-1990.

(15) Decher, G. *Science (Washington, D. C.)* **1997**, *277*, 1232-1237.

(16) Khor, E.; Lim, L. Y. *Biomaterials* **2003**, *24*, 2339-2349.

(17) Thandavamoorthy, S.; Bhat, G. S.; Tock, R. W.; Parameswaran, S.; Ramkumar, S. S. *Journal of Applied Polymer Science* **2005**, *96*, 557-569.

Danksagung

Die vorliegende Arbeit wurde in der Zeit von Mai 2006 bis Januar 2010 am Departement Chemie der Universität Basel unter der Leitung von Herrn Prof. Dr. Andreas Taubert durchgeführt.

Ich danke *Prof. Dr. A. Taubert* für das interessante Thema, das stete Interesse am Fortgang der Arbeit und die willkommene Motivation während schwierigen Zeiten. Ausserdem bedanke ich mich für die Möglichkeit, dass ich meine persönlichen und wissenschaftlichen Erfahrungen machen durfte und die Städte Potsdam und Berlin in mein Herz schliessen konnte.
Vielen Dank an *Prof. Dr. Wolfgang Meier* für Möglichkeit meine Dissertation in Basel zu machen. Danke für die Bereitstellung von Laboratorien, Geräten und die Unterstützung wenn ich sie gebraucht habe.
Danke an *Dr. Helmut Schlaad* für die Übernahme des Korreferats und die Zusammenarbeit während der Dissertation.
Prof. Dr. Thomas Pfohl für den Vorsitz meiner Verteidigung.

Dem Team vom Zentrum für Mikroskopie (ZMB) am Biozentrum der Universität Basel danke ich herzlich für die Hilfe bei der Rasterelektronenmikroskopie:
Gianni Morson: Danke für die Instandhaltung des REM im Anatomischen Institut- auch wenn nicht alle wissen, wie das Gerät zu bedienen ist…
Marcel Düggelin, Daniel Mathys: Danke für die exzellente Hilfestellung und die resultierenden Bilder.
Eva Bieler: Danke für die Hilfestellung, etliche lustige Stunden und deine Frohnatur.

Herzlichen Dank an die Mitglieder der *Arbeitsgruppe von A. Taubert* für die wissenschaftliche Unterstützung und die Experimente, die an der Universität Potsdam durchgeführt wurden.
Danke an die *Arbeitsgruppe von H. Schlaad* und weiteren Mitarbeitern am Max-Planck-Institut in Potsdam. Speziell gilt mein Dank *Dr. Christina Diehl*, welche die Thiol-en-click-Reaktion durchgeführt hat und mir wichtige Daten generiert hat.
Allen derzeitigen und ehemaligen Mitgliedern der *Arbeitsgruppe von W. Meier* danke ich für das gute Arbeitsklima. Mein Dank gilt vor allem *Dr. Rainer Nehring* für diverse interessante

Gespräche und die Durchsicht der vorliegenden Arbeit. Danke auch an *Dr. Cornelia Palivan* für die aufmunternden und motivierenden Worte während dem Zusammenschreiben und Bewerben.

Mein besonderer Dank gilt meiner *Mutter*, die mich vor allem während meines Studiums aber auch sonst immer in allem unterstützt hat, was ich angepackt habe.
Großer Dank gilt auch meinem Lebenspartner *Tobias Hess* für seine Geduld und Hilfe in jeder Lebenslage!

1 General Introduction: Literature overview

1.1 Polymer-controlled, bioinspired calcium phosphate mineralization from aqueous solution

This chapter introduces the most important calcium phosphate (CaP) crystal phases and their typical characteristics. Additionally, CaP mineralization from aqueous solutions with additives like polymers will be discussed. The influence of the additives for nucleation and crystal phase formation is described in the form of a literature overview. The most important polymeric additives are given. Furthermore, polyesters that are used for this work are introduced.

1.1.1 Important calcium phosphate crystal phases

Like many other compounds, calcium phosphate crystallizes in various crystal structures with different mechanical, thermal, and chemical stabilities. The most important crystal phases in the context of bioinspired mineralization are (i) amorphous calcium phosphate (ACP), (ii) brushite (dicalcium phosphate dihydrate, DCPD, $CaHPO_4*2\ H_2O$), (iii) β-tricalcium phosphate (calcium orthophosphate or tribasic calcium phosphate, $Ca_3(PO_4)_2$, β-TCP), (iv) octacalcium phosphate ($Ca_8H_2(PO_4)_6*5\ H_2O$, OCP), and (v) hydroxyapatite ($Ca_5(PO_4)_3OH$, HAP).[1,2]

In Nature, however, calcium phosphates (CaPs) – especially HAP – are rarely found as a neat compound because CaPs can easily exchange PO_4^{3-}, OH^-, or Ca^{2+} for other ions. For example, Sr^{2+}, Ba^{2+}, or Pb^{2+} can replace Ca^{2+}. In addition, ions like VO_4^{3-}, AsO_4^{3-}, F^-, Cl^-, and Br^- can substitute for PO_4^{3-} and OH^-, respectively. Other examples are Na^+, K^+, and CO_3^{2-}. Incorporation of the latter into HAP results in carbonated apatite, which is the main constituent of human bone. As a result, substituted apatites exist in a large variety of compositions and properties, which are controlled by the chemical environment within they were grown.[2] In the following table, the different crystal phases of calcium phosphates and their specific characteristics are listed.

Table 1.1. Calcium phosphate crystal phases and their characteristics.[1]

Crystal phases (Abbreviation, Common name)	**Chemical Formula Crystal system**	**Synthesis from aqueous solution at ambient conditions**	**pH of formation**	**Precursor for**	**Typical shape**	**Solubility product**	**Ca/P ratio**
Amorphous calcium phosphate[a] (ACP)	$Ca_3(PO_4)_2$ * n H_2O N/a	Yes	All	All crystalline phases	Beads		1.5
Dicalcium phosphate dehydrate (DCPD, Brushite)	$CaHPO_4$ * 2 H_2O Monoclinic, C2/c	Yes	Acidic (<4-5)	HAP Monetite	Large Plates (Large crystal face is 010)	$1.87*10^{-7}$ $(mol/l)^2$	1
Dicalcium phosphate anhydrous (DCPA, Monetite)	$CaHPO_4$ Triclinic, P1	Yes	Acidic (<4-5)	Brushite Apatite	Plates	$9.2*10^{-7}$ $(mol/l)^2$	1
α-Tricalcium phosphate[b] (α-TCP Whitlockite)	$Ca_3(PO_4)_2$	No	Basic				1.5
β-tricalcium phosphate[c] (β-TCP)	$Ca_3(PO_4)_2$	No	Basic			$2.8*10^{-29}$ $(mol/l)^5$	1.5
octacalcium phosphate (OCP)	$Ca_8H_2(PO_4)_6$*5 H_2O Triclinic, P1	Yes	Acidic (<5-6)	HAP	Layered (apatitic and hydrated layers)	$2.5*10^{-99}$ $(mol/l)^8$	1.33
Hydroxyapatite[d] (HAP)	$Ca_5(OH)(PO_4)_3$ Hexagonal, P63/m[g] Monoclinic[h]	Yes	Basic (>7)	OXA	Needles	$5.5*10^{-118}$ $(mol/l)^9$	1.67

Crystal phases (Abbreviation, Common name)	**Chemical Formula Crystal system**	**Synthesis from aqueous solution at ambient conditions**	**pH of formation**	**Precursor for**	**Typical shape**	**Solubility product**	**Ca/P ratio**
Chloroapatite (ClAP)	$Ca_5(Cl)(PO_4)_3$ Hexagonal, P63/m	Yes	Basic (>7)		Needles		1.7
Fluorapatite[e] (FAP)	$Ca_5(F)(PO_4)_3$ Hexagonal, P63/m	Yes	Basic (>7)		Needles	$5.0*10^{-123}$ (mol/l)[9]	1.7
Tetracalcium phosphate (TTCP, Hilgenstockite)	$Ca_4O(PO_4)_2$		Basic	HAP			2
Oxyapatite[f] (OXA)	$Ca_{10}O(PO_4)_6$	No	Basic			Water-soluble	
Monocalcium phosphate (MCP)	$CaH_4(PO_4)_2$	No	Acidic			Highly water-soluble	0.5
Monocalcium phosphate monohydrate (MCPM)	$CaH_4(PO_4)_2*H_2O$		Acidic			Water-soluble	0.5

[a] Two discrete forms ACP1& ACP2.

[b] Widely used as bone substitute.

[c] Stabilized by magnesium ions.

[d] Major inorganic component in bone and teeth.

[e] Highly stable in acid, favored over HAP at pH < 6.

[f] Decomposition product of HAP.

[g] Biological form.

[h] More stable than the biological form.

1.1.2 CaP mineralization control via water-soluble polymers

1.1.2.1 Homopolymers as additive

1.1.2.1.1 Poly(acrylates)

Bigi et al. have shown that sodium poly(acrylate) reduces the nucleation efficiency of OCP and significantly reduces the coherence length of the crystalline domains.[3] The reduction of the coherence length is roughly isotropic and indicates no preferential interaction of the polyelectrolyte with the growing crystals. Interestingly, a parallel publication by the same group has shown that the crystallization of HAP (not OCP) is strongly affected by poly(acrylic) acid (not sodium poly(acrylate)). In this case the authors reported a crystal face specific reduction of the coherence length of the resulting minerals.[4] A cross-comparison has not been made, although OCP was reported to hydrolyze and form HAP by a layer-by-layer mechanism. This hydrolysis was held responsible for the resulting acicular HAP morphology.[5,6] The authors suggest that the carboxylate-rich polyelectrolyte sodium poly(acrylate) adsorbs on the hydrated layer of the OCP, thus inhibiting its in situ hydrolysis to HAP.[5,6]

1.1.2.1.2 Poly(amino acid)s

Polyacrylic acid and poly(acrylates) have been used as synthetic analogs of proteins. However, poly(amino acids) are more closely related to the acidic proteins often found in bone and other biomaterials than poly(acrylates). In a direct comparison of poly(acrylates) and poly(amino acids), Bigi and coworkers have synthesized HAP in the presence of increasing concentrations of poly(acrylic acid) and poly(aspartate). Several structural modifications of the resulting composites as a function of polyelectrolyte content in the reaction solution have been reported.[7] The crystallinity of the HAP decreases with increasing polyelectrolyte concentration. Moreover, the particle morphology is strongly affected by the presence of the anionic polyelectrolytes: while HAP precipitated without polymer predominantly consists of tiny crystals with a platy morphology, HAP precipitated with poly(acrylic acid) and poly(aspartic acid) shows clusters of long and thin crystals.

Peytcheva et al.[8] have shown that poly(aspartates) are efficient growth modifiers for CaP. They have observed presumably amorphous CaP, “snowball”, “parachute”, and fibrillar structures that appear to be kinetic intermediates. They have also demonstrated that the size of the fibrillar entities depends on the molecular weight of the poly(aspartate). The authors

suggest that the formation of the observed structures is due to the influence of the polymer on the surface energies and crystal growth rates via polyelectrolyte adsorption on the growing particles. Similar fibrillar features have been made by Fowler et al. using the surfactant AOT (sodium dioctyl sulfosuccinate) as a template.[9] These authors have, however, not commented on the growth process and role of the additive.

Bigi et al.[7] and Füredi-Milhofer et al.[10,11] both propose that poly(aspartate) specifically interacts with OCP and HAP. Poly(aspartate) is quantitatively incorporated into the HAP crystals, leading to a reduction of the coherence length of the crystalline domains. As the composite crystals also show a remarkable trend towards aggregation, the authors propose that aspartic acid and poly(aspartate) interact with the exposed hydrated layer of OCP crystals. It is further suggested that this interaction takes place between the carboxylate groups of the macromolecules and the rows of calcium ions parallel to the direction in the hydrated layer.

Prior to Peytcheva et al.,[8] Hunter and coworkers have already shown that the chemistry of polyamino acids plays an important role in HAP nucleation control.[12] While poly(aspartic acid) is almost as efficient in inhibiting HAP nucleation as osteopontin, a highly phosphorylated bone protein, poly(glutamic acid) is over 1000 fold less effective. This suggests that Petcheva et al.[8] would have observed different CaP morphologies with poly(glutamate), because the results by Hunter et al.[12] imply that the poly(glutamate)-CaP interactions are much weaker than the poly(aspartate)-CaP interactions. The inhibition of CaP mineralization by osteopontin phosphopeptides has also been confirmed by Pampena et al.[13]

Fujisawa et al. have studied the interaction of osteonectin (a protein found in bone and teeth) with HAP.[14] After protein adsorption and digestion with trypsin, a small peptide was left adsorbed on the HAP surface. The peptide was identified as an amino terminal peptide rich in aspartic acid. To model this suspected HAP-binding site, the adsorption and mineralization of CaP with glutamic acid (Glu_6) and aspartic acid (Asp_6) oligopeptides was studied in electrophoresis or agar gels. While Glu_6 enhanced the nucleation and growth of CaP, Asp_6 inhibited mineralization. This general finding is in line with results by Hunter et al.,[12] but as the gels used in the later study[14] were rather poorly defined, it is difficult to draw a final conclusion.

In contrast to Hunter et al.[12] and Fujisawa et al.,[14] Tsortsos and Nancollas have shown that poly(-L-glutamate) and poly(-L-aspartate) are strong nucleation inhibitors for HAP in solution, but promote HAP and OCP nucleation when adsorbed on inorganic surfaces like germanium.[15] Both polymers adopt a random coil like conformation in solution. A train-loop

configuration of the polycarboxylates on the crystals was held responsible for the observed nucleation inhibition and promotion effects. This suggests that not only the polymer chemistry and conformation in solution is an important parameter to control mineralization, but that also the presence of surfaces can change the mineralization process dramatically.

So far, most studies have been concerned with HAP, but the influence of poly(amino acids) on OCP mineralization has also been studied. Burke et al. have studied the growth kinetics of OCP in presence of poly(aspartic acid) and phosphophoryn, a highly phosphorylated protein, rich in aspartic acid.[16] Phosphophoryn was found to be a less efficient growth inhibitor than poly(aspartic acid). This lower efficiency was assigned to the more efficient formation of β-sheets on the OCP crystal surface in the case of poly(aspartic acid). It would be interesting to compare the inhibition efficiency of the above proteins (phosphophoryn and osteopontin) for both HAP and OCP. Indeed, the data from Hunter et al.[12,17] suggest that there are differences between the two CaP crystal phases, especially if poly(glutamate) and poly(aspartate) are included in the comparison. However, this comparison has not been reported.

Nevertheless, more efficient formation of β-sheets in the case of poly(aspartic acid) on OCP[10,16] supports the claim that not only the concentration or the absolute number of adsorbed acid or phosphate groups is important for nucleation control. Also the configuration and conformation of a given (macro)molecule on a surface is to be considered as an additional parameter for mineralization control. A combined NMR and theoretical study has shown that oligopetides do adopt specific, preferred geometries on HAP surfaces.[18]

As a consequence, it is possible that also the development of a crystal surface *during* mineralization affects the way a polymer precipitates. For example, the surface structure of an adsorbed polymer and hence its influence on crystal growth need not be identical at all stages of a precipitation reaction.

Bigi et al. report that poly(-L-aspartate) inhibits the formation of OCP in aqueous solution and induces morphological and structural modifications.[19] Low poly(-L-aspartate) concentrations induce a reduction of the mean dimensions of the platelets and the formation of aggregates. Relatively high concentrations reduce the total amount of product, which precipitates as almost spherical aggregates with increasing structural disorder. Both poly(-L-aspartate) and poly(-L-glutamate) inhibit OCP hydrolysis, but poly(glutamate) is the more efficient inhibitor. Inhibition takes place through polyelectrolyte adsorption on the face of OCP crystals, which prevents the splitting of OCP crystals along their c-axis and the transformation into the final very long, needle like, apatitic crystals.

More recently, Bigi and coworkers have also studied the effect of single amino acids (glutamic and aspartic acid) on the mineralization of HAP.[20,21] The carboxylic acid moieties preferentially interact with the calcium ions of the HAP. Aspartic acid is incorporated into the minerals to a larger extent than glutamic acid. Glutamic acid induces disorder in the HAP structure. This study clearly shows that single amino acids can (with certain restrictions) be used as models to study CaP mineralization more quantitatively.

For example, Wong and Czernuszka have shown that phosphorylated serine, tyrosine, threonine, and arginine strongly affect CaP growth.[22,23] Phosphoserine accelerates the rate of precipitation. Furthermore, the transformation from OCP to HAP occurs earlier than in a control sample mineralized without amino acids and in the presence of the other three phosphorylated amino acids. Phosphoserine also promotes secondary nucleation, but hinders crystal growth.[24] Phosphotyrosine on the other hand completely inhibits the OCP-HAP transformation. Phosphorylated arginine and tyrosine slow down the overall crystallization rate compared to the control samples. Interestingly, these data contradict experiments with phosphorylated proteins, where a high number of phosphoserine units in the proteins was found to strongly inhibit (instead of nucleate) CaP mineralization.[12,13,16,17,25]

In a study to rationalize the inhibition by phosphorylated polymers, Füredi-Milhofer et al.[10,11] describe the effects of phosphate containing polypeptides, which can be viewed as an extension of the single-component poly(amino acid)s discussed so far, on CaP mineralization. Phosphophoryn and phosvitin (approximately 50 mol% of phosphoserine residues, but only 7 mol% of aspartic acid residues) both recognize the Ca-OPO-Ca-OPO chain motif which is part of the HA-layer of OCP. Therefore, the interaction of both proteins with OCP results in elongated crystals. This interaction was suggested to be favorable, because the phosphate groups of phosphophoryn are spaced at approximately the same distance along the extended protein chain as are the phosphate groups in the Ca-OPO-Ca-OPO chain motif of OCP.

Overall, these studies show that polyelectrolytes affect the (relative) growth rates or the mechanism of crystallization: nucleation, crystal growth, aggregation, and phase transformation are directly controlled by the polymer and its concentration. Several effects are related to this: crystal numbers, sizes, and size distributions change, crystal habits are modified, polymer is incorporated in the precipitate, and finally, the polymorph is also partly selected by the chemistry and presence of the polyelectrolyte. Older studies, e.g. refs.[10,11] suggest that some “epitaxial-like” interaction between the organic matrix or additive and the growing crystal is responsible for the observed results. But newer studies, e.g.[18] have also

shown that other effects like thermodynamic considerations or charge effects play a role in mineralization control as well.

1.1.2.1.3 Other Homopolymers

Other homopolymers have been used rarely as crystallization additives. Greish et al. have introduced an interesting new and completely different polymer template than the studies discussed so far: a polyphosphazene was functionalized with carboxylic acid side groups.[26] The acids coordinate Ca^{2+} and HAP precipitates through a dissolution-precipitation process under mild basic conditions. Prelot and Zemb have reported the formation of mesoporous hydroxyapatite from poly(ethylene oxide oleyl phosphate)[27] and Shkilnyy et al. have fabricated CaP hybrid nanoparticles using poly(ethylene imine) as a growth modifier,[28,29] Figure 1.1.

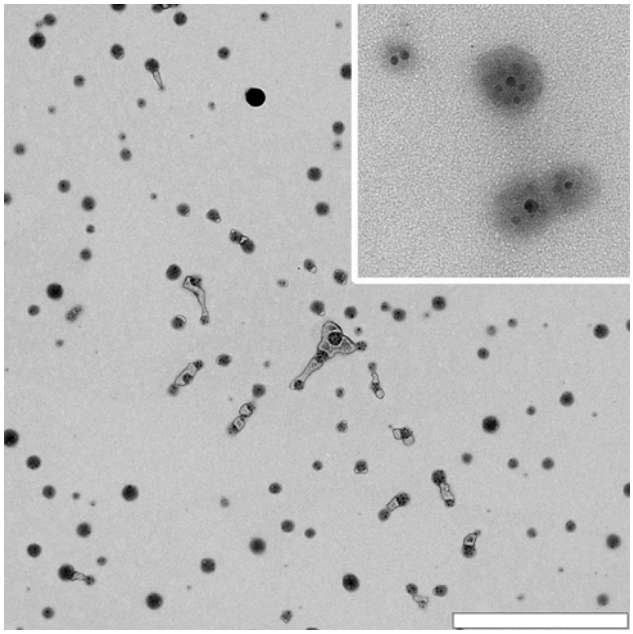

Figure 1.1. TEM image of CaP nanoparticles formed in the presence of PEI.[29] Scale bar is 1 μm. Image courtesy of A. Shkilnyy and B. Thiersch, University of Potsdam. Inset: magnified view showing the composite nature of the particles.

1.1.2.2 Biodegradable Polymers and Protein Mimics as additives

Bone is a highly structured protein/inorganic composite, where the main protein component is collagen. Many studies have used collagen of different origin, composition, structure and pre-treatment for the synthesis of CaP/protein composites, in particular for the

engineering of potential implant materials. These developments have been reviewed extensively both from a chemical and a biomedical perspective.[30-32]

Schwarz and Epple have shown that porous poly(glycolide) membranes can be mineralized with HAP and FAP. FAP forms elongated hexagonal prisms and HAP forms large hexagonal plates.[33] The polyglycolide acts as a specific environment directing nucleation and growth.

Ritzoulis et al. have shown that also casein, a milk protein, and olive oil-in-water emulsions lead to highly porous CaP after supercritical CO_2 extraction.[34] In a much more controlled approach, self-assembled peptide fibers have been shown to efficiently control CaP mineralization from aqueous solution.[35] Here the peptides were designed to self-assemble into fibers, which were thoroughly characterized. Among others, electron microscopy and electron diffraction showed that the CaP nanocrystals nucleated on the fiber surface all have the same crystallographic orientation, a finding, which was assigned to the surface chemistry and hence the ability of the peptide fibers to control CaP nucleation.

Bertozzi and coworkers have fabricated a poly(2-hydroxyethyl methacrylate) (pHEMA) hydrogel, which exposes carboxylate groups on the surface of the cross-linked pHEMA. Electrostatic interaction promotes CaP nucleation and growth on the surface and in the interior of the hydrogel. Variation of the hydrogel surface leads to various mineralization grades and the crystallinity of the resulting HAP.[36,37] In a subsequent study, the group reported an "emulation" of natural scaffolds for bone growth via the functionalization of poly(methacryl amide) and poly(methacrylate) hydrogels with amino acids and peptides that serve as CaP nucleating and mineral-binding ligands.[38]

Hartgerink and coworkers have taken this concept one step further and generated collagen-like synthetic peptides by an elegant combination of solid-phase synthesis and polymerization.[39] The resulting peptide polymers self-assemble into well-defined, quasi-collagenous fibers with diameters between 10 and 20 nanometers. This approach has several advantages over the expression in bacteria or the isolation of natural collagen: large amounts of material can be obtained, polymer properties like solubility or self-assembly can be exactly adjusted and polymers can be made to include non-biological functionalities. As a result, the approaches by Hartgerink and coworkers[35,39,40] and Bertozzi and colleagues[36-38] are probably among the most attractive pathways for the fabrication of well-controlled, biocompatible, biochemically active, and biodegradable materials for potential use in implants.

1.1.2.3 Carbohydrates as additives

Besides proteins, protein mimics and synthetic polymers, carbohydrates have also been studied as a scaffold for CaP mineralization. Initially, the effect of soluble carbohydrates was studied. Kamasaka et al. reported that phosphorylated oligosaccharides derived from potato starch inhibit CaP mineralization.[41] Because the saccharides, carrying two phosphate groups per monomer unit, are more efficient inhibitors than those with only one phosphate per monomer unit, it was concluded that the inhibition efficiency is related to the number of phosphate groups attached to each sugar molecule. Mäkinen and Söderling go more into detail. They have reported that the solubility of Ca salts and tooth enamel in aqueous solutions does also depend on the chemical structure of carbohydrates present in solution.[42]

Sulfated polysaccharides have a strong inhibitory effect on HAP and DCPD crystal growth and agglomeration.[43] The increase of negative zeta potential values after addition of polysaccharides suggests a strong binding of these polysaccharides to HAP and DCPD crystals. A similar observation was made for proteoglycan- and chondroitin-4-sulfate-controlled precipitation of HAP.[42,44] In summary, these data suggest that not only phosphated, but also sulfated carbohydrates could be interesting scaffolds for CaP/polymer hybrid materials with controllable properties, although Hunter et al. have found a weak inhibition of CaP precipitation with dextran sulfate.[17]

Cellulose hydrogels have some potential for orthopedic applications, but they lack osteoinduction. Barbosa and colleagues showed that this can be partly overcome by soaking the regenerated cellulose hydrogels in calcium chloride solution[45] or by chemically phosphorylating the hydrogels prior to mineralization.[46] More recently the same authors have shown that human bone marrow stromal cells not only proliferate on regenerated cellulose hydrogels but also deposit a layer of HAP.[47] These studies show that phosphorylation is an efficient means to increase the nucleation and crystallization efficiency of a synthetic or semi-synthetic biomaterial.

1.1.2.4 Homopolymers in multilayers

Homopolymers can also be deposited on many substrates using the approach of polyelectrolyte multilayers,[48] which has generated a tremendous scientific and commercial interest. Among others, polymer multilayers can be used for the fabrication of surfaces that favor or inhibit CaP nucleation. Ngankam et al. have shown that CaP nucleation is dramatically reduced if a polyelectrolyte multilayer is deposited on a silica surface.[49]

Surprisingly, the charge does not alter the nucleation efficiency, but changes the crystal phase from DCPD to HAP and OCP, respectively.

Ball et al. have extended this approach to polyamino acids and demonstrated that alternating multilayers of poly(L-glutamic acid) or poly(L-aspartic acid) and poly(L-lysine), respectively, can be used to tune the lag time before nucleation occurs.[50] Spoerke et al. have shown that the same type of approach is also viable for the modification of titanium surfaces.[51] Finally, Walsh et al. have shown that calcium phosphate films with adjustable porosities and morphologies can be grown at the air-water interface.[52] Here, poly(aspartate) present in the subphase, is used as a growth inhibitor preventing nucleation and growth in bulk aqueous solution.

These publications clearly demonstrate that homopolymers, (polymeric) surfactants, and polymer multilayers are efficient growth modifiers for calcium phosphate. The effect of polyacrylates, polygluatamates, and polyaspartates on mineralization from bulk solution has been studied in some detail, but even in these cases there is still a lack of quantitative understanding of the role and function of the polymeric additive. Because of this, it is still difficult, if not impossible, to predict the influence of a given polymer on the mineralization process. But as the additives like polymers influence the CaP nucleation, growth and properties, further investigations have to be done. Especially, this is important for water insoluble components.

1.1.3 CaP mineralization of insoluble scaffolds

Other approaches towards advanced calcium phosphate/organic hybrid materials include the mineralization of insoluble scaffolds or the mineralization in hydrogels. Hydrogels and polymer matrix systems have been extensively studied by several groups.[53-72] Insoluble scaffolds have also been studied; especially polyester matrices have been intensely investigated for bone substitutes and other applications.[73,74] In the following paragraphs, the most important polyesters are introduced. These polyesters have also been used for this work.

1.1.3.1 Poly(hydroxyl butyrates)

Mainly composites of CaP and Poly(hydroxyl butyrate) (PHB, see figure 1.2) and Poly(hydroxyl valerate) (PHV) and their copolymers were studied.[75-77] PHB is a water insoluble, biodegradable thermoplastic, which is produced commercially in bulk by biotechnology. Compared to polyglycolide, polylactide and their copolymers, PHBs possess a higher chemical stability towards hydrolysis, resulting in considerably longer degradation times.[78]

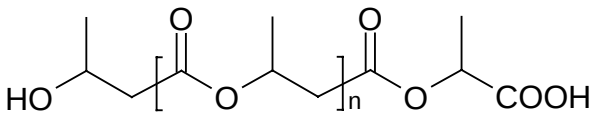

Figure 1.2. The structure of Poly(hydroxyl butyrate) (PHB)

In PHB/ CaP composites, the amount of HAP may also have an effect on the degradation time of the polyester. Doyle et al. showed that the more HAP was present in the composite, the more rapid was the deterioration in properties.[75] The crystallinity of PHB-HV was also varied by the presence of HAP particles. This is also true with TCP.[77] During degradation, compounds from PHB and PHV release acidic degradation products and neither pure HAP nor β-TCP are able to counter the acidic degradation of polyesters. The material based on PHB/PHV copolymer and ACP gave an alkaline pH and the cells from the experiment died after 10 days. In contrast, Linhart et al.[76] showed that a composite of ACP and PHB remained at an almost constant pH within the physiological range. Despite this observation, all groups take PBH/CaP-composites into consideration to have the potential for various medical applications.

1.1.3.2 Poly(caprolactones)

Composites of poly(caprolactone) (PCL, see figure 1.3) and CaP also have been studied. As PHB-CaP composites, PCL-TCP composites degrade faster than the polymer itself when implanted in an *in vivo* environment.[79]

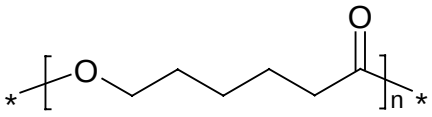

Figure 1.3. The structure of Poly(caprolactone) (PCL)

Poly(caprolactone) and its copolymers also can be used as scaffolds for CaP growth on the surface. Thin layers of CaP crystals are deposited on the surfaces of polymers to improve the osteoconductivity of the substrate, favoring biological responses on the surfaces and thus mimicking the reactions occurring in the natural calcified tissues without losing bulk properties of polymers.[80-84] Fiber mats of polymer/CaP composites were produced. Porter et al.[85] fabricated PCL-HAP composite nanowires via template synthesis without any solvent. Oliveira et al.[86] developed PCL-based scaffolds by a 3D plotting technique. Others used electrospinning (figure 1.4) to achieve high specific surface areas favoring cell adhesion and stimulate bone regeneration.[83,87] Polyester/CaP fibrous composites can also be fabricated by co-spinning of the components or from mineralization of CaP on pre-spun polyester fibers.[88,89] To build up fiber scaffolds, electrospinning may also be used for other polymers such as the previously discussed PHB and PHB-HV copolymers.[90]

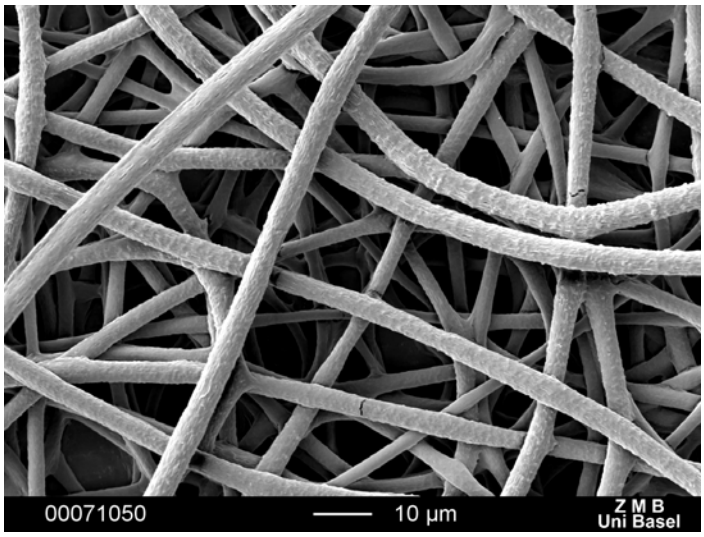

Figure 1.4: Electrospun fibres from poly(hydroxyl butyrate).

As already known from other polymer scaffolds, functional groups have mineral-nucleating effects. Song et al.[91,92] and Oliveira et al.[86] showed that mineralization is controlled by the specific surface chemistry. Therefore further research on fiber scaffolds from functionalized polymers and its effects on CaP mineralization is of great interest.

As the most of the known polyester/CaP composites are fabricated by classical methods like high pressure approaches, it is of note to study the mineralization of CaP from aqueous solution on polymeric scaffolds at ambient conditions.

This Thesis is focusing on electrospun scaffolds from functionalized biodegradable polyesters for tissue engineering. These polymers were chosen as they are biocompatible and biodegradable and therefore preferable for implantation for surgery.[93,94] A popular technique to synthesize these polyesters is via biotechnology. As we had no access to this method, we synthesized the polyester via ring opening polymerization (ROP). Nevertheless, we found a new way to functionalize these polyesters in a simple and efficient technique, the "thiol-ene click chemistry".[95,96] Thiol-ene click chemistry was chosen because a variety of thiols is commercially available and is biocompatible. Additionally this technique provides one way to introduce different functionalities to the polyester as acids, bases, amines, carboxylates, alcohols, etc. Polyesters with these different functionalities were synthesized to test their influence on the CaP growth.

The electrospinning method was chosen to create a homogenous polyester scaffold with a required huge surface area.

The second project was performed to develop a coating for implant materials (nitinol and titanium): chitosan and heparin. Coatings are necessary for implants as they prevent infections or induce incorporation into the human tissue. The challenging improvement of this project is that these coatings do not need a time consuming and therefore expensive pretreatment. The polyelectrolytes heparin and chitosan can be coated onto the implant materials without etching or precoating. The method of coating is the layer-by-layer technique.

1.2 References

(1) *Calcium Phosphates in Biological and Industrial Systems*; Kluwer Academic Publishers: Norwell-Dordrecht, 1998.

(2) Cazalbou, S.; Combes, C.; Eichert, D.; Rey, C. *J. Mater. Chem.* **2004**, *14*, 2148.

(3) Bigi, A.; Boanini, E.; Borghi, M.; Cojazzi, G.; Panzavolta, S.; Roveri, N. *J. Inorg. Biochem.* **1999**, *75*, 145.

(4) Bertoni, E.; Bigi, A.; Falini, G.; Panzavolta, S.; Roveri, N. *J. Mater. Chem.* **1999**, *9*, 779.

(5) Bigi, A.; Boanini, E.; Falini, G.; Panzavolta, S.; Roveri, N. *J. Inorg. Biochem.* **2000**, *78*, 227.

(6) Bigi, A.; Boanini, E.; Cojazzi, G.; Falini, G.; Panzavolta, S. *Crystal Growth & Design* **2001**, *1*, 239.

(7) Bigi, A.; Boanini, E.; Gazzano, M.; Kojdecki, M. A.; Rubini, K. *J. Mater. Chem.* **2004**, *14*, 174.

(8) Peytcheva, A.; Cölfen, H.; Schnablegger, H.; Antonietti, M. *Coll. Polym. Sci.* **2002**, *280*, 218.

(9) Fowler, C. E.; Li, M.; Mann, S.; Margolis, H. C. *J. Mater. Chem.* **2005**, *15*, 3317.

(10) Furedi-Milhofer, H.; Sarig, S. *Prog. Cryst. Growth Charact.* **1996**, *32*, 45.

(11) Furedi-Milhofer, H.; Moradian-Oldak, J.; Weiner, S.; Veis, A.; Mintz, K. P.; Addadi, L. *Conn. Tissue Res.* **1994**, *30*, 551.

(12) Hunter, G.; Kyle, C. L.; Goldberg, H. A. *Biochem. J.* **1994**, *300*, 723.

(13) Pampena, D. A.; Robertson, K. A.; Litinova, O.; Lajoie, G.; Goldberg, H. A.; Hunter, G. K. *Biochem. J.* **2004**, *378*, 1083.

(14) Fujisawa, R.; Wada, R.; Nodasaka, Y.; Kuboki, Y. *Biochim. Biophys. Acta* **1996**, *1291*, 53.

(15) Tsortos, A.; Nancollas, G. H. *J. Colloid Interface Sci.* **2002**, *250*, 159.

(16) Burke, E. M.; Guo, Y.; Colon, L.; Rhima, M.; Veis, A.; Nancollas, G. H. *Coll. Surf. B* **2000**, *17*, 49.

(17) Hunter, G. K.; Goldberg, H. A. *Proc. Natl. Acad. Sci. USA* **1993**, *90*, 8562.

(18) Huq, N. L.; Cross, K. J.; Reynolds, E. C. *J. Mol. Model.* **2000**, *6*, 35.

(19) Bigi, A.; Boanini, E.; Gazzano, M.; Rubini, K.; Torricelli, P. *Biomed. Mater. Eng.* **2004**, *14*, 573.

(20) Boanini, E.; Fini, M.; Gazzano, M.; Bigi, A. *Eur. J. Inorg. Chem.* **2006**, 4821.

(21) Boanini, E.; Torricelli, P.; Gazzano, M.; Giardino, R.; Bigi, A. *Biomaterials* **2006**, *27*, 4428.

(22) Wong, A. T.-C.; Czernuszka, J. T. *Coll. Surf. A* **1993**, *78*, 245.

(23) Wong, A. T.-C.; Czernuszka, J. T. *Coll. Surf. A* **1995**, *103*, 23.

(24) Wong, A. T.-C.; Czernuszka, J. T. *Mat. Res. Soc. Symp. Proc.* **1992**, *252*, 49.

(25) Onuma, K. *J. Phys. Chem B* **2005**, *109*, 8257.

(26) Greish, Y. E.; Bender, J. D.; Lakshmi, S.; Brown, P. W.; Allcock, H. R.; Laurencin, C. T. *J. Biomed. Mater. Res. A* **2006**, *76A*, 206.

(27) Prelot, B.; Zemb, T. *Mater. Sci. Eng. C, Biomimetic and Supramolecular Systems* **2005**, *25*, 553.

(28) Shkilnyy, A.; Friedrich, A.; Tiersch, B.; Schoene, S.; Fechner, M.; Koetz, J.; Schlaepfer, C.-W.; Taubert, A. *Langmuir* **2008**, *24*, 2102-2109.

(29) Skilnyy, A.; Thiersch, B.; Friedrich, A.; Koetz, J.; Schläpfer, C.-W.; Taubert, A. *J. Mater. Chem.*, submitted.

(30) Kalya, S.; Rosenthal, A. K. *Curr. Opin. Rheumatology* **2005**, *17*, 325.

(31) Landis, W. J. *Phosphorus, Sulfur and Silicon and the Related Elements* **1999**, 185.

(32) Landis, W. J.; Silver, F. H.; Freeman, J. W. *J. Mater. Chem.* **2006**, *16*, 1495.

(33) Schwarz, K.; Epple, M. *Chem. Eur. J.* **1998**, *4*, 1898.

(34) Ritzoulis, C.; Scoutaris, N.; Papademetriou, K.; Stavroulias, S.; Panayiotou, C. *Food Hydrocolloids* **2005**, *19*, 575.

(35) Hartgerink, J. D.; Beniash, E.; Stupp, S. I. *Science* **2001**, *294*, 1684.

(36) Song, J.; Saiz, E.; Bertozzi, C. R. *J. Am. Chem. Soc.* **2003**, *125*, 1236.

(37) Song, J.; Saiz, E.; Bertozzi, C. R. *J. Eur. Ceram. Soc.* **2003**, *23*, 2905.

(38) Song, J.; Malathong, V.; Bertozzi, C. R. *J. Am. Chem. Soc.* **2005**, *127*, 3366.

(39) Paramonov, S. E.; Gauba, V.; Hartgerink, J. D. *Macromolecules* **2005**, *38*, 7555.

(40) Niece, K. L.; Hartgerink, J. D.; Donners, J. J. J. M.; Stupp, S. I. *J. Am. Chem. Soc.* **2003**, *125*, 7146.

(41) Kamasaka, H.; Uchida, M.; Kusaka, K.; Yoshikawa, K.; Yamamoto, K.; Okada, S.; Ichikawa, T. *Biosci. Biotechnol. Biochem.* **1995**, *59*, 1412.

(42) Makinen, K. K.; Söderling, E. *Calcif. Tissue Int.* **1984**, *36*, 64.

(43) Boeve, E. R.; Cao, L. C.; Deng, G.; De Bruijn, W. C.; Schroder, F. H. *J. Urol.* **1996**, *155*, 368.

(44) Makinen, K. K.; Soderling, E.; Peacor, D. R.; Makinen, P. L.; Park, L. *Calcif. Tissue Int.* **1989**, *44*, 258.

(45) Granja, P. L.; Barbosa, M. A.; Pouysegu, L.; de Jeso, B.; Rouais, F.; Baquey, C. *J. Mater. Sci.* **2001**, *36*, 2163.

(46) Graff, A.; Winterhalter, M.; Meier, W. *Langmuir* **2001**, *17*, 919.

(47) Granja, P. L.; de Jeso, B.; Bareille, R.; Rouais, F.; Baquey, C.; Barbosa, M. A. *Eur. Cells Mater.* **2005**, *10*, 31.

(48) Decher, G. *Science* **1997**, *277*, 1232.

(49) Ngankam, P. A.; Lavalle, P.; Voegel, J. C.; Szyk, L.; Decher, G.; Schaaf, P.; Cuisinier, F. J. G. *J. Am. Chem. Soc.* **2000**, *122*, 8998.

(50) Ball, V.; Michel, M.; Boulmedais, F.; Hemmerle, J.; Haikel, Y.; Schaaf, P.; Voegel, J. C. *Crystal Growth & Design* **2006**, *6*, 327.

(51) Spoerke, E. D.; Stupp, S. I. *Biomaterials* **2005**, *26*, 5120.

(52) Walsh, D.; Boanini, E.; Tanaka, J.; Mann, S. *J. Mater. Chem.* **2005**, *15*, 1043.

(53) Busch, S.; Dolhaine, H.; DuChesne, A.; Heinz, S.; Hochrein, O.; Laeri, F.; Podebrad, O.; Vietze, U.; Weiland, T.; Kniep, R. *Eur. J. Inorg. Chem.* **1999**, *10*, 1643.

(54) Busch, S.; Schwarz, U.; Kniep, R. *Chem. Mater.* **2001**, *13*, 3260.

(55) Busch, S.; Schwarz, U.; Kniep, R. *Adv. Funct. Mater.* **2003**, *13*, 189.

(56) Gobel, K.; Simon, P.; Buder, J.; Tlatlik, H.; Kniep, R. *J. Mater. Chem.* **2004**, *14*.

(57) Kniep, R.; Busch, S. *Angew. Chem. Int. Ed. Engl.* **1996**, *35*, 2624.

(58) Iijima, M.; Iijima, K.; Moriwaki, Y.; Kuboki, Y. *J. Cryst. Growth* **1994**, *140*, 91.

(59) Iijima, M.; Moradian-Oldak, J. *J. Mater. Chem.* **2004**, *14*, 2189.

(60) Iijima, M.; Moriwaki, Y. *J. Cryst. Growth* **1989**, *96*, 59.

(61) Iijima, M.; Moriwaki, Y. *Calcif. Tissue Int.* **1990**, *47*, 237.

(62) Iijima, M.; Moriwaki, Y. *J. Cryst. Growth* **1991**, *112*, 571.

(63) Iijima, M.; Moriwaki, Y. *J. Cryst. Growth* **1998**, *194*, 125.

(64) Iijima, M.; Moriwaki, Y.; Kuboki, Y. *Curr. Topics Cryst. Growth Res.* **1995**, *2*, 1.

(65) Iijima, M.; Moriwaki, Y.; Kuboki, Y. *Connective Tissue Res.* **1997**, *36*, 51.

(66) Iijima, M.; Moriwaki, Y.; Kuboki, Y. *Connective Tissue Res.* **1998**, *38*, 171.

(67) Iijima, M.; Moriwaki, Y.; Yamaguchi, R.; Kuboki, Y. *Connective Tissue Res.* **1997**, *36*, 73.

(68) Iijima, M.; Takita, H.; Moriwaki, Y.; Kuboki, Y. *Comparative Biochemistry and Physiology, Part A: Molecular & Integrative Physiology* **1991**, *98A*, 379.

(69) Simon, P.; Carrillo-Cabrera, W.; Formanek, P.; Gobel, C.; Geiger, D.; Ramlau, R.; Tlatlik, H.; Buder, J.; Kniep, R. *J. Mater. Chem.* **2004**, *14*, 2218.

(70) Simon, P.; Schwarz, U.; Kniep, R. *J. Mater. Chem.* **2005**, *15*, 4992.

(71) Tlatlik, H.; Simon, P.; Kawska, A.; Zahn, D.; Kniep, R. *Angew. Chem. Int. Ed.* **2006**, *45*, 1905.

(72) Iwatsubo, T.; Sumaru, K.; Kanamori, T.; Shinbo, T.; Yamaguchi, T. *Biomacromolecules* **2006**, *7*, 95.

(73) Laurencin, C. T.; Khan, Y. In *Scaffolding in Tissue Engineering*; Ma, P. X., Ellisseeff, J., Eds.; CRC Taylor & Francis Group: Boca Raton-New York-Abingdon, 2006, p 253.

(74) Wei, G.; Ma, P. X. In *Scaffolding In Tissue Engineering*; Ma, P. X., Ellisseeff, J., Eds.; CRC Taylor & Francis Group: Boca Raton-New York-Abingdon, 2006, p 241.

(75) Doyle, C.; Tanner, E. T.; Bonfield, W. *Biomaterials* **1991**, *12*, 841-7.

(76) Linhart, W.; Lehmann, W.; Siedler, M.; Peters, F.; Schilling, A. F.; Schwarz, K.; Amling, M.; Rueger, J. M.; Epple, M. *Journal of Materials Science* **2006**, *41*, 4806-4813.

(77) Chen, L. J.; Wang, M. *Biomaterials* **2002**, *23*, 2631-2639.

(78) Doyle, C.; Tanner, E. T.; Bonfield, W. *Biomaterials FIELD Full Journal Title:Biomaterials* **1991**, *12*, 841-7.

(79) Yeo, A.; Rai, B.; Sju, E.; Cheong, J. J.; Teoh, S. H. *J. Biomed. Mater. Res., Part A* **2007**, *84A*, 208-218.

(80) Yefang, Z.; Hutmacher, D. W.; Varawan, S. L.; Meng, L. T. *Int J Oral Maxillofac Surg* **2007**, *36*, 137-45.

(81) Kim, H.-W.; Knowles, J. C.; Kim, H.-E. *Journal of Materials Science: Materials in Medicine* **2005**, *16*, 189-195.

(82) Degirmenbasi, N.; Kalyon, D. M.; Birinci, E. *Colloids and Surfaces, B: Biointerfaces* **2006**, *48*, 42-49.

(83) Wutticharoenmongkol, P.; Sanchavanakit, N.; Pavasant, P.; Supaphol, P. *Macromolecular Bioscience* **2006**, *6*, 70-77.

(84) Wutticharoenmongkol, P.; Sanchavanakit, N.; Pavasant, P.; Supaphol, P. *Journal of Nanoscience and Nanotechnology* **2006**, *6*, 514-522.

(85) Porter, J. R.; Henson, A.; Popat, K. C. *Biomaterials* **2009**, *30*, 780-788.

(86) Oliveira, A. L.; Costa, S. A.; Sousa, R. A.; Reis, R. L. *Acta Biomaterialia* **2009**, *5*, 1626-1638.

(87) Erisken, C.; Kalyon, D. M.; Wang, H. *Biomaterials* **2008**, *29*, 4065-4073.

(88) Ito, Y.; Hasuda, H.; Kamitakahara, M.; Ohtsuki, C.; Tanihara, M.; Kang, I.-K.; Kwon, O. H. *Journal of Bioscience and Bioengineering* **2005**, *100*, 43-49.

(89) Yang, F.; Wolke, J. G. C.; Jansen, J. A. *Chemical Engineering Journal (Amsterdam, Netherlands)* **2008**, *137*, 154-161.

(90) Kwon, O. H.; Lee, I. S.; Ko, Y.-G.; Meng, W.; Jung, K.-H.; Kang, I.-K.; Ito, Y. *Biomedical Materials (Bristol, United Kingdom)* **2007**, *2*, S52-S58.

(91) Song, J.; Saiz, E.; Bertozzi, C. R. *Journal of the European Ceramic Society* **2003**, *23*, 2905-2919.

(92) Song, J.; Saiz, E.; Bertozzi, C. R. *Journal of the American Chemical Society* **2003**, *125*, 1236-1243.

(93) Holland, S. J.; Tighe, B. J.; Gould, P. L. *Journal of Controlled Release* **1986**, *4*, 155-180.

(94) Kemnitzer, J. E.; McCarthy, S. P.; Gross, R. A. *Macromolecules* **1992**, *25*, 5927-5934.

(95) Charles , E. H.; Christopher , N. B. *Angewandte Chemie International Edition*, *49*, 1540-1573.

(96) ten Brummelhuis, N.; Diehl, C.; Schlaad, H. *Macromolecules (Washington, DC, United States)* **2008**, *41*, 9946-9947.

2 Methods and general background

2.1 Scanning Electron Microscopy (SEM)[1]

Scanning electron microscopy provides images of a surface or a small object. Scanning electron microscopy is characterized by a huge magnification range (from 10-fold to about 200'000-fold) and a high depth of focus. By scanning the sample with an electron beam, different signals are generated. These can be registered by different detectors. After conversion in an electric signal, an image of the surface or object is generated. Because the electron beam interacts in many ways with the sample, not only surfaces and their topography can be displayed but also material contrast and chemical composition. Chemical characterization can be achieved by X-ray spectroscopy.

The electron beam can be generated in a variety of ways. Mostly, electrons are released from a source by electrical heating. Tungsten filaments and lanthanum hexaboride cathodes are heated up and electrons are released from the metal surfaces. The released electrons only survive in high vacuum. A vacuum of about 10^{-6} mbar is therefore needed for the electrons to pass through the column to the sample. In the column, the electrons are bundled to a narrow beam. The objective lens is responsible scanning this beam across the sample with a defined speed and order. As the electron beam hits every point of the sample *sequentially*, all signals can be correlated with a location on the sample, including chemical information and an impression of the topography. The magnification can be adjusted by variation of the scanned area: the smaller the area, the higher the magnification.

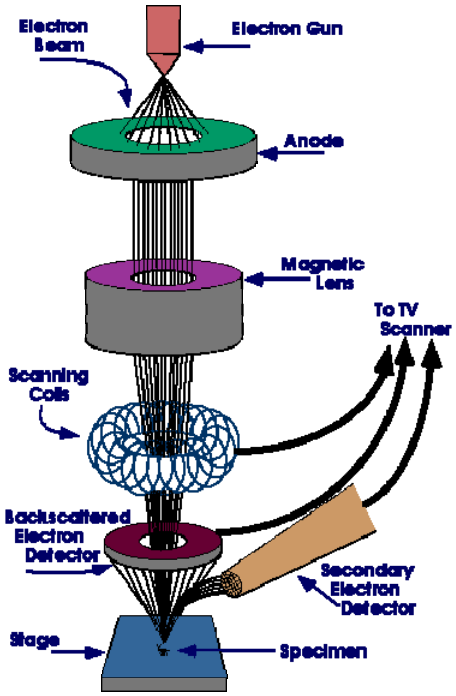

Figure 2.1: Principle of an SEM. A beam of electrons is produced at the top of the microscope by an electron gun. The electron beam follows a vertical path through the microscope, which is held within a vacuum. The beam travels through electromagnetic fields and lenses, which focus the beam down toward the sample. Once the beam hits the sample, electrons and X-rays are emitted from the sample, which are used for image generation.[2]

The electrons of the scanning beam (= primary electrons) penetrate into the sample and interact with the sample atoms, for example by knocking out electrons. These knocked-out electrons (= secondary electrons) are low-energy. Most frequently, atoms at the surface are ionized. Alternatively, primary electrons may scatter on an atom nucleus (analogous to Rutherford scattering). These backscattered electrons have more energy. In addition, inner electrons of the atomic shell can be ejected. The incident beam may excite an electron in an inner shell, ejecting it from the shell while creating an electron hole where the electron was. An electron from an outer, higher-energy shell then fills the hole, and the difference in energy between the higher-energy shell and the lower energy shell is released in the form of X-ray. The number and energy of the X-rays emitted from a sample is measured by an energy dispersive spectrometer (EDS). As the energy of the X-rays is characteristic for the difference in energy between the two shells, this allows the elemental composition of the specimen to be detected.

Figure 2.2 shows all the different electrons described above (any many more). They can individually be detected by dedicated detectors such as backscattered (BSE), secondary

(SE), X-ray (EDS), Auger, cathodoluminescence, electron beam induced current (EBIC), and other detectors. This enables the separate investigation of different aspects such as morphology-chemical composition correlation by combining the signals from the SE (or BSE) detector with the signals from the EDS detector.

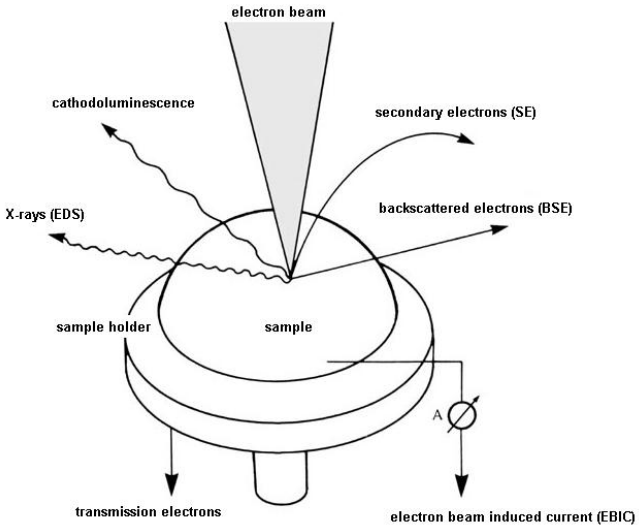

Figure 2.2: Schematic illustration of the different induced signals in SEM.

Because the SEM utilizes vacuum conditions and high energy electrons to form an image, special sample preparations are necessary. All water must be removed from the samples because the water would vaporize in the vacuum and lead to a deterioration of the image. As the sample is penetrated by charged particles (electrons), the sample must also be conductive. If an insulating sample is to be imaged, a conductive coating must be applied before introducing it into the microscope. Conductive coatings are prepared by carbon evaporation or sputter coating a metallic film of a few nanometers in thickness on the sample.

The sputter coater uses an electric field, argon gas, and metallic target of the desired metal coating. The sample is placed in a small, evacuated chamber. Argon ions are then produced by applying a high voltage to the gas. The argon cations are attracted to the negatively charged metal target and knock out metal ions (gold, platinum, silver, etc.) from the target. These metal atoms are then deposited on the samples and form a uniform and a few nm thin, conductive metal film on the sample. Standard targets are gold, platinum and platinum/gold alloys are used for higher magnification and very small features, as it forms a smooth surface and does not aggregate to islands. Carbon coatings are mostly used for analytical measurements such as EDS, where a strong metal line from the coating disturbs the measurement.

2.2 Contact angle measurement[3]

Contact angle analysis measures the wettability of a surface by determination of the surface tension of a liquid droplet at its interface with a homogenous surface (see figure 2.3). The contact angle is the angle of the liquid at the interface relative to the plane of the (model) surface. A drop of water producing a large contact angle indicates a hydrophobic surface. As a result, the surface is poorly wetted and the solid surface free energy is low. A drop of water producing a small contact angle on a surface indicates a hydrophilic surface. This condition reflects good wetting, good adhesiveness, and higher surface energy. Wetting and surface energies can be quantified by the Young equation, see figure 2.3. Young's equation also enables a general classification of surfaces, see Table 2.1.

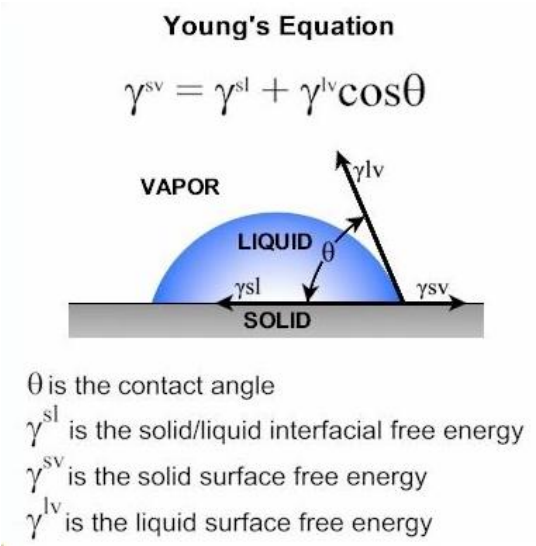

Figure 2.3: A water droplet on a solid surface. The angle formed between the solid/liquid interface and the liquid/vapor interface is referred to as a the contact angle θ.[4]

Table 2.1: Classification of surfaces according to contact angles and wettabilities.

	Contact angle	Wettability
$\gamma^{sv} = \gamma^{lv}$, $\gamma^{sl} = 0$	$\theta = 0$, $\cos\theta = 1$	Complete wetting
$\gamma^{sv} \neq \gamma^{lv} \neq \gamma^{sl}$	$0 < \theta < 90°$, $1 > \cos\theta > 0$	Partial wetting
$\gamma^{sv} = \gamma^{sl}$	$\theta > 90$, $\cos\theta = 0$	No wetting

Materials like Teflon (polytetrafluorethylene, PTFE) have apolar surfaces which are not well wetted by water. The hydrophobicity further increases with increasing surface

roughness, leading to surfaces on which drops of water assume a nearly spherical shape. These surfaces are called super-hydrophobic. Water easily runs off such surfaces carrying with it surface contaminants, which are only weakly adsorbed to such surfaces, also known as the “lotus effect”.

In general, contact angle measurements provide a useful initial estimation of the physical properties of a surface. However, contact angle measurements need to be analyzed with care as a number of factors including operator error, surface roughness, surface heterogeneity, contaminated fluids, and sample geometry can influence the overall result. Nevertheless, contact angle measurement is one of the most sensitive and inexpensive surface analysis techniques.

2.3 Nitinol

Nitinol (an acronym for Nickel Titanium Naval Ordnance Laboratory) is a shape memory alloy made of nickel and titanium. Nitinol shows a unique phase transition in the crystal structure, see figure 2.4. Above its transformation temperature, Nitinol is superelastic. If a mechanical stress is induced, the alloy immediately returns to its pre-stressed position after removing this stress. The reason for the superelasticity is the stress induced phase transformation from the high temperature phase Austenite into the low temperature phase Martensite. The strain related to this phase transformation is fully reversible after removing the stress. Below its transformation temperature, Nitinol displays the shape memory effect. After deformation of the alloy in its low temperature phase Martensite, the shape will remain until the material is heated above the transformation temperature for the Austenite phase. Then it changes back to its pre-deformed, original shape.

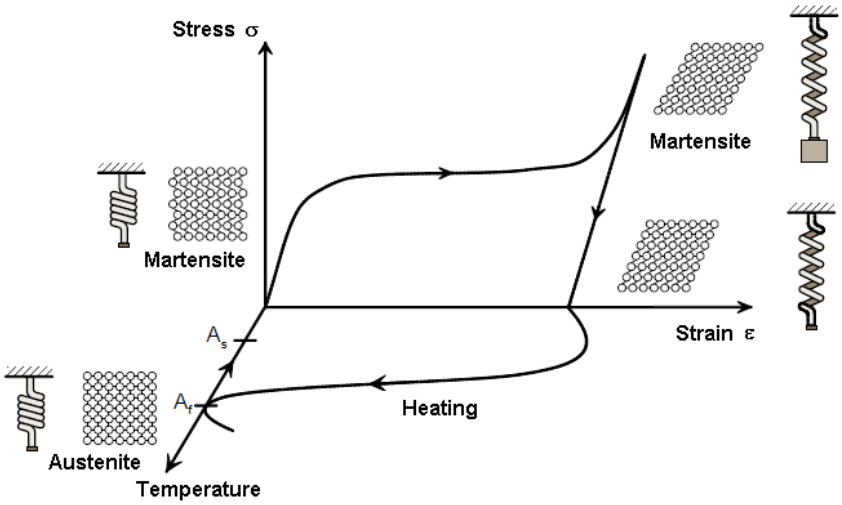

Figure 2.4: The martensite-austenite transformation. The crystal structure and the mechanical properties of the metal are altered as a result of the temperature change. A_S= austenite start temperature, A_f= austenite finish temperature.[5]

Nitinol is typically composed of a nearly equal mixture of nickel (50-55.6 wt. %) and titanium. Making small changes in this composition can change the transition temperature of the alloy. For this reason, Nitinol may or may not be superelastic at room temperature. These unique properties of Nitinol in a wide range of temperatures make it suitable for many applications, particularly in medicine. The medical industry ask for minimally invasive surgical and diagnostic procedures where Nitinol is the enabling component in an increasing number of devices such as endoscopic instruments, stents, filters, and orthopedic devices.[6]

2.4 Layer-by-Layer technique[7]

The Layer-by-Layer (LbL) technique enables the creation of nanometer-scale multilayered films or coatings on arbitrarily shaped objects. The LbL technology uses the electrostatic attraction of charged polymers (= polyelectrolytes) to surfaces. A positively charged surface adsorbs polyanions from the solution until the surface is recharged, the surface is then negatively charged. Hence, the amount of deposited polymer is self-regulated and results in reproducible layers with a thickness in the nanometer (1-5 nm) range. Repeating the deposition step with a polycation results in a positively charged surface on which another polyanion can adsorb from solution. This method, developed by Decher and co-workers about

15 years ago, therefore allows the buildup of polyelectrolyte multilayer films on almost any kind of surface, and with a large choice of polyelectrolytes.[7] The initial material can be metal, plastic, ceramic, natural materials, etc. and the LbL assembled material can consist of polymers, nanoparticles, proteins, or other substances.[8,9]

Multilayers formed by alternating adsorption of anionic and cationic polyelectrolytes are an excellent and original way for the synthesis of ultrathin functional films. The ease of their formation and the possibility to include specific molecules, proteins, or particles into the layers offer almost infinite possibilities for tuning the film architecture and properties.[8,10-12] Water, rather than toxic or hazardous solvents can be used, and practically any water-soluble or dispersible building blocks that have either charges or hydrogen-bonding capability can be considered and built into the resulting films.

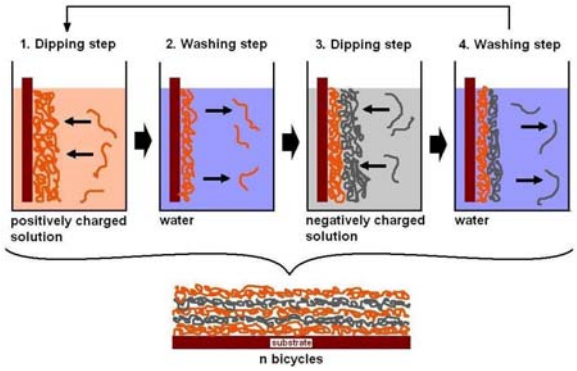

Figure 2.5: Principle of LbL. Alternating and consecutive adsorption of polycations (orange) and polyanions (gray) on a negatively charged surface.[7] Other building blocks like proteins, charged particles, etc. can also be used.

2.5 Electrospinning[13]

The process of spinning fibers within an electrostatic field is known as electrospinning. High voltage is used to create an electrically charged jet of polymer solution which dries in flight to leave a polymer fiber on a collector, Figure 2.6. The electrospinning setup consists of a pipette or syringe to hold the polymer solution, two electrode, and a high voltage supply (10 kV and higher). One electrode is attached to the needle, the other one is connected to the collector.

During spinning, the syringe pump forces a constant flow of the polymer solution through the syringe needle. When a sufficiently high voltage is applied between the two electrodes, the liquid becomes charged. Electrostatic repulsion counteracts the surface tension of the solution and at a critical voltage, a jet of liquid ejects from the surface. This point of eruption is known as the Taylor cone, figure 2.6. After the cone formation, a charged liquid jet is formed. The jet is then elongated by chaotic motion caused by electrostatic repulsion, becoming thinner with every loop. As the jet penetrates the atmosphere, the solvent evaporates in flight due to the large surface area of the jet. The polymer fibers are then deposited in the form of a web ("non-woven") on the grounded collecting device.

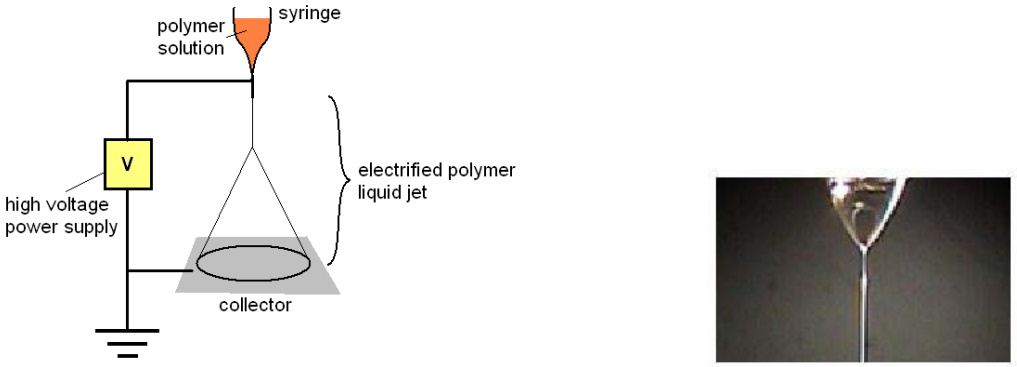

Figure 2.6: Left: principle of electrospinning,[14] right: Taylor cone.[15]

The collector can be made of any shape according to the requirements, like flat plate, rotating drum, etc. By varying the setups, electrospinning can produce different nanofibrous structures with two- or three-dimensional shapes, including aligned nanofibers, tubular structures, and core-shell nanofibers.[16-18] The simplicity, flexibility, and versatility make electrospinning one of the most popular technique for micro- and nanofibrous fabrication today.

2.6 References

(1) http://pages.unibas.ch/zmb/rem.html.

(2) www.purdue.edu/REM/rs/graphics/sem2.gif.

(3) Palzer, S.; Hiebl, C.; Sommer, K.; Lechner, H. *Chemie Ingenieur Technik* **2001**, *73*, 1032-1038.

(4) Zisman W, A. In *Contact Angle, Wettability, and Adhesion*; AMERICAN CHEMICAL SOCIETY: WASHINGTON, D.C., 2009, p 1.

(5) Kaack, M. **2002**.

(6) Pelton, A. R.; Stöckel, D.; Duerig, T. W. *Materials Science Forum* **2000**, *327-328*, 63-70.

(7) Decher, G. *Science (Washington, D. C.)* **1997**, *277*, 1232-1237.

(8) Lvov, Y.; Decher, G.; Sukhorukov, G. *Macromolecules* **1993**, *26*, 5396-9.

(9) Ariga, K.; Hill, J. P.; Ji, Q. *Physical Chemistry Chemical Physics* **2007**, *9*, 2319-2340.

(10) Lvov, Y.; Ariga, K.; Ichinose, I.; Kunitake, T. *J. Am. Chem. Soc.* **1995**, *117*, 6117-23.

(11) Caruso, F.; Lichtenfeld, H.; Giersig, M.; Moehwald, H. *J. Am. Chem. Soc.* **1998**, *120*, 8523-8524.

(12) Michel, M.; Arntz, Y.; Fleith, G.; Toquant, J.; Haikel, Y.; Voegel, J.-C.; Schaaf, P.; Ball, V. *Langmuir* **2006**, *22*, 2358-2364.

(13) Thandavamoorthy, S.; Bhat, G. S.; Tock, R. W.; Parameswaran, S.; Ramkumar, S. S. *Journal of Applied Polymer Science* **2005**, *96*, 557-569.

(14) *An introduction to electrospinning and nanofibers*; Ramakrishna, S.; Fujihara, K.; Teo, W.-E.; Lim, T.-C.; Ma, Z., Eds.; World Scientific, 2005.

(15) http://web.mit.edu/aeroastro/labs/spl/images/colloid_2.jpg.

(16) Yang, F.; Murugan, R.; Wang, S.; Ramakrishna, S. *Biomaterials* **2005**, *26*, 2603-2610.

(17) Bognitzki, M.; Czado, W.; Frese, T.; Schaper, A.; Hellwig, M.; Steinhart, M.; Greiner, A.; Wendroff, J. H. *Advanced Materials (Weinheim, Germany)* **2001**, *13*, 70-72.

(18) Dersch, R.; Liu, T.; Schaper, A. K.; Greiner, A.; Wendorff, J. H. *Journal of Polymer Science, Part A: Polymer Chemistry* **2003**, *41*, 545-553.

3 Electrospinning of polyesters for bone tissue engineering

3.1 Introduction

Tissue engineering is an interdisciplinary technology combining materials engineering, cell biology, and genetic engineering to bring about artificial tissues or organs, such as skin, cartilage for joints, heart valves, bone, etc. Scaffold materials are key components in the development of tissue-engineered bone constructs for critical bone defects. Ideally, a scaffold should have the following characteristics for successful implantation and further function[1]:

- Biocompatible, biodegradable, and bioresorbable
- mechanical properties similar to those of the target tissue *in vivo*
- three dimensional
- suitable chemical and biochemical functionality

Electrospun composites combine a high chemical and structural flexibility unique large surface area to volume ratio, facile manipulation, and the ability to provide an appropriate vehicle to direct stem cells into specific lineages.[2,3] One of the main goals of using electrospun fiber mats in medical technology is to induce seeded cells to produce extracellular matrix (ECM) and regenerate the native tissue structure. Scaffolds made of bioresorbable polymeric fibers mimic the typical ECM architecture allowing the growth of cells within the scaffold and the replacement of the scaffold itself. Cells attach and organize around fibers with diameters smaller than the diameter of cells.[4]

Of particular interest to the current study is the modification of electrospun materials for bone tissue engineering by tailoring the physical properties of the scaffold. One critical factor governing ECM production and subsequent mineralization is the availability of phosphate and calcium within the given matrix. Past research has revolved around composite scaffolds, where a mineral component is incorporated into the matrix material. The important features of CaP particles are their chemical composition, overall size features, and degradation time. Past studies have shown beneficial effects caused by the addition of calcium phosphate to electrospun materials such as very low cytotocicity, increased cell proliferation,

and increased mineralization.[3,5,6] Fabrication of such scaffolds can be successfully achieved either by dispersing inorganic crystals into the polymer solution before electrospinning or by adsorbing inorganic crystals on the surface of the scaffold after electrospinning.

There are a number of issues, including pore size and morphology, porosity, mechanical properties, surface properties, and biodegradability, which must be considered in scaffold design. Of these, pore size and porosity are the critical features that affect cell attachment, proliferation, and migration. Higher cell viability, cell migration and infiltration inside the scaffold are typically achieved for fibrous mats with higher porosity.[7] Moreover, the degradation rate should match the rate of tissue regeneration, whereas scaffold should provide enough mechanical support during degradation.[8]

Commonly used biodegradable polymers include synthetic and natural polymers. Degradable polyesters are among the most widely used synthetic materials for electrospun tissue-engineering scaffolds because they are biodegradable and their degradation products can easily be metabolized. Examples of polyesters include poly(lactic acid) (PLA), poly(glycolic acid) (PGA), poly(caprolactone) (PCL), poly(3-hydroxybutyrate-co-3-hydroxyvalerate) (PHB-HV), and their copolymers. For bone tissue mimics, long degradation times are needed, which is why semicrystalline polymers with high degrees of polymerization such as PCL, PLA, PHBV, and their copolymers are often used. Degradation times can be controlled by varying the monomer ratios in a copolymer (which, depending on the monomer type, affects the crystallinity) and by thickness of electrospun fibers.[8]

Nanofibrous PLA has been used as scaffold for nerve regeneration, bone tissue engineering, vascular engineering, and stem cell tissue engineering.[9-11] The ease of fabrication and low cost make PCL an attractive polymer for the fabrication of electrospun nanofibers. Besides, the electrospinning process re-organizes the PCL chains and the electrospun nanofibers have thus a higher crystallinity than unprocessed PCL.[12] Similar to PLA, electrospun PCL has been used in skin tissue engineering, bone regeneration, and heart tissue engineering.[13-15] Finally, a number of studies have investigated tissue engineering with electrospun poly(3-hydroxybutyrate) (PHB); to reduce its brittleness PHB is often copolymerized with 3-hydroxyvalerate in various ratios, forming PHB-HV. For example, Ito et al.[16] fabricated hydroxyapatite (HA)/PHB-HV nanofiber composite by soaking the electrospun nanofibrous membrane in simulated body fluid (SBF). HA deposition greatly increased the hydrophilicity of the scaffold and the number of attached cells on the electrospun membrane was compared to a cast film, although combination with HA did not significantly affect cell adhesion.

Other approaches forcing hydrophilicity are needed to improve cytocompatibility. Surface modification has long been recognized as a potential tool for enhancing the biocompatibility of the surface of a material. Researchers have focused on immobilizing biomolecules, such as collagen, gelatin, chitosan and peptides, onto the surfaces of polymeric scaffolds to improve their hydrophilicity and hence the cytotoxicity of the surface of the electrospun fibrous scaffolds.[17]

3.2 Results

3.2.1 The electrospinning apparatus

The principle of an electrospinning device was already shown in figure 2.6 (left) in chapter 2.5. Figure 3.1 shows the homebuilt electrospinning setup used in the current study. The syringe pump (a) controls the flow of the polymer solution in the reservoir syringe. Initial experiments with gravitation as driving force for solution flow also worked, but the velocity is strongly affected by the viscosity of the solution and therefore, gravitation is not applicable to all polymer solutions. From the syringe, the solution is pumped through a Teflon tube (b) to the needle or capillary (c). Between the needle and a metallic, grounded, collector, a high voltage is applied. The voltage is generated by a power supply (d) which, in our case, produces voltages from zero to 30 kV with almost no current. A flat collector (e) was sufficient, thought a rotating drum would be preferable to get larger scaffolds. To collect the scaffolds, aluminum foil (f) was deposited onto the conducting and grounded collector (e). With this approach even unsuccessful experiments such as bead spreading or dropping could be cleaned up just by removing the foil. Successful samples can be collected rapidly by exchanging the aluminum foil for a fresh one.

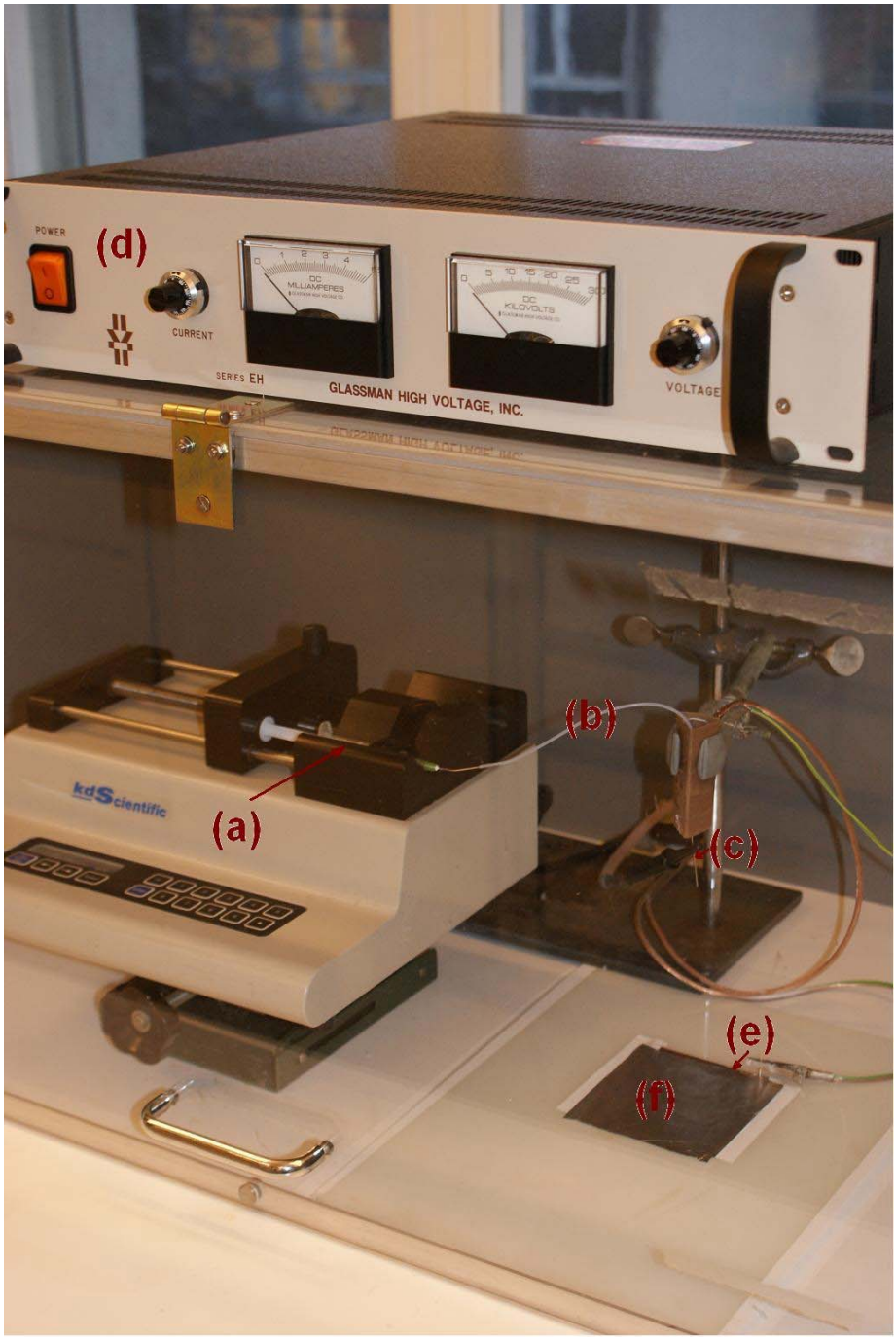

Figure 3.1: Homemade electrospinning setup with (a) syringe pump with syringe, (b) Teflon tube, (c) needle/capillary connected to high voltage, (d) high voltage supply, (e) grounded collector, and (f) aluminum foil.

3.2.2 Process parameters and fiber morphology

The principle (see also chapter 2.5) of electrospinning and many publications[18-21] suggest that the following parameters affect the outcome of an electrospinning experiment:

System parameters:

- polymer chemistry (molecular weight, molecular weight distribution, architecture (branched, linear, …), chemical composition, …)
- solution properties (viscosity, conductivity, surface tension, …)
- ambient parameters (temperature, humidity)

Process Parameters:

- electric potential between capillary and collector
- flow rate of the polymer solution
- concentration of the polymer solution
- distance between needle and collector

This chapter focuses on electrospinning of polyesters such as PCL, PHB, and PHB-HV, and the mineralization of the resulting fiber mats with CaP. Commercially available polyesters were used to establish the electrospining process. To investigate the effects of some key process parameters, we conducted electrospinning at different conditions. The parameters studied were needle-collector distance, applied voltage and flow rate.

3.2.2.1 Electrospinning of Poly(ε-caprolactone) (PCL)

A solution of PCL (MW= 80 kDa) in chloroform was electrospun at different voltages (15- 25 kV), flow rates (0.15- 1.5 ml/ h), and needle-collector distances (3- 13 cm). The distance between the needle and the grounded collector has a significant impact on morphology of the electrospun nanofibers. As the distance between the tip and grounded plate decreases from 10 to 3 cm, more uniform and beadless nanofibers are obtained in all PCL samples, figure 3.2. An increase from 10 to 13 cm, in contrast, provides more time for the whipping instability, which, in principle, is advantageous for a successful electrospinning process.[21]

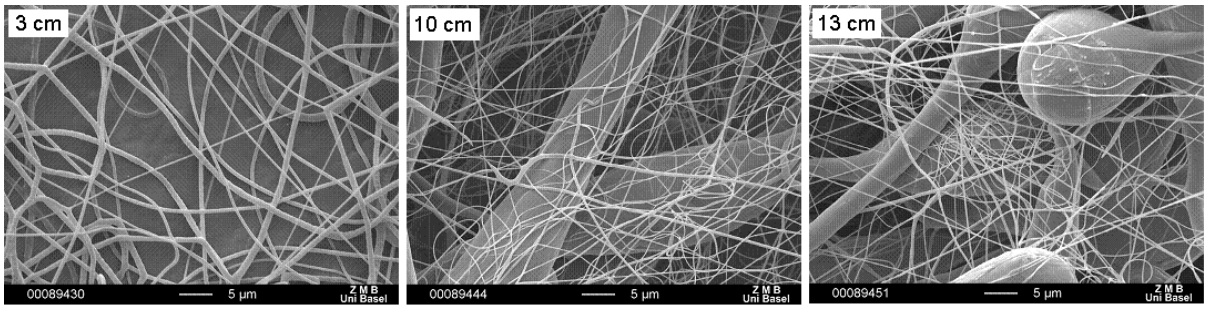

Figure 3.2: Effect of increasing needle-collector distance on 7 wt % PCL electrospun at 15 kV and 0.5 ml/ h.

In order to avoid or reduce bead formation however, higher voltages are needed. Indeed, increasing the high voltage from 15 kV (Figure 3.2) to 25 kV (Figure 3.3) shows that the fibers again become thinner and more uniform at the same needle-collector distance, the same flow rate, and the same polyester concentration.

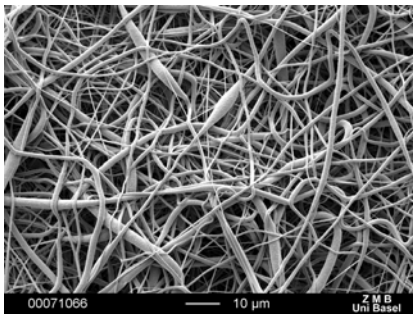

Figure 3.3: Fibers spun at 25 kV, from a 7 wt % PCL solution in dichloromethane, 12 cm needle-collector distance, and a flow rate of 0.5 ml/ h. Compare Figure 3.2 for effect of high voltage.

The effect of voltage is further confirmed by additional experiments, figure 3.4. Electrospinning was performed at several voltages from 15- 25 kV, whereas the other parameters (concentration, distance and flow rate) were kept constant. Fiber formation could be observed at 15 kV for the first time with the set parameters (that is, no fiber formation occurs below 15 kV). Increasing the voltage to 20 and 25 kV induces rather dramatic changes in the overall fiber morphology. The beads observed at 15 kV almost disappear and only occasional bulges form within the fibers. The average fiber diameter increases with increasing voltage, but becomes more uniform.

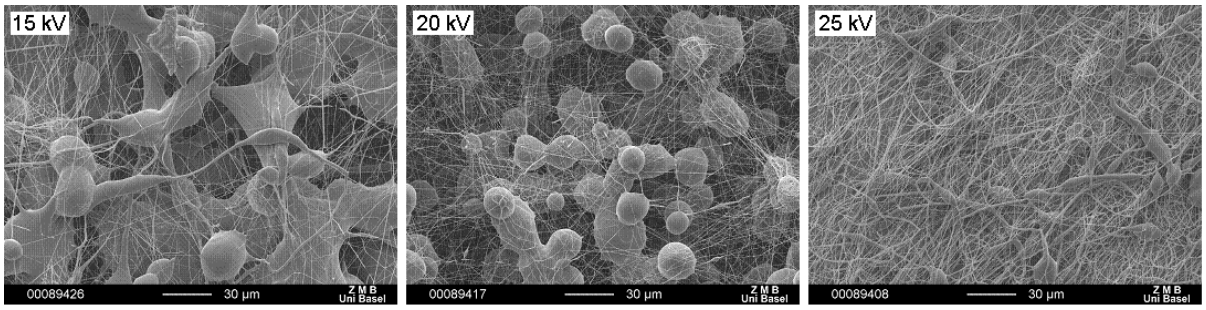

Figure 3.4: Effect of increasing electric potential on the fiber morphology of fiber mats electrospun from 7 wt % PCL electrospun at 0.5 ml/ h and 10 cm needle-collector distance.

Figure 3.5 shows the effect of different flow rates from 0.15 -1.5 ml/ h on the fiber morphology. At low flow rates (0.15 ml/ h), lots of beads form. Flow rates above 0.3 ml/ h show less beads but more bulges and thick, elongated features in the fibers. At the same time the diameter distribution of the electrospun fibers becomes broader. A slow flow rate is preferred to observe small diameter distribution, but it has to be fast enough to avoid excessive bead formation.

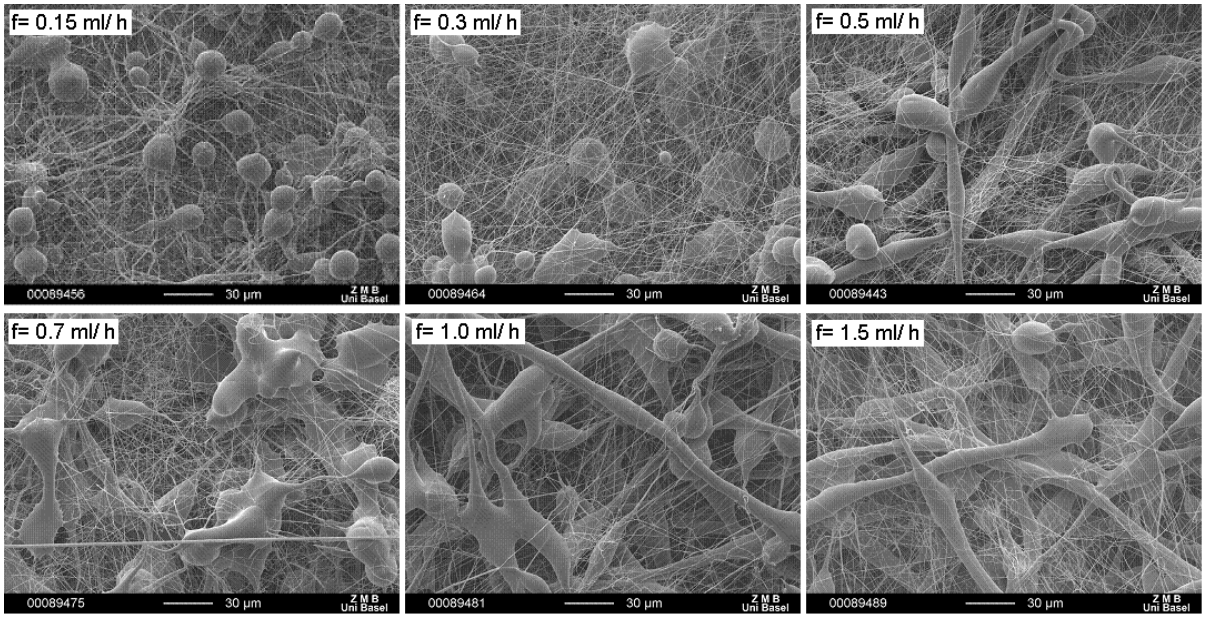

Figure 3.5: Effect of increasing electric potential on 7 wt % PCL electrospun at 15 kV and 10 cm needle-collector distance.

3.2.2.2 Electrospinning of Poly(3-hydroxyl butyrate-co-3-hydroxyl valerate) (PHB-HV)

PHB and PHB-HV (provided by Manfred Zinn, EMPA St. Gallen) were dissolved in chloroform at a concentration of 10 wt %. The concentration of HV in the copolymers was 3 wt, 6 wt, and 20 wt %, respectively. The solutions were electrospun at 25 kV, 10 cm needle-collector distance, and with a flow rate of 0.5 ml/ h. Electrospinning of PHB and all PHB-HV leads to uniform fibers. The spun fiber mats were rather small (diameter about 1 cm) but robust and therefore easy to handle.

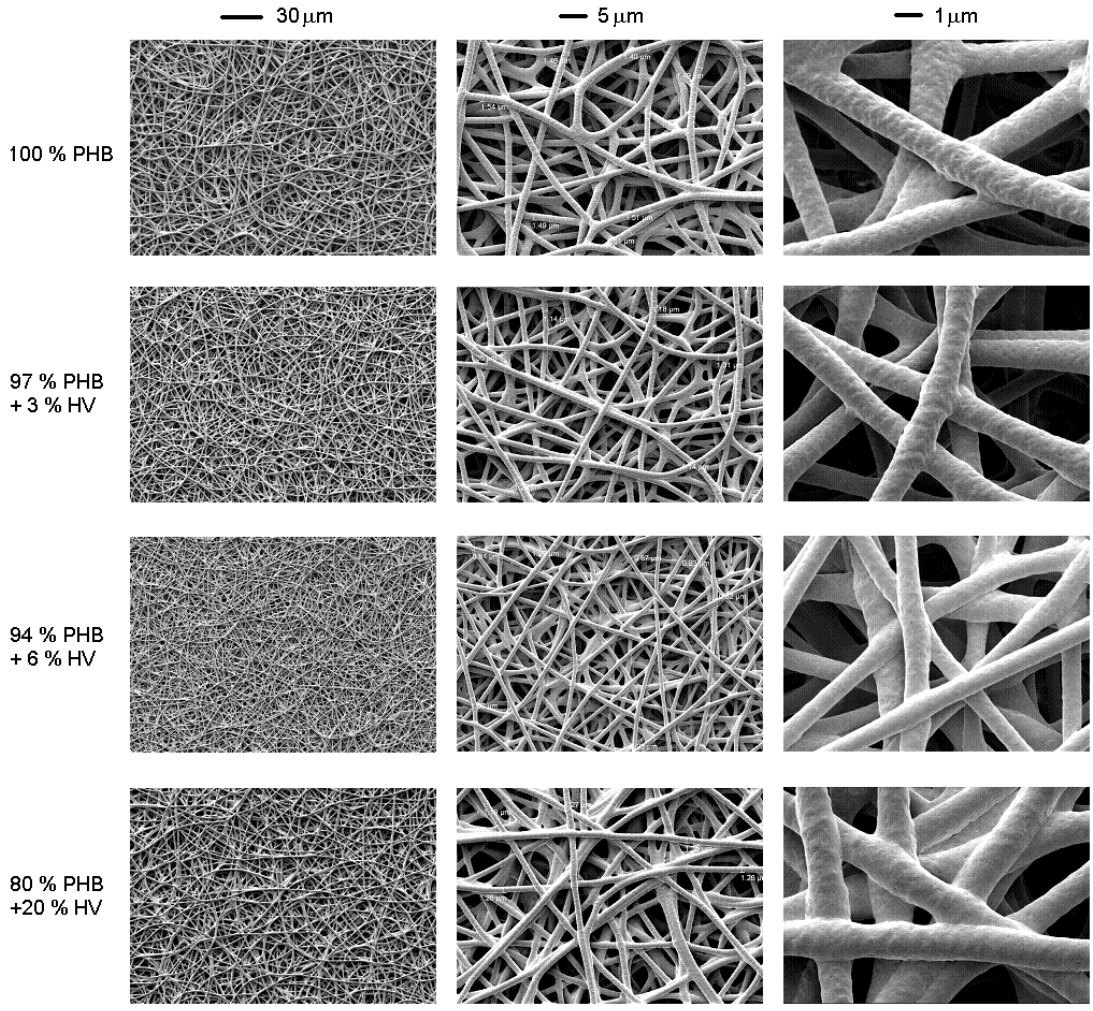

Figure 3.6: Overview of the morphology of PHB and PHB-HV with different HV percentage but equal concentration, voltage, flow rate and distance parameters.

With increasing HV fraction, the fiber diameter initially decreases. Pure PHB fibers have diameters of 1.5 ± 0.2 µm, indicating a rather narrow diameter distribution. With increasing HV fraction, the average diameters decrease from 1.23 ± 0.1 µm (3 wt % HV) to

0.95 ± 0.3 µm (6 wt %). Lower diameters are thus associated with broader diameter distributions. Finally, PHB-HV fibers from polymers with 20 wt % HV result in an increasing average fiber diameter of 1.27 ± 0.08 µm. The fiber diameters and their distribution are given in figure 3.7.

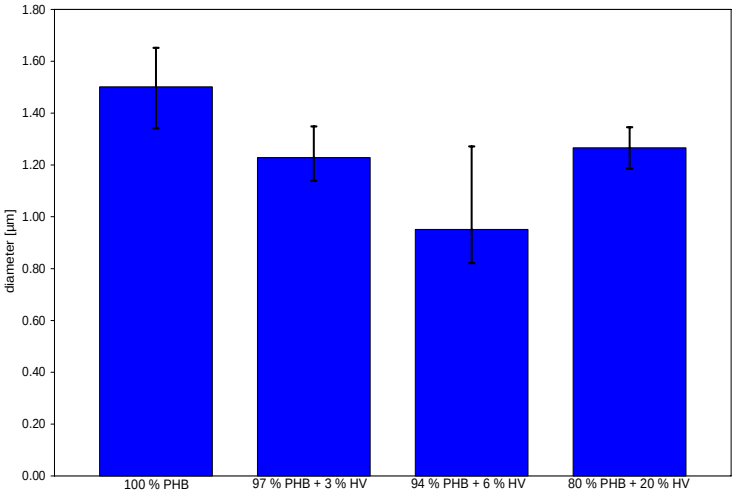

Figure 3.7: Comparison of PHB and PHB-HV fiber diameters with respect to their HV amount in the copolymer.

3.2.2.3 Calcium phosphate mineralization on the electrospun polyester scaffolds

To learn if CaP mineralizes on the polyester scaffolds, precipitation of CaP from simulated body fluid (SBF) was carried out. SBF has inorganic ion concentrations similar to those of human extracellular fluid. SBF has been used for both the evaluation of the bioactivity of artificial materials *in vitro*, but also for the biomimetic coating of apatite on various materials. The ion concentrations of SBF are given in table 3.1[22].

Table 3.1. Ion concentrations of the simulated body fluid[22] and human blood plasma.

Ion	Concentration (mmol/l)	
	Simulated body fluid (SBF)	Human blood plasma
Na^+	142.0	142.0
K^+	5.0	5.0
Mg^{2+}	1.5	1.5
Ca^{2+}	2.5	2.5
Cl^-	147.8	103.0

HCO_3^-	4.2	27.0
HPO_4^{2-}	1.0	1.0
SO_4^{2-}	0.5	0.5

SEM images of mineralized fiber mats after ten days soaking in SBF is shown in figure 3.8. Crystals precipitate onto the PCL fibers and EDS analysis (figure 3.9) confirms the presence of calcium and phosphorus, implying that the deposits observed in the SEM are calcium phosphate particles. EDS also detects sodium, magnesium, and chlorine, but in low amounts compared to the calcium and phosphorus peaks. EDX analysis of crystals in the edges of the fiber nodes (arrows) detected mainly sodium and chlorine, implying the formation of sodium chloride. These deposits can be removed by rinsing with water right after taking the scaffold out of the SBF solution.

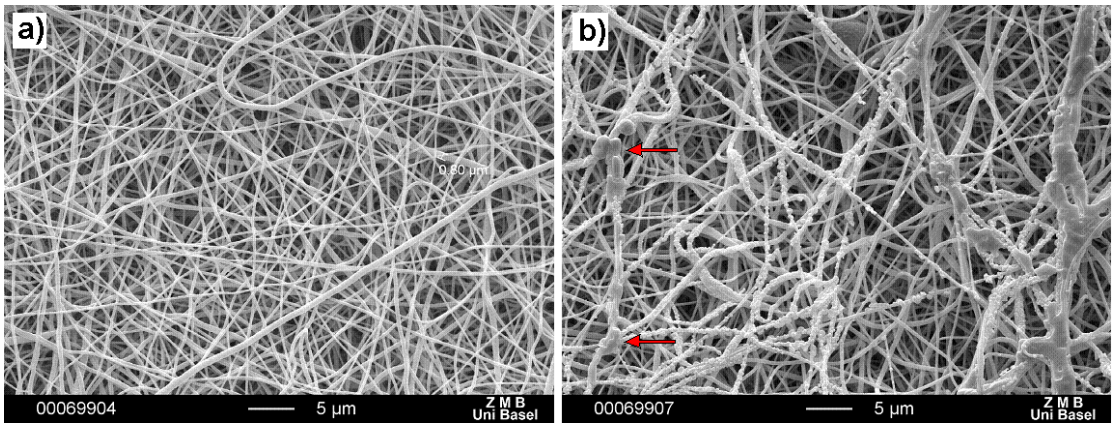

Figure 3.8: a) PCL fibers; b) PCL fibers with precipitated CaP on the surface. Arrows show sodium chloride particles.

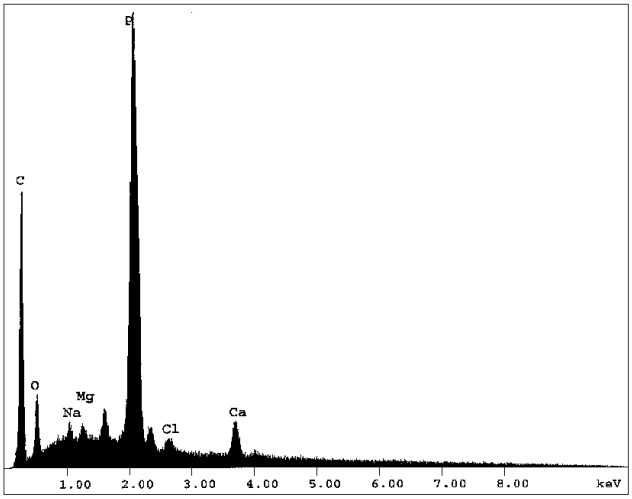

Figure 3.9: EDX spectrum of PCL fibers mineralized in SBF for ten days.

3.3 Discussion

For the electrospinning process, different parameters have an influence to the morphology of the resulting fibers. They can be separated into a chemistry-related and a process-related part, see Chapter 3.2.2. On the processing side, the vapor pressure of the solvent, the needle-collector distance, the applied voltage, and the flow rate are the most important parameters to consider.

The vapor pressure of the solvent should be suitable such that it evaporates quickly enough for the fiber to form before the jet reaches the collector. The viscosity and surface tension of the solvent must neither be too large to prevent the jet from forming nor too small to allow the polymer solution to drain freely from the needle. Solvents like chloroform and dichloromethane are suitable for electrospinning polymers from solutions, although highly concentrated solutions are needed. Low concentration solutions form droplets due to the influence of surface tension.

In the current study, PCL solutions in dichloromethane and chloroform with concentrations of about 7 wt % to 15 wt % polymer were prepared and electrospun. Spinning with high concentrations (more than 10 wt %) of PCL did not work because of the high viscosity of the solutions. Either the needle would get clogged or the solvent evaporated from the drop at the end of the needle before the Taylor cone formed and the jet could spread out.

This is unlike some other studies, where PCL was spun from solutions with PCL weight fractions of up to 15 wt %.[23] At the moment, the reason for this different behavior is not clear, but as in publications the needle diameters are not given, it is possible that large needle diameters also enable the spinning of highly viscous solutions. Others spun PCL out of solvent mixtures like dichloromethane/N,N-dimethyl formamide (DMF)[17,19] or dichloromethane/methanol.[24] Addition of ionic salts like sodium chloride (NaCl) have an effect on solution conductivity resulting in beadless fibers with smaller diameters.[25,26] This already illustrates that there is a vast parameter space to be explored and that a large, consistent study on spinning parameters would be highly desirable. At the moment, we can conclude that our polymers are efficiently spun with our setup at 7 wt%.

It has also been known for a while that the structure and morphology of electrospun fibers is affected by the needle to collector distance. The gap between the capillary and the grounded surface should not be too small to avoid shortcuts and sparks between the electrodes. It should be large enough for the solvent to evaporate in time for the fibers to form. Electrospinning from aqueous polymer solutions require more distance to dry fiber

formation than systems that use highly volatile organic solvents.[27] From this work it can be concluded, that increasing distance leads to decreased average fiber diameters. But these larger gaps may ask for higher voltage, because otherwise fibers are not formed and only drops can be observed at the collector.

The flow rate of the polymer solution from the syringe is another important process parameter as it influences the jet velocity. In accordance with literature it was found that the fiber diameter increases with an increase in the polymer flow rate.[20] Thereby, it has to be pointed out that very slow solution flow and high viscosity may cause blockage or lead to spread droplets or short fibers with many beads.

The power supply is the next important parameter which affects the morphology of the electrospun fibers. It should be adequate to overcome the viscosity and surface tension of the polymer solution to form the jet from the capillary. Deitzel et al. showed that an increase in applied voltage causes a change in the shape of the jet initiation and hence the structure and morphology of fibers.[28] From the observations in chapter 3.2, and from different publications[21], it is to conclude that the diameter of the PCL fibers produced by electrospinning from chloroform becomes more uniform with larger needle-collector distance, higher electrospinning voltage, and slow flow rate.

This general behavior can be adopted for other polyesters with high molecular weights such as PHB and PHB-HV. The viscosity of the solutions decreased with increasing amount of HV. The fiber diameters also decrease with increasing amount of HV until 6 wt %, but fibers from PHB-HV with 20 wt % HV become thicker again. This cannot be explained by the viscosity, but with different electrical conductivity as postulated by Sombatmankhong et al.[29]

These authors electrospun fibers from pure PHB, pure PHB-HV (5 mol % HV) and from mixtures of the two polymers. They showed that the electrical conductivity was a maximum in the solution containing equal amounts of both polymers (50:50 PHB/PHB-HV). Minimum conductivity was measured for the pure PHB and PHB-HV solution. The average fiber diameter of the spun PHB/PHB-HV blend solutions was larger than those of the electrospun fibers from pure polymer solutions. The largest average diameter was measured for the 50:50 PHB/PHB-HV blend solution. This corresponds to the largest electrical conductivity of the 50:50 PHB/PHB-HV solution. We may thus infer that in our case, the diameter variation is also (at least partially) related to the changes in electrical conductivity in the polymer solutions. Possibly, this finding can be generalized for other solvents or solvent mixtures or other polymers, but so far there are no data available from the literature. We may however hypothesize that even strong effects such as the bead formation reported for the PCL

could (again at least partly) be related to conductivity issues. This hypothesis is further supported by the observation that the addition of NaCl also affects the fiber diameters of electrospun PCL.[25,26]

Additionally, CaP mineralization on electrospun scaffolds was carried out. After 10 days of immersion of the PCL and PHB/PHB-HV electrospun scaffolds in SBF, the fibers are only slightly coated with CaP. In contrast to other groups[30,31], the scaffolds used in the current study were not pre-treated before the mineralization from aqueous solution. Yang et al.[30] activated the PCL surface by plasma surface treatment before soaking the scaffolds into 10x SBF, which is ten times more concentrated than the "normal" SBF. Li et al.[31] coated gelatin and poly(styrene sufonate) sodium salt (PSS) through layer-by-layer deposition on the PCL fiber surface, followed by mineralization in 10x SBF. After a few hours, the PCL scaffolds were fully covered with CaP but the porous structure was lost after six hours of incubation in both studies.

Both groups also observed that the (calcium phosphate) coatings improved the wettability of the electrospun PCL scaffold. For comparison, Li et al. also reported mineralization on "naked" PCL fibrous scaffolds.[2] The fibers were then only slightly coated with CaP, in contrast to the earlier examples activated with gelatin. This result is confirmed by the current study and demonstrates that the scaffolds have to be activated by including functional groups in or on the fibers to enforce calcium phosphate mineralization.

Instead of modifying the electrospun polyester by plasma treatment or additional polymer coatings, the polyester could in principle also be chemically modified by covalent addition of functional groups. These functional groups can, for example, be introduced via the thiol-ene click reaction. This method is a, simple, fast, cheap, and versatile tool to introduce a broad range of functionalities into organic molecules.[32,33]

3.4 Experimental section

3.4.1 Solution preparation

PCL was diluted with a concentration of 7 % wt and 9 % wt in dichloromethane or chloroform under stirring at room temperature. PHB and PHB-HV were weighted in pyrex tubes and chloroform was added to get concentrations of 14 % wt, 9 % wt, 7.5 % wt and 5 % wt. The closed and sealed (with parafilm) pyrex tubes were then heated up to 120 °C in an autoclave for 15 minutes. After intense stirring and cooling to room temperature, the viscous solution was ready to use.

3.4.2 Electrospinning

Electrospinning was performed on a homemade electrospinning apparatus (see chapter 3.2.1). The parameters used for resulting fibers were:

- Concentration: 5 to 14 % wt
- Flow rate: 0.15 to 1.5 ml/h
- Voltage: 10 to 25 kV
- Distance (needle to collector): 3 to 23 cm
- Solvent: dichloromethane or chloroform

3.4.3 Mineralization of the electrospun scaffolds by soaking in simulated body fluid (SBF)

To mineralize the polyester scaffolds, a fresh SBF had to be prepared. Sodium chloride (NaCl, 136.8 mM), potassium chloride (KCl, 3.0 mM), magnesium chloride hexahydrate ($MgCl_2$ * 6 H_2O, 1.5 mM), and calcium chloride hexahydrate ($CaCl_2$ * 6 H_2O, 2.5 mM) were weighted in a cleaned plastic bottle. 1000 ml of bidistilled water were added and the pH was set to 7.4 by addition of 1M HCl solution. This mixture represents the calcium-based stock solution. The phosphate stock solution was prepared likewise using sodium sulfate decahydrate (Na_2SO_4 * 10 H_2O, 0.5 mM), sodium hydrogen carbonate ($NaHCO_3$, 4.2 mM), and dipotassium hydrogenphosphate trihydrate (K_2HPO_4 * 3 H_2O, 1.0 mM). The two stock solutions were mixed in the ratio of 1:1 just before use. The fibrous mat was then added and the mixture was agitated at 37 °C for ten days. The scaffold was removed

and dried in a vacuum oven over night. PHB scaffolds were rinsed intensively with water before drying to remove residual NaCl.

3.5 References

(1) Agarwal, S.; Wendorff, J. H.; Greiner, A. *Polymer* **2008**, *49*, 5603-5621.

(2) Li, W.-J.; Tuli, R.; Huang, X.; Laquerriere, P.; Tuan, R. S. *Biomaterials* **2005**, *26*, 5158.

(3) Li, C.; Vepari, C.; Jin, H.-J.; Kim, H. J.; Kaplan, D. L. *Biomaterials* **2006**, *27*, 3115.

(4) Laurencin, C. T.; Ambrosio, A. M. A.; Borden, M. D.; Cooper, J. A., Jr. *Annual Review of Biomedical Engineering* **1999**, *1*, 19-46.

(5) Wutticharoenmongkol, P.; Sanchavanakit, N.; Pavasant, P.; Supaphol, P. *Macromolecular Bioscience* **2006**, *6*, 70-77.

(6) Yuan, H.; Yang, Z.; Li, Y.; Zhang, X.; De Bruijn, J. D.; De Groot, K. *Journal of Materials Science: Materials in Medicine* **1998**, *9*, 723.

(7) Zhu, X.; Cui, W.; Li, X.; Jin, Y. *Biomacromolecules* **2008**, *9*, 1795-1801.

(8) Dong, Y.; Liao, S.; Ngiam, M.; Chan, C. K.; Ramakrishna, S. *Tissue Engineering, Part B: Reviews* **2009**, *15*, 333-351.

(9) Yang, F.; Murugan, R.; Wang, S.; Ramakrishna, S. *Biomaterials* **2005**, *26*, 2603-2610.

(10) Woo, K. M.; Chen, V. J.; Ma, P. X. *Journal of Biomedical Materials Research, Part A* **2003**, *67A*, 531-537.

(11) Woo Kyung, M.; Jun, J.-H.; Chen Victor, J.; Seo, J.; Baek, J.-H.; Ryoo, H.-M.; Kim, G.-S.; Somerman Martha, J.; Ma Peter, X. *Biomaterials* **2007**, *28*, 335-43.

(12) Lim, C. T.; Tan, E. P. S.; Ng, S. Y. *Applied Physics Letters* **2008**, *92*, 141908/1-141908/3.

(13) Venugopal, J.; Ramakrishna, S. *Tissue Engineering* **2005**, *11*, 847-854.

(14) Zhang, Y. Z.; Venugopal, J.; Huang, Z. M.; Lim, C. T.; Ramakrishna, S. *Biomacromolecules* **2005**, *6*, 2583-2589.

(15) Shin, M.; Yoshimoto, H.; Vacanti, J. P. *Tissue Engineering* **2004**, *10*, 33-41.

(16) Ito, Y.; Hasuda, H.; Kamitakahara, M.; Ohtsuki, C.; Tanihara, M.; Kang, I.-K.; Kwon, O. H. *Journal of Bioscience and Bioengineering* **2005**, *100*, 43-49.

(17) Mattanavee, W.; Suwantong, O.; Puthong, S.; Bunaprasert, T.; Hoven, V. P.; Supaphol, P. *ACS Applied Materials & Interfaces* **2009**, *1*, 1076-1085.

(18) Chen, M.; Patra, P. K.; Warner, S. B.; Bhowmick, S. *Biophysical Reviews and Letters* **2006**, *1*, 189-214.

(19) Kim, H.-j.; Jung, Y.-h.; Khil, M.-s.; Kim, H.-y.; Bang, H.-J. *Journal of the Korean Fiber Society* **2004**, *41*, 424-432.

(20) Megelski, S.; Stephens, J. S.; Chase, D. B.; Rabolt, J. F. *Macromolecules* **2002**, *35*, 8456-8466.

(21) Thandavamoorthy, S.; Bhat, G. S.; Tock, R. W.; Parameswaran, S.; Ramkumar, S. S. *Journal of Applied Polymer Science* **2005**, *96*, 557-569.

(22) Kokubo, T.; Takadama, H. *Handbook of Biomineralization: Medical and Clinical Aspects* **2007**, 97-108.

(23) Prabhakaran, M. P.; Venugopal, J. R.; Chyan, T. T.; Hai, L. B.; Chan, C. K.; Lim, A. Y.; Ramakrishna, S. *Tissue Engineering Part A* **2008**, *14*, 1787-1797.

(24) Luong-Van, E.; Grøndahl, L.; Chua, K. N.; Leong, K. W.; Nurcombe, V.; Cool, S. M. *Biomaterials* **2006**, *27*, 2042.

(25) Moghe, A. K.; Hufenus, R.; Hudson, S. M.; Gupta, B. S. *Polymer* **2009**, *50*, 3311-3318.

(26) Zong, X.; Kim, K.; Fang, D.; Ran, S.; Hsiao, B. S.; Chu, B. *Polymer* **2002**, *43*, 4403-4412.

(27) Buchko, C. J.; Chen, L. C.; Shen, Y.; Martin, D. C. *Polymer* **1999**, *40*, 7397-7407.

(28) Deitzel, J. M.; Kosik, W.; McKnight, S. H.; Beck Tan, N. C.; DeSimone, J. M.; Crette, S. *Polymer* **2001**, *43*, 1025-1029.

(29) Sombatmankhong, K.; Suwantong, O.; Waleetorncheepsawat, S.; Supaphol, P. *Journal of Polymer Science, Part B: Polymer Physics* **2006**, *44*, 2923-2933.

(30) Yang, F.; Wolke, J. G. C.; Jansen, J. A. *Chemical Engineering Journal (Amsterdam, Netherlands)* **2008**, *137*, 154-161.

(31) Li, X.; Xie, J.; Yuan, X.; Xia, Y. *Langmuir* **2008**, *24*, 14145.

(32) Alessandro, D. *Angewandte Chemie International Edition* **2008**, *47*, 8995-8997.

(33) Charles , E. H.; Christopher , N. B. *Angewandte Chemie International Edition*, *49*, 1540-1573.

4 Synthesis of modified polyesters

4.1 Introduction

One of the biggest disadvantages of electrospun polyesters is the lack of chemical and biochemical functionality, such as cell recognition signals and functionalities to enforce, for example, cell growth and CaP nucleation. This has restricted their wider application. The design and fabrication of scaffolds using appropriate biomaterials is a key, but limiting step for the creation of functional engineered tissues and their applications.[1] The native ECM is comprised of a complex network of structural and regulatory proteins, which provides resident cells with specific ligands for cell adhesion and migration, and modulates cell proliferation and functions. Naturally occurring materials, such as collagen, elastin, silk protein, fibrinogen, chitosan, dextran, and hyaluronic acid have been electrospun into nanofibers.[2-5]

Although these fibrous scaffolds mimic the molecular and structural properties of the native ECM, they have a problem with mechanical stability and the 3D structure rapidly disintegrates under aqueous conditions.[4] One ambition for scaffold research should thus aim at the synthesis of functional polyester scaffolds with high mechanical stability. One possibility to achieve higher mechanical stability is the combination of a robust polyester with appropriate functional groups. These groups can either enhance CaP mineralization and/or serve as (bio)chemical signals for a certain process. Moreover, the mineralization of the polymeric scaffold will further enhance the stability of the scaffold.

In this chapter, the synthesis of a polyester is described. This polyester carries double bonds in its side chains, which can be used for further modifications after polymerization to introduce new functionalities. For this thesis, the polyester was modified with thioglucose acetate as a model reaction. The modified polyester then was electrospun to reach the three dimensional structure. To gain additional mechanical stability, the electrospun polyester scaffolds were mineralized with CaP.

4.2 Results and discussion

4.2.1 Synthesis of poly(α-allylvalerolactone-*co*-valerolactone)

The goal of this part of the work was the synthesis of a "platform" polyester, that is, a base polymer that can be extensively characterized and then functionalized with a broad range of functional groups. The advantage of this approach is that it avoids batch to batch variations in polymer composition: initially the base polymer is synthesized and then the batch is split into *n* sub-batches that can be functionalized with different groups such as acids, bases, peptide, sugars, chiral groups, ligands, …., while keeping the molecular weight, molecular weight distribution, and the fraction of functional groups the same between the different sub-batches.

Our approach towards the base polyester was the production of a polyester which carries terminal double bonds in its side chains. As the approach via biosyntheses like the one for PHB and PHB-HV was not accessible, a "classical" synthetic approach was developed. This included the synthesis of a new monomer followed by polymerization and functionalization. Functionality was achieved by modification via "thiol-ene" click chemistry.[6,7] With this approach, any desired functionality can be established by reaction of a thiol with the double bond of the polyester.

Several pathways lead to the desired monomer with free terminal double bonds in the side chain (**1, 9**). Initially, the ring opening polymerization (ROP) of lactones was taken to start the retro synthesis of the target monomer, figure 4.1. ROP leads to polymers with high molecular weight and low polydispersities.[8] For that, monomers like tetrahydro-pyranone (**2**) are needed. Also other substituted lactones may result in the desired monomer, it does not matter where the double bond is inserted. Even the length of the substituted chain (with the functional double bond) does not matter.

Besides insertion of oxygen through Bayer-Villiger reactions, lactones are often synthezised out of diols.[9] One reaction to obtain lactones is an acid-catalyzed intra-esterification. Another mechanism is the oxidative cyclization. A typical procedure for the oxidative cyclization of diols was found to synthesize monomer **2**.[9] The required diol (**3**) should therefore already carry the double bond. For insertion of the double bond, Grignard reaction was chosen where vinylmagnesium bromide reacts with hydroxyaldehyde **4**. This reaction step decides where the double bond is placed in the lactone and in the resulting

polyester. The hydroxyaldehyde **4** should be received by simple acidic ring opening of the corresponding commercially available dihydropyran **5**.[10-13]

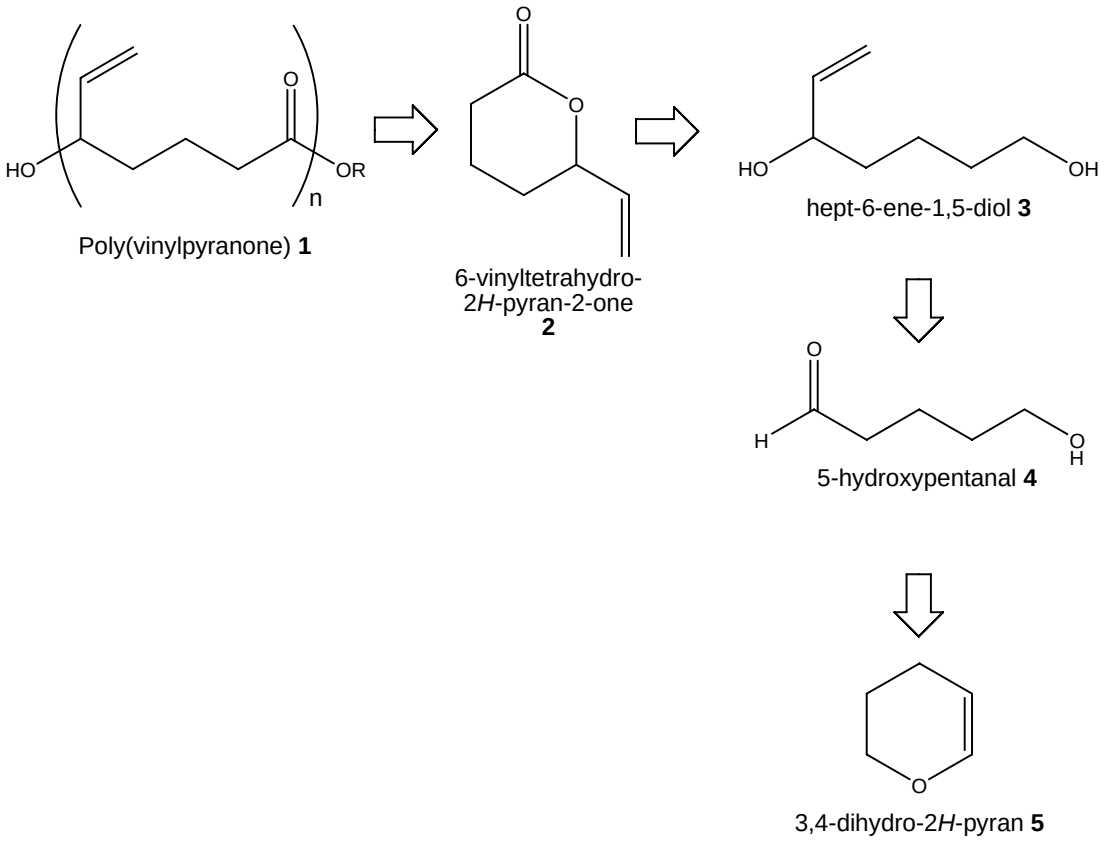

Figure 4.1: Retro synthesis of the poly(vinylpyranone) **1**.

The acidic ring opening of the dihydropyran **5** to the hydroxypentanal **4** first seemed to result in very little conversion because ^{1}H-NMR analysis showed a very small peak ar 9.76 ppm for the free aldehyde **4** (see figure 4.2).

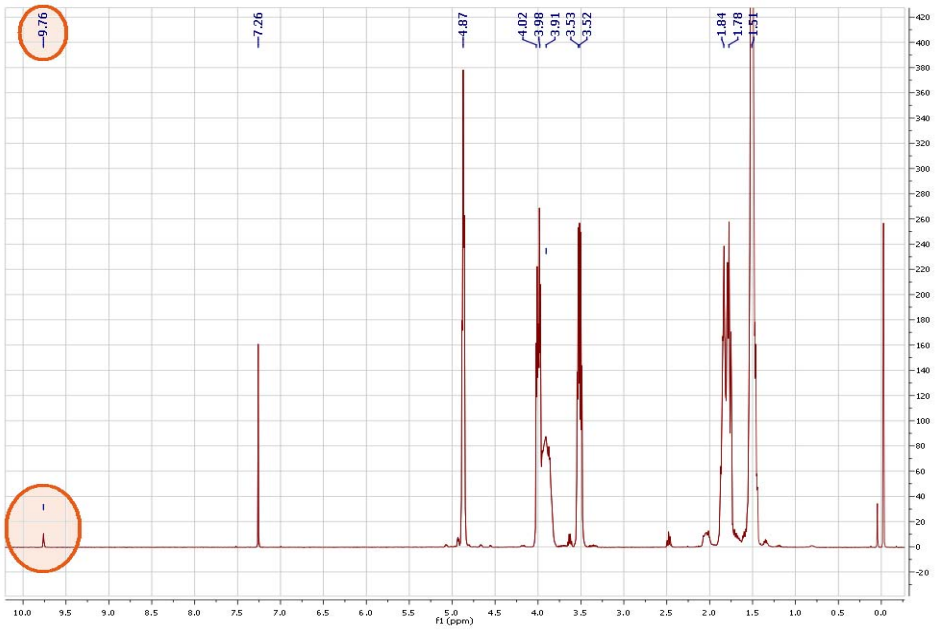

Figure 4.2: 1H-NMR of the alcohol **6** and the aldehyde **4**. The marked peak belongs to the hydrogen of the free aldehyde from **4**.

More detailed analysis, however, showed that the closed conformation **6** (tetrahydro-*2H*-pyran-2-ol) is present (see figure 4.3). Comparison with literature showed identical results and therefore the product (alcohol by majority) was used for the next synthesis step. With conversion of the small fraction of the free aldehyde **4** to the diol **3**, the equilibrium was forced to **4** and resulted in good yield of the diol **3**. Thus the syntheses including Grignard reaction worked well and in satisfying yields. Unfortunately, the oxidative cyclization from **3** to **2** did not result in any conversion.

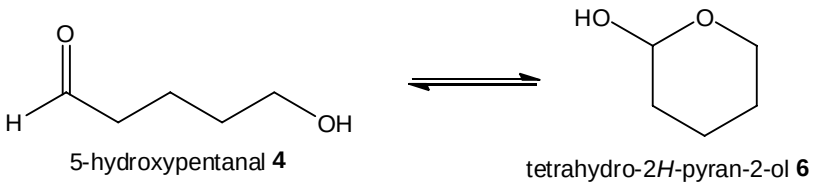

5-hydroxypentanal **4** tetrahydro-2*H*-pyran-2-ol **6**

Figure 4.3: Equilibrium between the aldehyde **4** and the closed form **6**.

Instead of trying different oxidation reagents or searching for better parameters of the synthesis, a different pathway yielded the desired monomer **6**.[14] Alkylation of lactones directly leads to the tetrahydro-3-(2-propenyl)-2-pyranon (α-allylvalerolactone, AVL, **7**) by a one step reaction of allyl bromide (**8**) with δ-valerolactone (VL, **9**)[14] (figure 4.4). This promising approach resulted in the product **7** at a yield of 20 %. Optimization of the procedure was aimed by addition of butyl lithium (BuLi)[15]. Implementation with fresh BuLi

yielded in desired product but not in better yield. Addition of chlorotrimethylsilane (TMSCl), modifying the procedure by making the LDA less basic but even more nucleophilic and favouring the alkylation at α-position, yielded in a conversion of 15 %. With all efforts made, the yields published by other authors[15,16] were not obtained. Nevertheless, the procedure proved reproducible and robust, such that enough monomer for further polymerization could be obtained.

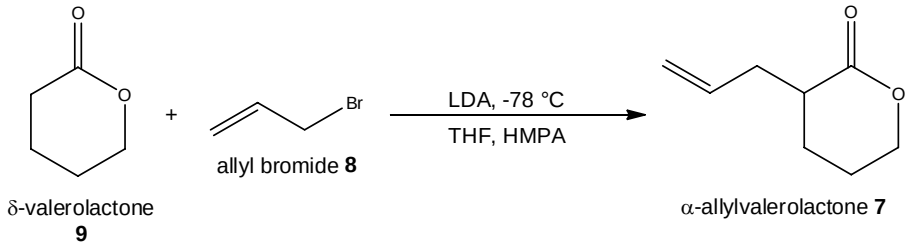

Figure 4.4: One-step reaction to get the desired monomer for further ROP.

Figure 4.5 shows the ^{1}H-NMR spectrum of AVL **7**. The peaks at 5.80 ppm and 5.09 ppm correspond to the hydrogen atoms of the double bond (number 7 & 8). The peak at 4.30 ppm corresponds to the hydrogen atoms bound to the carbon near the oxygen from the lactone. The hydrogen atoms bound to the carbon atoms 2 and 6 are observed at 2.62, 2.54 and 2.31 ppm. The less affected hydrogens at the carbons in position 3 and 4 show their peak in the range from 2.06 to 1.57 ppm.

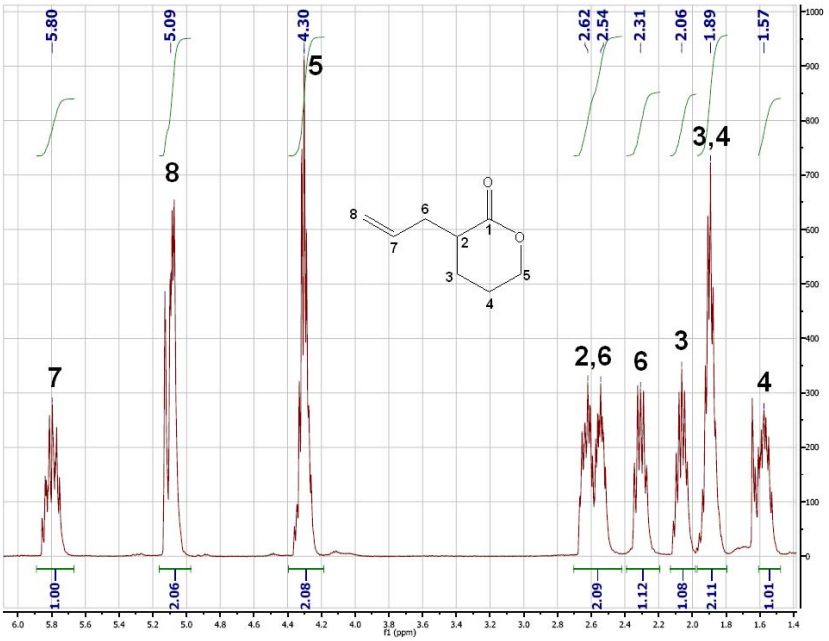

Figure 4.5: ^{1}H-NMR spectrum of α-allylvalerolactone **7**.

For ROP, the procedure of Parrish et al.[15] was initially chosen as this group polymerized exactly the same monomer. Copolymerization of **7** with VL (**9**) was carried out as described in the literature, resulting in poly(α-allylvalerolactone-*co*-valerolactone) (PAVL-VL, **10**). Copolymerization with VL (**9**) leads to polymers with higher crystallinity than homopolymerization of AVL and therefore rather to a solid product which is important for electrospinning.

The synthesis with a stannous catalyst ($Sn(OTf)_2$) yielded polymers with molecular weights of about 1000-2500 g/mol. In addition, the resulting molecular weights varied strongly from batch to batch. An alternative approach using a protocol by Lou et al.[8] yielded polymers with molecular weight around 3000 g/mol. Polymers with these molecular weights are too small for further use by electrospinning since the product is an oil rather than a solid.

With both polymerization procedures a diblock-copolymer was obtained, as can be seen from the ^{13}C-NMR spectra.[16,17] Figure 4.6c shows the carbonyl carbons and carbons of the AVL double bond in detail. The peaks at 175.5 ppm and 175.1 ppm correspond to the carbonyl carbon of the PAVL, whereas the ones at 173.6 ppm and 173.3 ppm come from the backbone of VL. The smaller peak (at 175.5 ppm and 173.6) corresponds to the carbonyls of the AVL and VL backbone within a statistical copolymer. This means the VL and AVL monomers are randomly arranged within the polymer and it is also called heterogeneous copolymer. The peaks at 175.1 ppm and 173.3 ppm respectively correspond to the AVL and VL backbone from a PAVL-*block*-PVL copolymer, indicating that the VL monomers are arranged block-wise, and, consequently, the AVL monomers are also arranged block-wise.

The peaks from the double bond at 135.4 ppm and 135.1 ppm also indicate that the copolymer occurs as block copolymer showing the same phenomenon like the carbonyl peaks. From the intensities of the peaks one can see, that the copolymer is more block-like but with heterogeneous regions. This can be explained via the copolymerization parameters, although they have not been determined quantitatively.

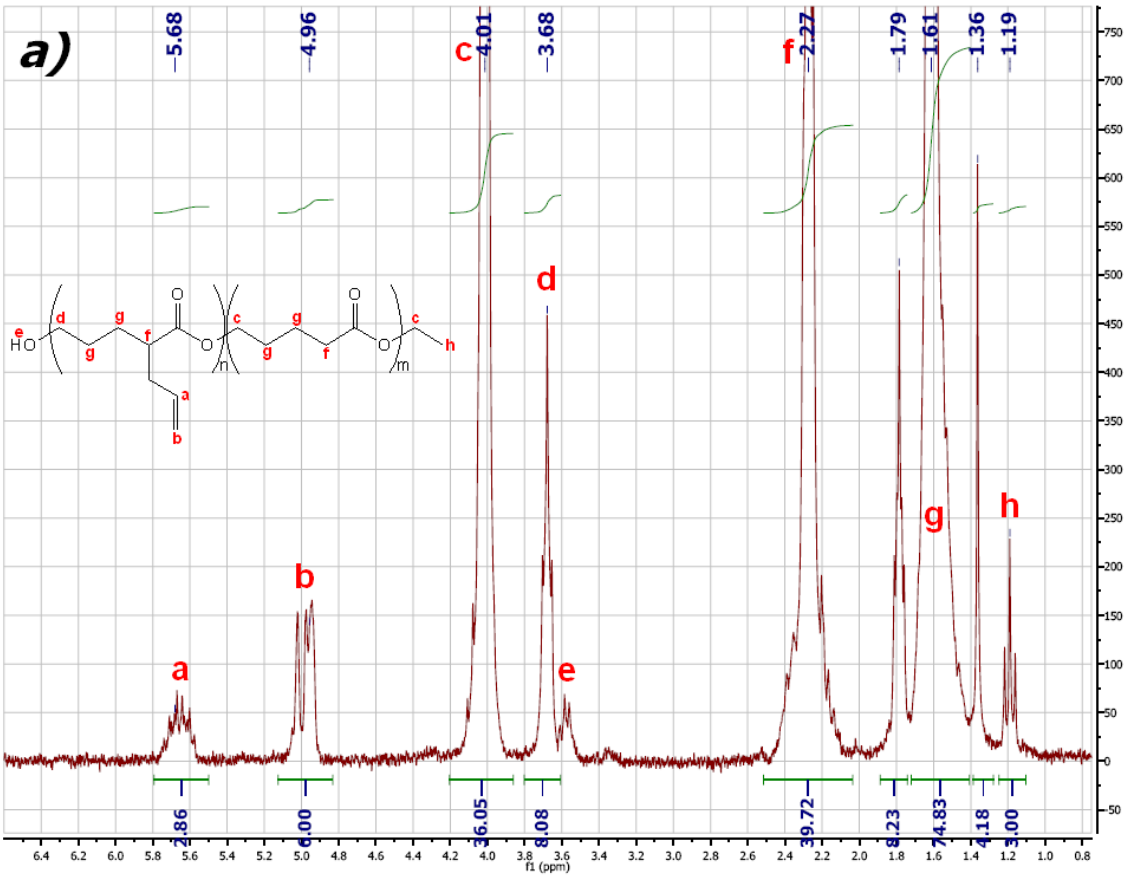
a)
5.68
4.96
4.01
3.68
2.27
1.79
1.61
1.36
1.19
a
b
c
d
e
f
g
h
2.86
6.00
36.05
8.08
39.72
8.23
14.83
4.18
3.00
f1 (ppm)

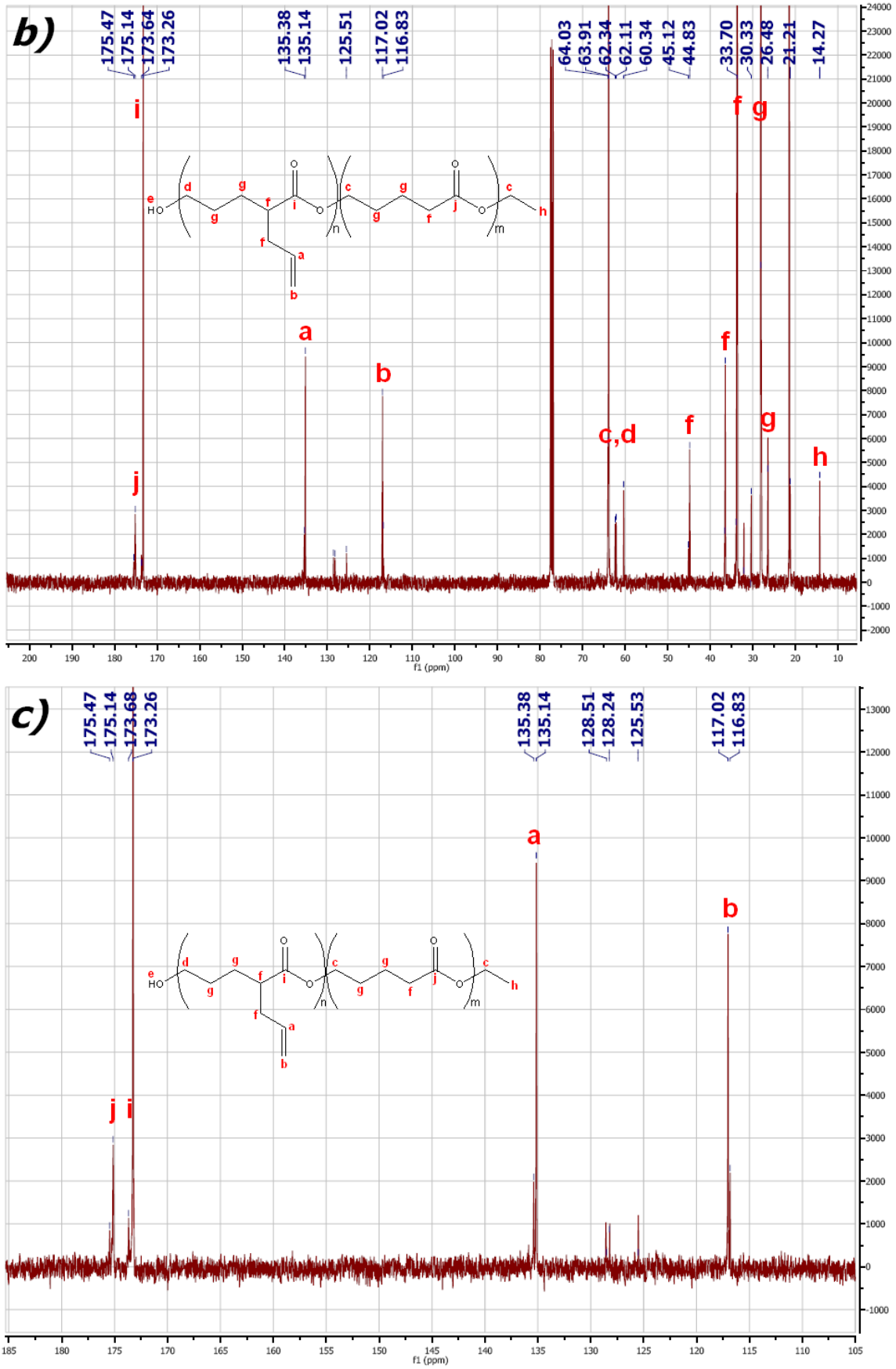

Figure 4.6: a) ^{1}H- and b) ^{13}C-NMR spectrum of poly(α-allylvalerolactone-*co*-valerolactone) **10.** Figure 4.6c shows the carbonyl carbons and the carbons from the double bond in detail.

4.2.2 Functionalization of poly(α-allylvalerolactone-*co*-valerolactone)

To systematically analyse the effect of different functional groups on nucleation and growth of CaP on polyester fibrous scaffolds, different functionalities have to be incorporated to get adjustable properties. Postpolymerization modification is an essential method of adopting functionality to simple polymers. Such modification reactions must be very selective because side reactions at the macromolecular level lead to ill-defined polymer structures and it is hard to purify such products. Click chemistry is a general concept introduced by Sharpless et al.[18] By definition, a click reaction must be feasible under simple reaction conditions, be modular, be wide in scope, give very high yields, generate only inoffensive byproducts, and be stereospecific. The radical addition of mercaptans onto double bonds can be considered as click reaction, as the reaction can be performed under feasible and mild conditions and goes to completion within a day.[19]

The free-radical addition of thiols onto double bonds, the "thiol-ene click" reaction (see figure 4.7), is a highly efficient tool used for polymerization and modifications of polymers.[19-21] The PAVL-VL products **(10)** were therefore used for further conversion by addition of different thiols. In this reaction, the thiols attach to the double bonds of the polyester by exposure to UV light (see figure 4.7).[6,7]

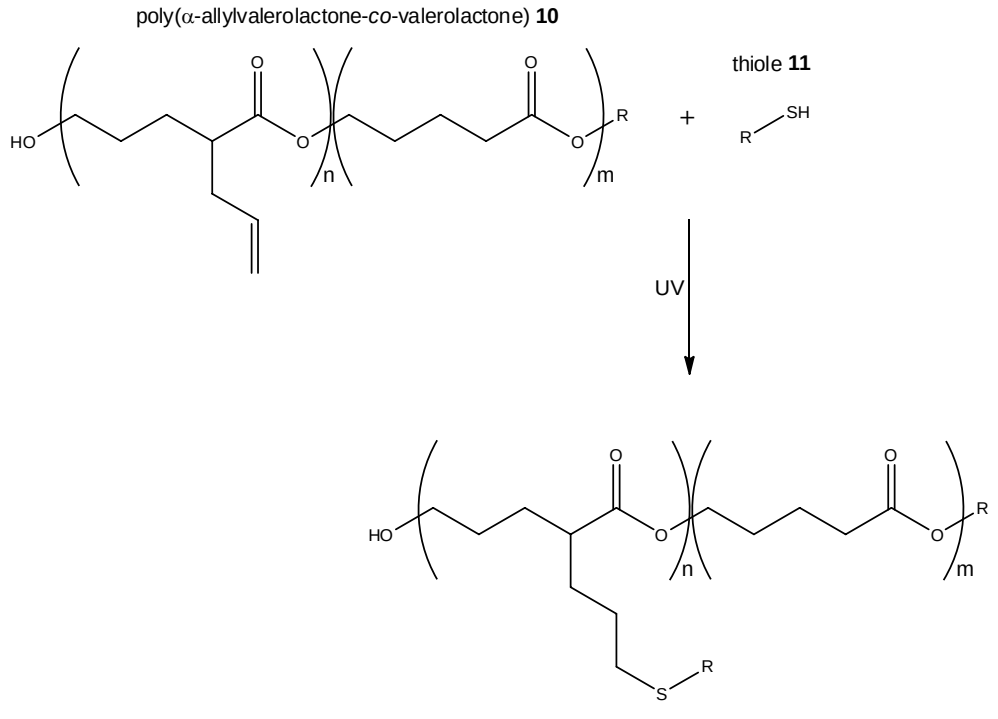

Figure 4.7: Addition of a thiol to a double bond.

The polyester **10** was functionalized to nearly full conversion by using thiols like thioglucose tetraacetate according to Schlaad et al.[19] In the ^{1}H-NMR spectrum in figure 4.8, the peaks from double bond hydrogens disappeared, while peaks from the thiol appear, showing that the addition of the thiol, the thioglucose tetraacetate (**11**), worked. Additionally, the change in molecular weight is clearly visible in the GPC data, figure 4.9. The black line corresponds to the PAVL-VL **(10)**, whereas the red and green lines correspond to the modified polymer after addition of thioglucose tetraacetate **12**. The molecular mass changes significantly after addition of the thiol **11**.

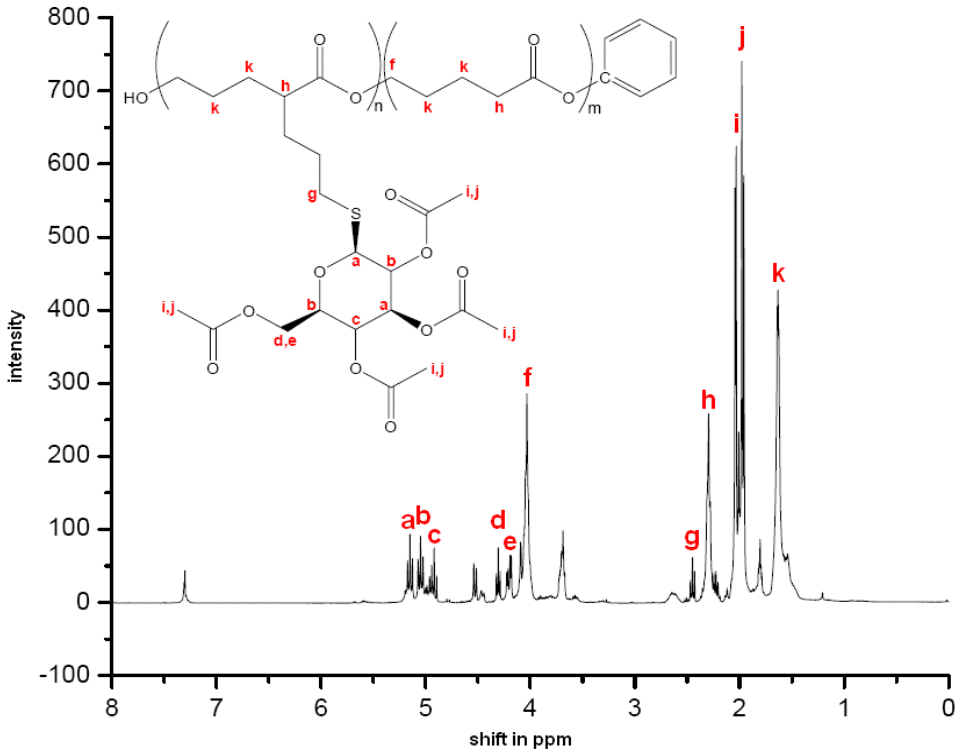

Figure 4.8: ^{1}H-NMR of the modified PAVL-VL.

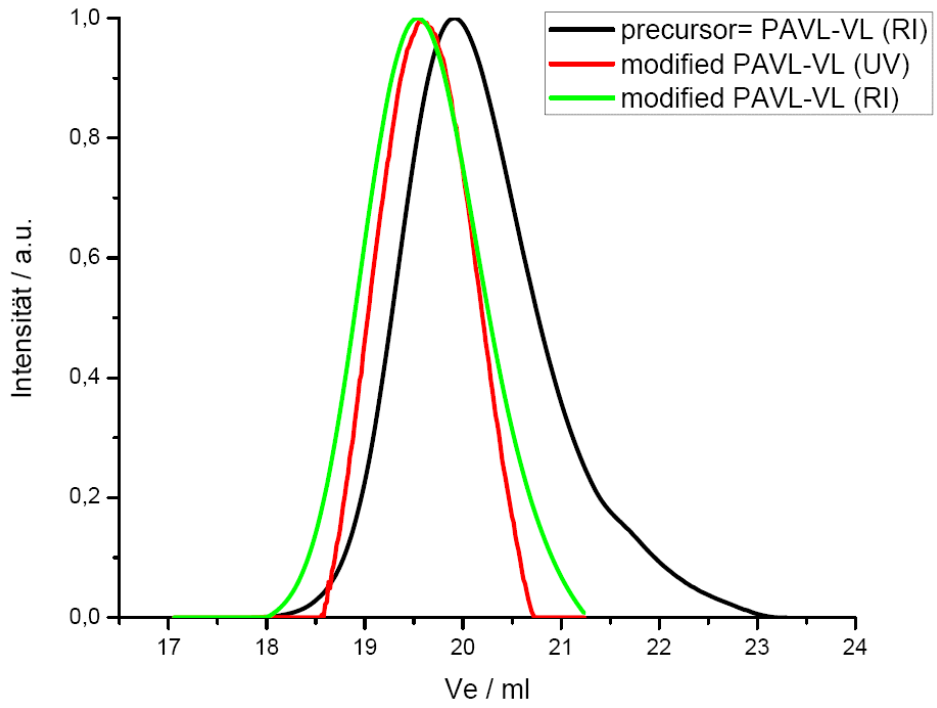

Figure 4.9: GPC spectrum of the used PAVL-VL **(10)** and the resulting modified PAVL-VL **11**.

After functionalization with thioglucose tetraacetate, scaffolds were prepared by electrospinning.

The disadvantage of this approach is that the electrospun matrices may differ from polymer to polymer because of different functional modifications. The electrospinning parameters have to be changed for every different polymer to get comparable three dimensional polyester scaffolds. One way to avoid this complication is the electrospinning of the precursor polymer **10** followed by thiol-ene modification. This sequence provides a uniform matrix after electrospinning, which enables the production of multiple scaffolds with identical fiber diameters, pore sizes, etc. Their only difference would then be the chemical properties of the fiber surface, which as been introduced after electrospinning via thiol-ene reaction. Unfortunately, however, the molecular weight of the precursor polymer was too small for this approach to be tested during the time of the thesis.

4.3 Experimental section

All reactions, except the synthesis of 5-hydroxypentanal, were carried out in dry flasks and dry solutions under argon. Tetrahydrofuran (THF), dichloromethane (DCM), and δ-valerolactone were distilled immediately before use. Hexamethyl phosphoramide (HMPA) was purchased from Aldrich, distilled prior to use, and stored over 3 Å molecular sieve under argon. All other reagents were used as received. Ethyl ester for extractions was used in technical grade. Other solvents were used in purum quality.

4.3.1 Synthesis and characterization of α-allylvalerolactone (AVL) and its precursors

4.3.1.1 Synthesis of 5-Hydroxypentanal (4)

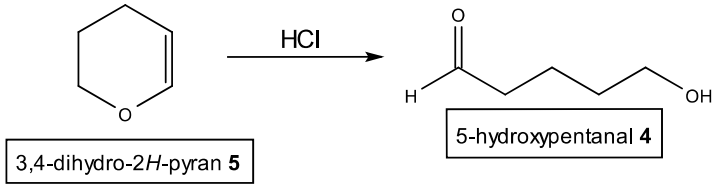

To 30 ml of 1 M HCl (30 mmol, 0.25 eq.) in a 100-ml round-bottomed flask, 3,4-dihydro-2H-pyran **5** (10 ml, 9.22 g, 109.6 mmol, 1.0 eq.) was slowly added. The mixture was stirred for about 30 minutes. The homogenous solution was set to pH 7 by addition of 1 M NaOH. The solution was extracted three times with diethyl ether. The organic phase was dried over $MgSO_4$ and evaporated under reduced pressure. Distillation of the resulting residue (at 70-72 °C/ 10 mbar) yielded a viscous oil (5.94 g, 53 %).

^{1}H-NMR (400 MHz; $CDCl_3$; *δ*/ ppm): 9.76 (s, 1H, aldehyde), 4.87 (s, 1H), 4.06-3.94 (m, 1H), 3.62-3.49 (m, 1H), 1.96-1.73 (m, 2H), 1.62-1.40 (m, 4H)

^{13}C-NMR (100 MHz; $CDCl_3$; *δ*/ ppm): 94.6 (s), 64.1 (s), 32.1 (s), 25.4 (s), 20.5 (s)

4.3.1.2 Synthesis of Hept-6-ene-1,5-diol (3)

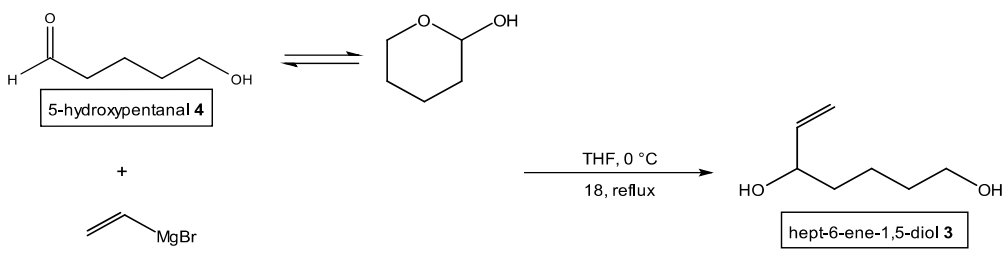

Vinylmagnesium bromide (1 M in THF, 49 ml, 49 mmol, 2.0 eq.) was added dropwise over 40 minutes to a cooled (0 °C) and stirred solution of 5-hydroxypentanal **4** (2.5 g, 24 mmol, 1.0 eq.) in 25 ml THF under argon. The resulting brownish solution was warmed to room temperature for 40 minutes and was heated to reflux for about 18 hours. The solution was cooled in an ice bath and quenched by careful addition of saturated ammonium chloride solution (8 ml). After filtration of the precipitate, the solution was extracted with diethyl ether. The organic phases were dried over $MgSO_4$ followed by evaporation under reduced pressure. The resulting yellowish oil was purified by column chromatography (silica, 18 cm, 2 cm in diameter, ethyl acetate) to yield in a light amber coloured oil (2.78 g, 89 %).

R_f (ethyl acetate): 0.45

^{1}H-NMR (400 MHz; $CDCl_3$; δ/ ppm): 5.94-5.81 (dm, 1H, J^{HH}= 5.87, CH_2=C*H*), 5.26-5.09 (dd, 2H, J^{HH}= 5.17, CH_2=CH), 4.16-4.08 (m, 1H, HO-C*H*-), 3.68-3.63 (m, 2H, HO-CH_2-), 1.98 (s, br, 1H, OH), 1.88 (s, br, 1H, OH), 1.66-1.32 (m, 6H)

FTIR (ν/ cm^{-1}): 3332 (intense, $\nu_{O\text{-}H}$), 2935 (intense, $\nu_{as\ C\text{-}CH2\text{-}C}$), 2866 (intense, $\nu_{sym\ C\text{-}CH2\text{-}C}$), 1645 (weak, $\nu_{C=C}$), 1426 (medium, δ_{CH2}), 1070 (medium, $\nu_{C\text{-}OH}$)

4.3.1.3 Synthesis of 6-Vinyl-tetrahydro-pyran-2-one (2)

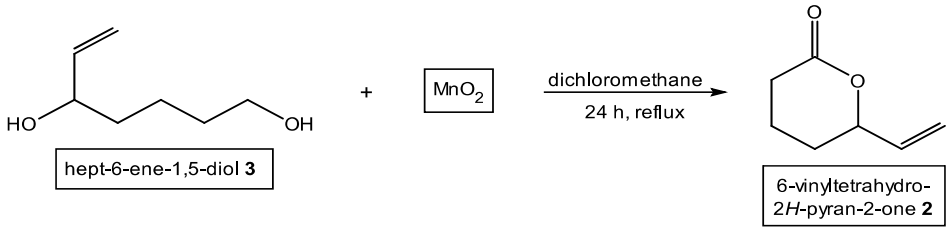

A mixture of hept-6-ene-1,5-diol **3** (260.4 mg, 2.00 mmol, 1.0 eq.) and MnO_2 (3.48 g, 40.0 mmol, 20.0 eq) in 10 ml dichloromethane was stirred at reflux for 24 hours. At this time, control by thin-layer chromatography did not show any conversion. The mixture was cooled to room temperature and was filtered through Celite. The solvent was removed by evaporation under reduced pressure. Characterization by IR spectroscopy did not show any C=O vibration and in the ^{13}C NMR spectrum, no carbonyl carbon was present.

^{13}C-NMR (100 MHz; $CDCl_3$; δ/ ppm): 141.6 (s), 114.9 (s), 73.2 (s), 62.7 (s), 37.0 (s), 32.7 (s), 21.9 (s)

FTIR (ν/ cm^{-1}): 3332 (intense, $\nu_{O\text{-}H}$), 2935 (intense, $\nu_{as\ C\text{-}CH2\text{-}C}$), 2866 (intense, $\nu_{sym\ C\text{-}CH2\text{-}C}$), 1645 (weak, $\nu_{C=C}$), 1426 (medium, δ_{CH2}), 1070 (medium, $\nu_{C\text{-}OH}$)

4.3.1.4 Synthesis of Tetrahydro-3-(2-propenyl)-2-pyranone (= α-allylvalerolactone, AVL) (7)

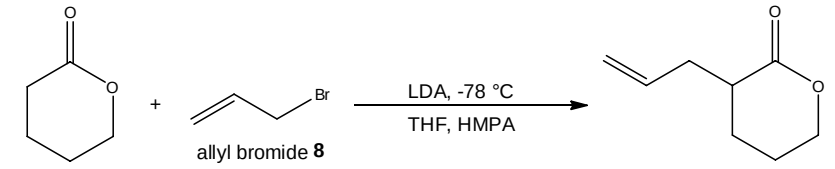

To a stirred solution of LDA (2M LDA solution in THF/heptane/ethylbenzene, 11 ml, 22.0 mmol, 1.1 eq.) at –78 °C a solution of VL (1.86 ml, 2.00 g, 20.0 mmol, 1.0 eq.) in THF (20 ml) was added drop wise over 50 minutes. After the addition of VL was complete, the mixture was stirred for 30 minutes at –78 °C. Afterwards, allyl bromide (2.08 ml, 2.90 g, 24 mmol, 1.2 eq.) in HMPA (4.20 ml, 4.33 g, 24.0 mmol, 1.2 eq.) was added dropwise within 20 minutes. After addition of allyl bromide, the reaction mixture was heated to –30 °C under stirring for four hours. The reaction mixture was quenched with saturated aqueous NH_4Cl (20 ml) and was transferred to an extraction funnel. The organic phases were separated and washed two times with saturated NH_4Cl. The aqueous phase was extracted with THF. The combined organic phases were dried over $MgSO_4$, filtered, and evaporated under reduced pressure. The crude product was purified by column chromatography (silica 40, 18 cm, 8 cm in diameter, hexane/ethyl acetate 6:1). After drying at high vacuum, a brownish oil was obtained (380 mg, 14 %).

R_f (hexane/ethyl acetate 1:1): 0.57

Elementary analysis (for $C_8H_{12}O_2$): calculated C 68.55, H 8.63, O 22.83; found C 68.37, H 8.54, N 0.0

^{1}H-NMR (400 MHz; $CDCl_3$; δ/ ppm): 5.86-5.75 (m, 1H, H_2C=C*H*-), 5.14-5.07 (m, 2H, *H_2*C=CH), 4.36-4.27 (m, 2H), 2.67-2.58 (m, 1H), 2.58-2.52 (m, 1H), 2.38-2.25 (m, 1H), 2.12-2.03 (m, 1H), 1.96-1.83 (m, 2H), 1.64-1.53 (m, 1H)

^{13}C-NMR (100 MHz; $CDCl_3$; δ/ ppm): 174.17 (*C*=O), 135.30 (H_2C=*C*H), 117.77 (H_2*C*=CH), 68.84, 39.54, 35.59, 24.20, 21.91

4.3.1.5 Synthesis of AVL by addition of BuLi

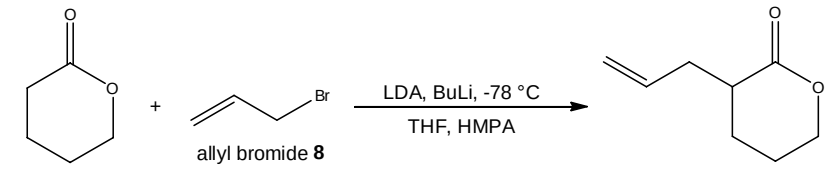

To a stirred solution of LDA (10.7 g, 100.0 mmol, 1.1 eq.) in THF (200 ml), BuLi (1.3 M in cyclohexane, 76.9 ml, 100.0 mmol, 1.1 eq.) was added at –78 °C. Then VL **9** (8.40 ml, 90.0 mmol, 1.0 eq.) in THF (50 ml) was added dropwise within 50 minutes. After the addition of the **9**, the mixture was stirred for 40 minutes at –78 °C. After this, allyl bromide **8** (9.30 ml, 108.0 mmol, 1.2 eq.) in HMPA (18.9 ml, 108.0 mmol, 1.2 eq.) was added slowly drop wise within 40 minutes. After addition of allyl bromide **8**, the reaction mixture was heated to –40 °C and held at that temperature in a cooling thermostat with continued stirring over night. The reaction mixture was quenched with saturated aqueous NH_4Cl (200 ml) and transferred to an extraction funnel. The organic phase was separated and washed two times with saturated NH_4Cl. The aqueous phase was extracted with THF. The combined organic phases were dried over $MgSO_4$, filtered, and evaporated under reduced pressure. The crude product was purified by column chromatography (silica 40, 10 cm, 6 cm in diameter, hexane/ethyl acetate 6:1). After drying, a brownish oil was obtained.

R_f (hexane/ethyl acetate 1:1): 0.57

Elementary analysis (for $C_8H_{12}O_2$): calculated C 68.55, H 8.63, O 22.83; found C 68.37, H 8.54, N 0.0

^{1}H-NMR (400 MHz; $CDCl_3$; δ/ ppm): 5.86-5.75 (m, 1H, H_2C=C*H*-), 5.14-5.07 (m, 2H, *H_2*C=CH), 4.36-4.27 (m, 2H), 2.67-2.58 (m, 1H), 2.58-2.52 (m, 1H), 2.38-2.25 (m, 1H), 2.12-2.03 (m, 1H), 1.96-1.83 (m, 2H), 1.64-1.53 (m, 1H)

^{13}C-NMR (100 MHz; $CDCl_3$; δ/ ppm): 174.17 (*C*=O), 135.30 (H_2C=*C*H), 117.77 (H_2*C*=CH), 68.84, 39.54, 35.59, 24.20, 21.91

4.3.1.6 Synthesis of AVL by addition of TMSCl

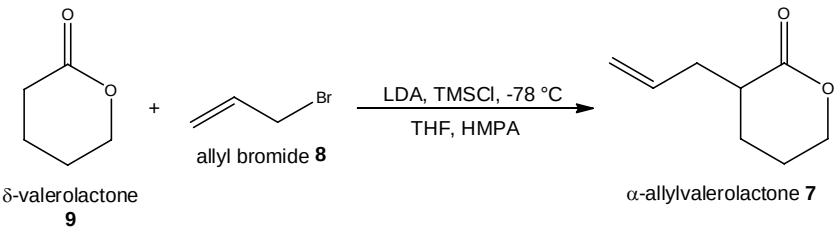

To a solution of LDA (2M LDA solution in THF/heptane/ethylbenzene, 47.4 ml, 94.8 mmol, 1.1 eq.), TMSCl (7.42 ml, 10.3 g, 94.8 mmol, 1.1 eq.) was added at –78 °C. VL (8.00 ml, 8.63 g, 86.2 mmol, 1.0 eq.) in THF (80 ml) was then added drop wise within 1.5 hours. After the addition of VL **9**, the mixture was stirred for 30 minutes at –78 °C. Then, allyl bromide **8** (9.30 ml, 108.0 mmol, 1.2 eq.) in HMPA (18.9 ml, 108.0 mmol, 1.2 eq.) was added slowly drop wise within 30 minutes. After addition of the allyl bromide **8**, the reaction mixture was heated to –40 °C with continued stirring over night. The reaction mixture was quenched with saturated aqueous NH_4Cl (80 ml) and transferred to an extraction funnel. The organic phase was separated and washed twice with saturated NH_4Cl. The aqueous phase was extracted with THF. The combined organic phases were dried over $MgSO_4$, filtered, and evaporated under reduced pressure. The crude product was purified by column chromatography (silica 40, 13 cm, 8 cm in diameter, hexane/ethyl acetate 2:1). After drying at high vacuum, a brownish oil was obtained (1.80 g, 15 %).

R_f (hexane/ethyl acetate 1:1): 0.57

Elementary analysis (for $C_8H_{12}O_2$): calculated C 68.55, H 8.63, O 22.83; found C 68.37, H 8.54, N 0.0

^{1}H-NMR (400 MHz; $CDCl_3$; δ/ ppm): 5.86-5.75 (m, 1H, H_2C=C*H*-), 5.14-5.07 (m, 2H, *H_2*C=CH), 4.36-4.27 (m, 2H), 2.67-2.58 (m, 1H), 2.58-2.52 (m, 1H), 2.38-2.25 (m, 1H), 2.12-2.03 (m, 1H), 1.96-1.83 (m, 2H), 1.64-1.53 (m, 1H)

^{13}C-NMR (100 MHz; $CDCl_3$; δ/ ppm): 174.17 (*C*=O), 135.30 (H_2C=*C*H), 117.77 (H_2*C*=CH), 68.84, 39.54, 35.59, 24.20, 21.91

4.3.1.7 Synthesis and characterization of the polyester PAVL-VL

4.3.1.7.1 Polymerization of PAVL-VL by addition of stannous catalyst

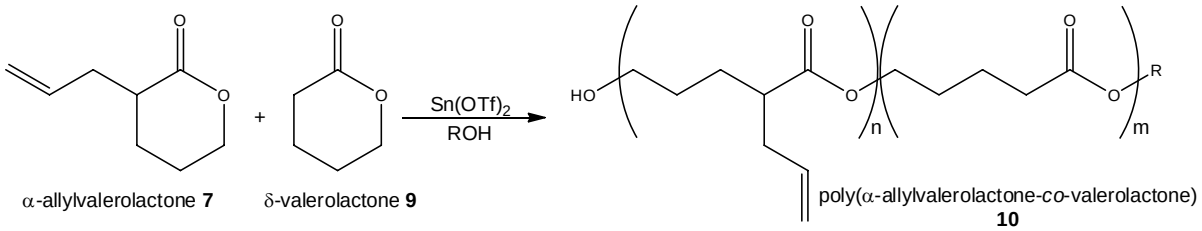

To a mixture of ethanol (7.58 µl, 5.99 mg, 0.13 mmol, 0.07 eq.) and THF (80 µl), a solution of $Sn(OTf)_2$ (70.0 µl, 1.13 mg, 2.70 µmol, 1.35 meq.) in THF (75 µl) was added. The mixture was stirred for 30 minutes at room temperature. VL **9** (0.60 g, 6.00 mmol, 3.0 eq.) and freshly distilled AVL **7** (0.28 g, 2.0 mmol, 1.0 eq.) were added in THF (5 ml). After 2.5 hours of

stirring at room temperature, the mixture was precipitated in cold methanol (80 ml) to yield a very fine white powder. The powder was dissolved in methanol and freeze-dried (0.57 g, 49 %).

GPC (THF, *poly(styrene)*): MW≈ 2500 g/mol, PDI: 1.26

^{1}H-NMR (400 MHz; $CDCl_3$; δ/ ppm): 5.68 (m, H_2C=C*H*), 4.95 (m, *H_2*C=CH), 4.01 (m, -C*H_2*-O), 3.68 (m, HO-C*H_2*), 2.34 (m, -*H_2*C-COO-, H_2C=CH-C*H_2*-), 1.61 (m, -C*H_2*-C*H_2*-), 1.19 (t, O-CH_2-C*H_3*)

^{13}C-NMR (100 MHz; $CDCl_3$; δ/ ppm): 175.0 (C=O_{AVL}), 173.1 (C=O_{VL}), 135.4 (H_2C=*C*H), 117.0 (H_2*C*=CH), 64.0 (-O-*C*H_2-), 45.0 (-H*C_{AVL}*-COO-), 36.5 (-HC$_{AVL}$-*C*H_2-CH=CH_2), 33.7 (-H_2*C_{VL}*-COO-), 28.0 (-*$C_{AVL/VL}$*H_2-CH_2-), 26.4 (-CH_2-*C_{AVL}*H_2-CH-), 21.5 (-CH_2-*C_{VL}*H_2-), 14.2 (O-CH_2-*C*H_3)

4.3.1.7.2 Polymerization of PAVL-VL initiated by alcohol/ HCl*Et_2O

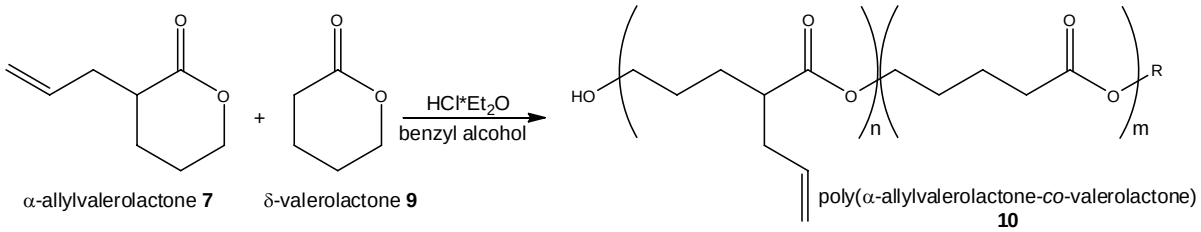

α-allylvalerolactone **7** δ-valerolactone **9** poly(α-allylvalerolactone-*co*-valerolactone) **10**

To a cooled solution (0 °C) of AVL **7** (1.40 g, 0.01 mol, 1.0 eq.) and VL **9** (3.00 g, 0.03 mol, 3.0 eq.) in DCM (5 ml), benzyl alcohol (6.21 µl, 6.49 mg, 0.06 mmol, 6.0 meq.) and HCl (2M in ethyl ether, 0.15 ml, 0.31 mmol, 31 meq.) in DCM (5 ml) were added. The reaction mixture was stirred and warmed to room temperature over night. The mixture was precipitated in ice-cooled hexane to yield a very fine powder. The filtrate was evaporated and re-precipitated in cooled methanol. The resulting product was not completely dry and therefore a very viscous oil (2.48 g, 56 %).

GPC (THF, *poly(styrene)*): MW≈ 3000 g/mol, PDI: 1.26

^{1}H-NMR (400 MHz; $CDCl_3$; δ/ ppm): 7.39-7.31 (m, benzyl), 5.78-5.67 (m, H_2C=C*H*), 5.12-5.01 (m, *H_2*C=CH), 4.18-3.99 (m, -C*H_2*-O), 3.65-3.60 (m, HO-C*H_2*), 2.47-2.21 (m, -*H_2*C-COO-, H_2C=CH-C*H_2*-), 1.79-1.50 (m, -C*H_2*-C*H_2*-)

^{13}C-NMR (100 MHz; $CDCl_3$; δ/ ppm): 173.5 (C=O), 135.3 (H_2C=*C*H), 128.6 (*C_6*H_5), 128.2 (*C_6*H_5), 117.2 (H_2*C*=CH), 64.1 (-O-*C*H_2-), 45.0 (-H*C_{AVL}*-COO-), 36.6 (-HC$_{AVL}$-*C*H_2-CH=CH_2), 33.9 (-H_2*C_{VL}*-COO-), 28.2 (-*$C_{AVL/VL}$*H_2-CH_2-), 26.4 (-CH_2-*C_{AVL}*H_2-CH-), 21.6 (-CH_2-*C_{VL}*H_2-)

4.4 References

(1) Mattanavee, W.; Suwantong, O.; Puthong, S.; Bunaprasert, T.; Hoven, V. P.; Supaphol, P. *ACS Applied Materials & Interfaces* **2009**, *1*, 1076-1085.

(2) Lee, J.-J.; Yu, H.-S.; Hong, S.-J.; Jeong, I.; Jang, J.-H.; Kim, H.-W. *Journal of Materials Science: Materials in Medicine* **2009**, *20*, 1927-1935.

(3) Meng, W.; Kim, S.-Y.; Yuan, J.; Kim, J. C.; Kwon, O. H.; Kawazoe, N.; Chen, G.; Ito, Y.; Kang, I.-K. *Journal of Biomaterials Science, Polymer Edition* **2007**, *18*, 81-94.

(4) Sell, S.; Barnes, C.; Smith, M.; McClure, M.; Madurantakam, P.; Grant, J.; McManus, M.; Bowlin, G. *Polymer International* **2007**, *56*, 1349-1360.

(5) Schenke-Layland, K.; Rofail, F.; Heydarkhan, S.; Gluck, J. M.; Ingle, N. P.; Angelis, E.; Choi, C.-H.; MacLellan, W. R.; Beygui, R. E.; Shemin, R. J.; Heydarkhan-Hagvall, S. *Biomaterials* **2009**, *30*, 4665-4675.

(6) ten Brummelhuis, N.; Diehl, C.; Schlaad, H. *Macromolecules (Washington, DC, United States)* **2008**, *41*, 9946-9947.

(7) Lutz, J.-F.; Schlaad, H. *Polymer* **2008**, *49*, 817-824.

(8) Lou, X.; Detrembleur, C.; Jerome, R. *Macromolecules* **2002**, *35*, 1190-1195.

(9) Phillips, D. J.; Graham, A. E. *Synlett* **2008**, 649-652.

(10) Zakharkin, L. I.; Gavrilenko, V. V.; Maslin, D. N.; Khorlina, I. M. *Tetrahedron Letters* **1963**, 2087-90.

(11) Black, G. P.; Murphy, P. J.; Thornhill, A. J.; Walshe, N. D. A.; Zanetti, C. *Tetrahedron* **1999**, *55*, 6547-6554.

(12) Stork, G.; Zhao, K. *Tetrahedron Letters* **1989**, *30*, 287-90.

(13) Woods, G. F., Jr. *Organic Syntheses* **1947**, *27*, No pp given.

(14) Molander, G. A.; Harris, C. R. *Journal of the American Chemical Society* **1995**, *117*, 3705-16.

(15) Parrish, B.; Quansah, J. K.; Emrick, T. *Journal of Polymer Science, Part A: Polymer Chemistry* **2002**, *40*, 1983-1990.

(16) Duda, A.; Biela, T.; Libiszowski, J.; Penczek, S.; Dubois, P.; Mecerreyes, D.; Jerome, R. *Polymer Degradation and Stability* **1998**, *59*, 215-222.

(17) Nakayama, A.; Kawasaki, N.; Aiba, S.; Maeda, Y.; Arvanitoyannis, I.; Yamamoto, N. *Polymer* **1998**, *39*, 1213-1222.

(18) Kolb, H. C.; Finn, M. G.; Sharpless, K. B. *Angewandte Chemie, International Edition* **2001**, *40*, 2004-2021.

(19) Gress, A.; Voelkel, A.; Schlaad, H. *Macromolecules (Washington, DC, United States)* **2007**, *40*, 7928-7933.

(20) Sumerlin, B. S.; Vogt, A. P. *Macromolecules (Washington, DC, United States)*, *43*, 1-13.

(21) Kade, M. J.; Burke, D. J.; Hawker, C. J. *Journal of Polymer Science, Part A: Polymer Chemistry*, *48*, 743-750.

5 Polymer/CaP as coating for implant materials

5.1 Introduction

Surfaces of implant materials influence cell adhesion by assisting or inhibiting cell adhesion and growth. Depending on the application, a simple, fast and efficient coating of implant materials such as nitinol and titanium is required. Polymer/CaP hybrids can not only be used as stand-alone composite but also for coating other materials. This chapter focuses the coating of implant materials by polymers and CaP.

Charged polymers, such as chitosan and heparin, were deposited as multilayer onto titanium and Nitinol. The coating procedure with polymers based on electrostatic forces is known as the layer-by-layer deposition.[1] After coating the titanium and nitinol surface with polymer multilayers, CaP was mineralized onto these multilayers. As the polyelectrolyte multilayer influences the CaP nucleation[2] and the surface properties (roughness, wettability, …) of the resulting film, this additional treatment is interesting for a further tuning of implant surface characteristics.

5.2 Surface modification of nickel-titanium alloy and titanium surfaces via a polyelectrolyte multilayer/calcium phosphate hybrid coating

Sylvia Schweizer,[1] Thomas Schuster,[1] Mathias Junginger,[2] Gerd Siekmeyer,[3,]* and Andreas Taubert[1,2,4,]*

1 Department of Chemistry, University of Basel, CH-4056 Basel, Switzerland.

2 Institute of Chemistry, University of Potsdam, D-14476 Golm, Germany.

3 ADMEDES Schüssler GmbH, D-75179 Pforzheim, Germany.

4 Max-Planck-Institute of Colloids and Interfaces, D-14476, Golm, Germany.

* Corresponding author: G.S., ADMEDES Schüssler GmbH, Rastatter Str. 15, D-75179 Pforzheim, Germany. Email: gsiekmeyer@admedes.com, Tel.: ++49 (0)7231 92 23 141.

* Corresponding author: A.T., Institute of Chemistry, University of Potsdam, Karl-Liebknecht-Str. 24-25, Building 26, D-14476 Golm, Germany, Tel.: ++49 (0)331 977 5773, Email: ataubert@uni-potsdam.de

Abstract

The report shows that simple layer-by-layer (LbL) deposition of positively charged chitosan and negatively charged heparin can be used to efficiently modify the native surface of both NiTi and Ti without any previous treatments. Moreover, mineralization of the polymer multilayers with calcium phosphate leads to surfaces with low contact angles around 70° and 20º for NiTi and Ti, respectively. This suggests that a polymer multilayer/calcium phosphate hybrid coating could be useful for making NiTi or Ti implants that are at the same time antibacterial (via the chitosan), suppress blood clot formation (via the heparin), and favor fast endothelialization (via the improved surface hydrophilicity compared to the respective neat material).

Introduction

NiTi shape memory alloys have in the recent past gained increasing attention from the biomaterials community. This is due to an interesting combination of properties of these materials: NiTi alloys are mechanically stable, yet flexible, and biocompatible. They are therefore interesting for a variety of applications in medicine, most notably in cardiovascular stents.[3-6] NiTi has also been suggested as a material for spine and other repairs, in particular for repairs where a stiff implant like steel would dramatically reduce the mobility and hence the quality of life of a patient.[4,5,7]

One of the major concerns in the context of both cardiovascular and spine repair are infections during or after the operation. In principle, infections can be prevented by including anti-inflammatory agents or antibiotics into the implants. They leak out during some time after the operation. The incorporation of anti-proliferating drugs and wound healing agents into advanced stents, known as drug eluting stents, has also been promoted.[8,9] Indeed, drug-eluting stents reduce restenosis.[10-13] However, drug eluting stents have also shown severe side effects such as an increased risk of thrombosis, poor attachment between stent and arterial wall and aneurysms. Finally, endothelialization and healing on the stent surface were delayed.[14-18]

Besides infections, the deposition of plaque on a stent must (ideally) be avoided or at least minimized.[19] Plaque rupture is fatal due to the exposure of a highly coagulant surface and thrombus formation.[20] Finally, the implant surface must be such that it favors fast endothelialization, as this may minimize restenosis and could also favor protection against thrombosis.[21-26] As a result, there is a need for simple, efficient, and cost-effective stent modification processes yielding stents which fulfill the above requirements.

Several approaches to functionalize NiTi implants for the above and other requirements have been reported, including chemical etching, polishing, laser, heat, and ion beam treatments, coating with calcium phosphate, and functional polymer coatings.[4,6,8,12,19,27-42] Functional polymer coatings, including biofilms and plasma polymers have attracted increasing interest in the recent past.[12,34,41,43-48] This is because the polymer composition can be adapted for a special requirement like antibacterial activity. Moreover, polymers are cheap, easy to process, and available in large quantities.

In a recent study, Meng et al. showed that a mixed coating of heparin and chitosan, using the well-known layer-by-layer technique,[49-51] successfully promotes a fast endothelialization and intimal healing after stent implantation.[52] In addition, this specific coating was found to be anti-adhesive and antibacterial. Finally it was also shown to have a

good hemocompatibility.[52,53] As a result, mixed chitosan/heparin surface coatings are interesting candidates for the fabrication of (multi)functional coatings on NiTi stents.

One of the drawbacks of the procedure reported by Meng et al. is the fact that the stents had to be pretreated using a rather time-consuming procedure before using the LbL self assembly technique. In a sense, this alleviates the advantage of the LbL process, which is, although not very fast, easily automated and can hence be easily upscaled and included in a production line, for example for the preparation of complex polymer membranes or coatings.[1,39,54-60]

The current report demonstrates that NiTi can be modified with biocompatible polymers such as chitosan and heparin without time-consuming pre-treatments. Instead of a rather long and occasionally tedious polishing process, we have used a simple washing process using deionized water as the sole purification step before depositing the polymer multilayer. In order to evaluate the feasibility of the approach, we have also studied the deposition of chitosan/heparin film on titanium wire. In both cases (NiTi and Ti), chitosan/heparin multilayer films can be deposited. The resulting polymer multilayer is stable and retains its original structure even if the implant is bent up to 37º, which could be important for implants under mechanical load. Moreover, mineralization of the polymer multilayers with calcium phosphate leads to surfaces with a low contact angles around 70° and 20º for NiTi and Ti, respectively. This suggests that a polymer multilayer/calcium phosphate hybrid coating could be useful for making NiTi or Ti implants that at the same time are antibacterial (via the chitosan),[53] suppress blood clot formation (via the heparin), and favor fast endothelialization (via the improved surface hydrophilicity compared to the respective neat material).

Experimental Section

Materials. Chitosan from crab shell with a deacetylation degree > 85%, titanium wire with a diameter of 2 mm (both Sigma-Aldrich), heparin sodium salt from porcine intestinal mucosa, calcium nitrate tetrahydrate (both Fluka), and ammonium hydrogen phosphate (ChemPur) were used as received. NiTi stents and tubes were obtained from ADMEDES Schüssler. Bidistilled water was used for all solutions and rinsing steps.

Sample preparation. Chitosan was dissolved in aqueous HCl with a pH below 2. Upon complete dissolution of the chitosan, the solution pH was adjusted to 5.3 with 1M KOH. Heparin was dissolved in pure water and upon complete dissolution, the pH was adjusted to

8.5 with 1M KOH. After extensive rinsing with pure d.i. water, bare NiTi and Ti substrates were coated by alternatively immersing them in a chitosan and heparin solution of 1 mg/mL for 20 to 30 minutes, followed by rinsing with water, immersion in the other polymer solution etc. at room temperature. The first polyelectrolyte layer deposited was Chitosan. Deposition ended after 10, 15, 20, … bilayers always with heparin as the last electrolyte layer. For mineralization, $Ca(NO_3)_2$*4 H_2O and $(NH_4)_2HPO_4$ were dissolved in water to yield solutions with a concentration of 0.7 M and 0.25 M, respectively. After mixing these solutions, the pH of the resulting suspension was adjusted to pH 8.1 with 1M KOH. Subsequently, the polymer multilayer-coated substrates were immersed into the suspension and shaken for a week at room temperature. After rinsing with water, all substrates were dried in air.

Characterization. Raman spectra were acquired with a Witec confocal Raman microscope Witec confocal Raman microscope (CRM 200) equipped with an objective from Nikon (10x, NA=0.25) and a linear polarized laser (diode pump Green laser, l = 532 nm, CrystaLaser). Atomic force microscopy (AFM) was done on a PicoLE (Molecular Imaging) with silicon nitride cantilevers for contact mode (Veeco NanoProbe^{TM} Tips, DNP-S1) with a force constant of 0.12 N/m, as given by the manufacturer. Images were recorded in height, amplitude, and phase modes and were flattened for further evaluation. Measurements were performed on the dry materials at room temperature. For scanning electron microscopy (SEM) and energy dispersive X-ray spectroscopy (EDXS), the NiTi tubes and Ti wires were sputter-coated with a 10 nm silver, platinum, or gold layer. Samples were imaged using a Philips XL30 FEG ESEM operated at 10 kV. EDX spectra were obtained at 10 kV using an EDAX X-ray detector. Contact angles were obtained with a Krüss Tensiometer K100 using the Wilhelmy plate method.

Results

1. NiTi alloys (Nitinol). Figure 5.1 shows a Raman spectrum of a NiTi tube coated with 10 layers of chitosan and heparin, respectively, which was subsequently mineralized with calcium phosphate. Bands at 433, 593, and 966 cm^{-1} can be assigned to PO_4^{3-} vibrations (ν_2, ν_4, and ν_1, respectively) in either hydroxyapatite (HAP) or octacalcium phosphate (OCP).[61] Bands at 1302, 2863, and 2886 cm^{-1} are due to C-H bending and symmetric stretch vibrations, respectively. A band at 1446 cm^{-1} can be assigned to CO_2^- symmetric stretch vibrations. Raman spectroscopy therefore clearly shows that both the polymers and calcium phosphate have been deposited on the NiTi tubes.

Interestingly, IR spectroscopy in reflection mode only gave poor spectra that could not be interpreted further. We assign this phenomenon to the fact that the NiTi surface of our tubes is highly reflective, which could lead to a rather noisy background.

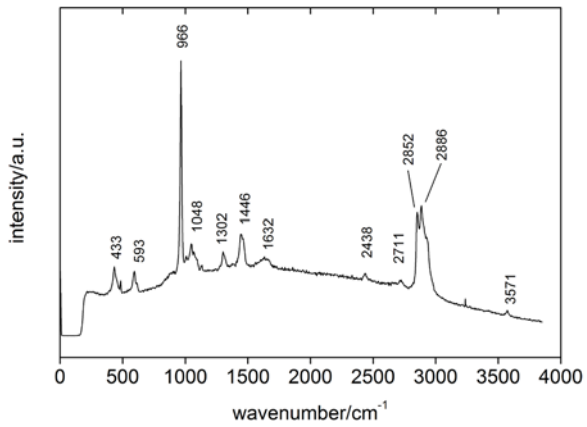

Figure 5.1. Raman spectrum of a NiTi tube coated with 10 layers of chitosan and 10 layers of heparin after mineralization with calcium phosphate.

Figure 5.2 shows scanning electron microscopy (SEM) images of various NiTi surfaces. The pure NiTi has a smooth surface with a few scratches, dents, and protrusions. No other features could be observed. NiTi coated with polymer multilayers exhibit the same smooth surface, although on a qualitative level it seems that the scratches are less clearly visible. Still, there are some dents and protrusions, but the protrusions seem to have "softer" boundaries. Moreover, these samples show a strong response towards the electron beam. In many cases, bubble-like features were observed in the coated samples upon irradiation and black traces were left after recording high magnification images. This indicates that, although the surface admittedly only slightly changes in the SEM, there is an organic (electron beam sensitive) coating on the NiTi surface.

On samples where the calcium phosphate has been grown directly onto the bare NiTi show large crystals and a rather rough surface compared to the bare NiTi. In contrast, samples mineralized after coating with the polyelectrolyte multilayers have a smooth and uniform surface and only a few small dots indicative of some larger crystals are visible. Higher magnification SEM images also show that in the presence of the polymer film, the whole surface is covered with small nanoparticles with diameter of ca. 100 nm and below. These are thought to be calcium phosphate nanoparticles, as they are only visible after the mineralization process.

In summary, SEM thus shows that (i) there is a polymer coating on the NiTi surfaces and (ii) that the polymer coating is necessary for the synthesis of small calcium phosphate nanoparticles that are homogeneously distributed on the surface. Overall, SEM thus confirms Raman spectroscopy in that SEM shows that there is a clear difference between the different samples and there is evidence for both polymer and calcium phosphate deposition on the NiTi surface. Energy-dispersive X-ray spectroscopy (EDS) failed due to the rapid charging and subsequent electron beam induced surface damage. This implies that after treatment with the polymer solutions and the calcium mineralization suspension a new surface forms, which is beam sensitive. These findings support our above interpretation and Raman spectroscopy because the bare NiTi did not show such a behavior.

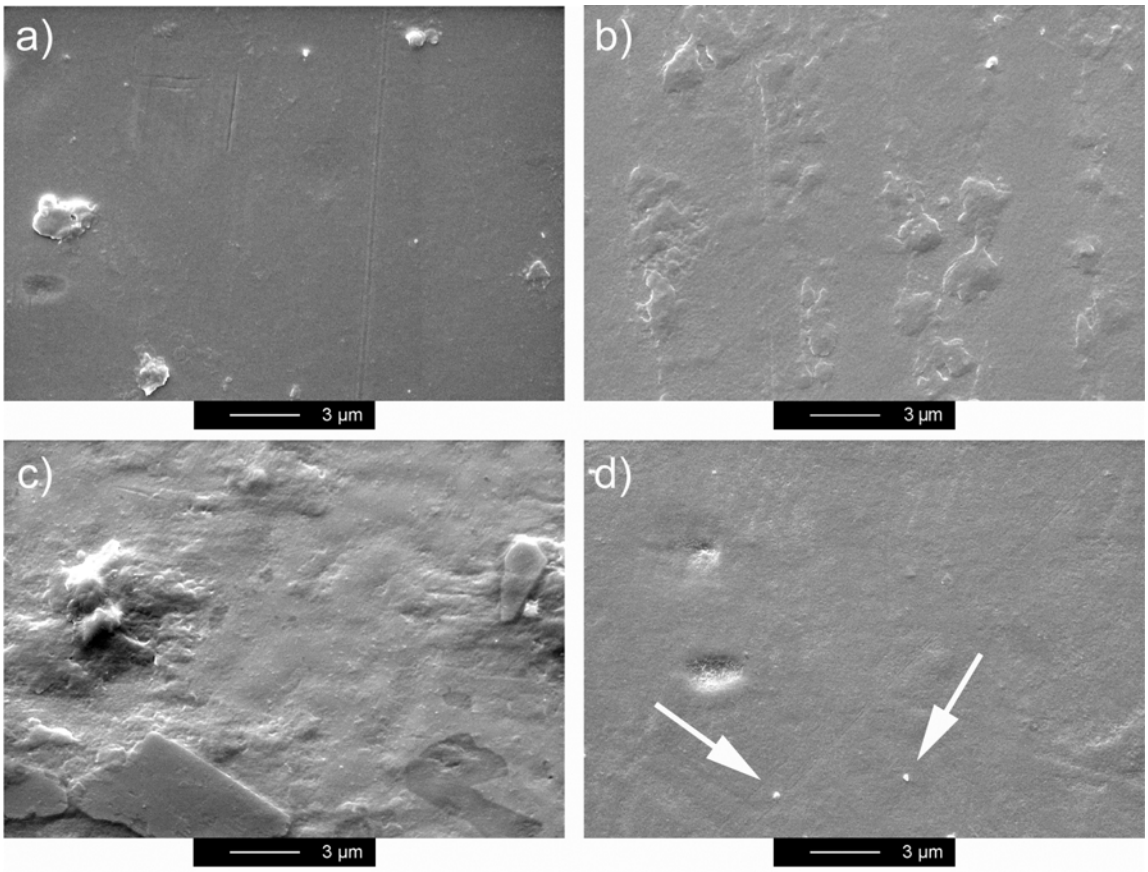

Figure 5.2. SEM images of (a) a bare NiTi surface, (b) 20 layers of polyelectrolyte, (c) mineralized NiTi tube (no polymer), (d) 20 layers of polyelectrolyte mineralized with calcium phosphate. Arrows in (d) point to presumed calcium phosphate protrusions formed on the polymer multilayer. These crystals are much smaller than the large crystals observed in the absence of the polymer multilayer (panel c). It must be noted that the whole surface shown in (d) is uniformly coated with small features such as the ones indicated by the arrows, but they are much harder to see, presumably, because they are covered to some extent by the polymer film.

Figure 5.3 shows atomic force microscopy (AFM) images of the same samples. AFM supports SEM and gives further insight into the surface structure, which has not been accessible via SEM due to beam damage. AFM of the bare NiTi surface shows that, while the surface appears flat in the SEM, there are still some height differences. Typical features are plateaus and holes on the order of a few hundred nanometers in diameter and up to ca. 40 nm in depth. Upon coating with polymer multilayers, the surface roughness decreases to ca. one half that of the bare NiTi. In addition, much smaller features with dimensions on the order of 50 nm become visible. We assign these to some microstructure imposed on the sample by the presence of two different polymers, heparin and chitosan.

Interestingly, mineralization of the bare NiTi leads to (besides the larger features observed in the SEM) a very smooth surface with a roughness of only a few nanometers, where some of the originally present holes (Figure 5.3a) have been filled with calcium phosphate. Furthermore, the structure exhibits small features with sizes on the order of a few nanometers.

Finally, if the polymer-coated NiTi is mineralized, the surface roughness and the feature dimension are comparable to that of the bare NiTi. This surface exhibits features with a dimension of ca. 100 nm, which we assign to calcium phosphate nanoparticles grown on the polymer multilayers. The particle size is rather uniform and most particles exhibit a rod-like shape, which is often observed for calcium phosphate, especially octacalcium phosphate or hydroxyapatite.[62,63] It is important to note that these particles are the same as those observed in the SEM, but as there is no beam damage with the AFM, AFM shows that indeed the whole surface is relatively uniformly coated with small calcium phosphate particles, *if* there is a polymer multilayer on the NiTi surface. AFM thus clearly shows that the two particles indicated with the arrows in Figure 5.2 are simply two very nicely visible particles, but that there are many others around these particles. Possibly, they are partly embedded in the polymer coating, which greatly reduces contrast and therefore visibility in the SEM.

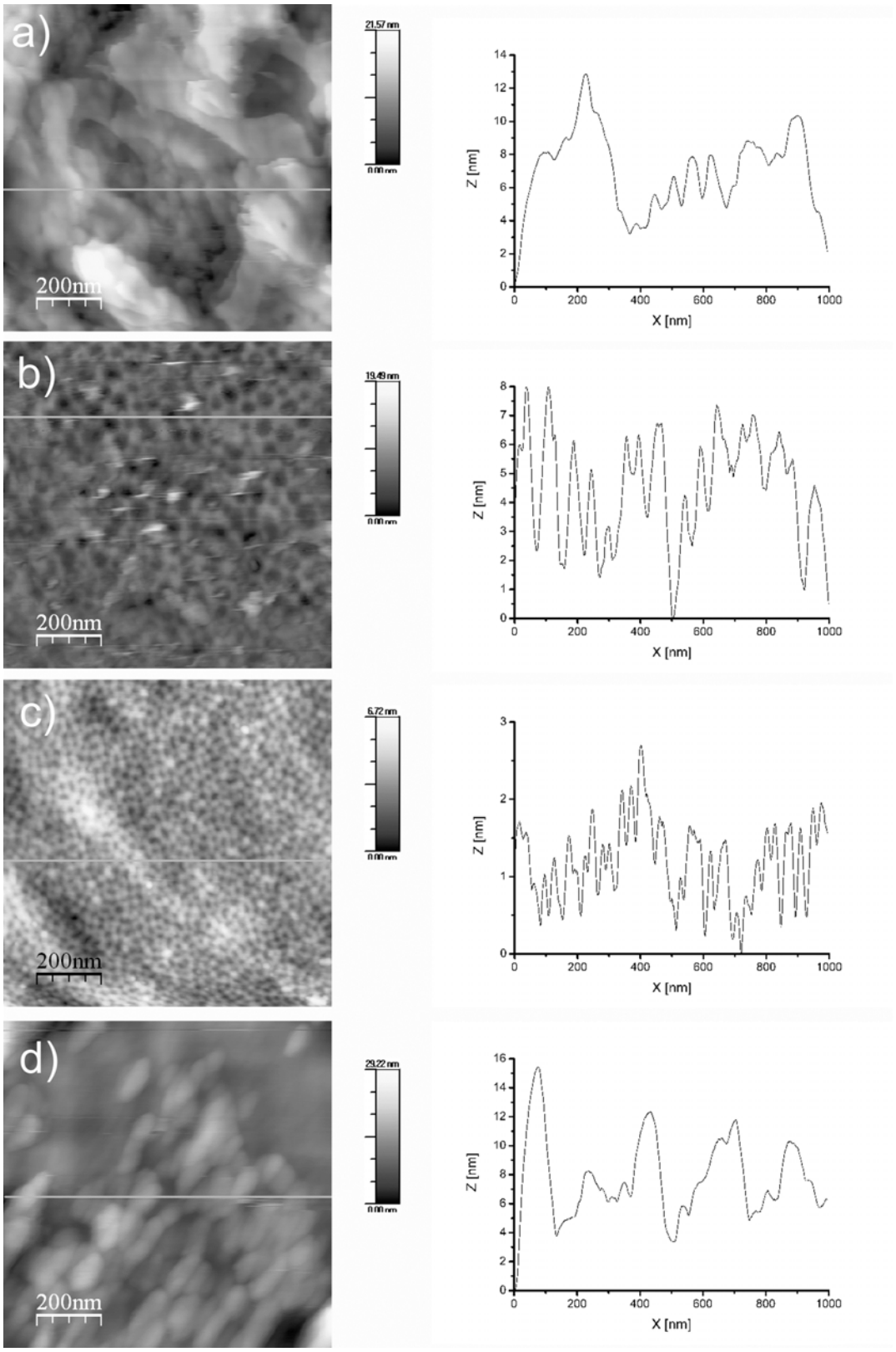

Figure 5.3. AFM images of the samples shown in Figure 2 and corresponding height profiles. (a) Bare NiTi surface, (b) 20 layers of polyelectrolyte, (c) mineralized NiTi surface (no polymer), (d) 20 layers of polyelectrolyte, followed by mineralization. Lines in the images show the location of the height profiles. Note that the height profiles are not on the same z-scale.

Table 5.1 shows contact angles obtained for the samples shown in Figures 5.2 and 5.3. The contact angle of bare NiTi is over 100º, whereas the coated samples all have contact angles that are below 100º. The lowest contact angle is observed with a hybrid coating consisting of both polyelectrolyte multilayer and calcium phosphate. This suggests that a combination of both components is needed for low contact angles.

Table 5.1. Contact angles for NiTi and various coatings. Meng et al.[52] have shown that 10 LbL layers are sufficient to leave contact angle unchanged, even with much thicker coatings. To ensure uniform behavior, we have thus focused on systems with 20 layers.

Sample	**Contact angle/º**
Blank (no coating)	106.6 ± 0.3
20 layers of polyelectrolyte (PEL)	83.3 ± 0.8
calcium phosphate	83.3 ± 4.0
20 layers of PEL/calcium phosphate	72.8 ± 1.8

Figure 5.4 shows that the coating on the NiTi tubes remains intact even during bending up to 37º with a radius of 5 mm. This measurement was done one a homebuilt device; the angle of 37° has no significance, we simply wanted to evaluate the stability of the polymer/calcium phosphate coating under strong bending conditions to determine if the film ruptures under mechanical stress. Resistance to mechanical stress is important for applications in vivo: If a coated NiTi implant is to be used in cardiovascular or spinal cord repair, it is under constant mechanical stress by a blood vessel or by movements of the body. This requires that also the coating be mechanically stable and sustain mechanical forces such as those typically found in blood vessels or along the spine. Figure 5.4 therefore shows that despite a rather large bending angle, the surface coating remains intact and that even after mineralization, the film is not disrupted. Interestingly, this holds for both the mineralized polymer multilayers and for the calcium phosphate layer on bare NiTi.

Obviously, our experiment is a qualitative test and more detailed studies under cyclic loading conditions are underway. However, tests with the real stent implantation device, a small Teflon tube, within which the stent is loaded, have shown that no mechanical damage of the coating occurs upon ejection from the device. This thus indicates that the films are stable enough to survive the friction forces that act on the coated stent during implantation.

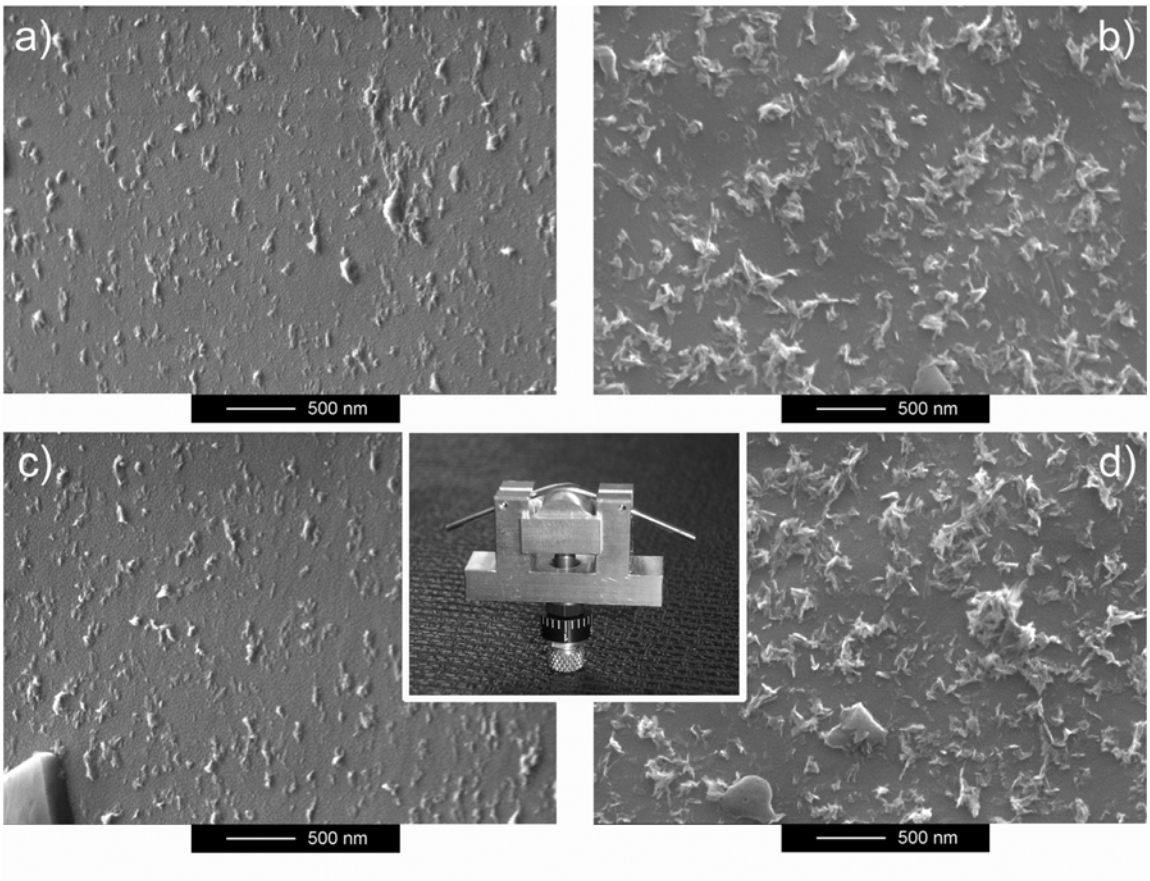

Figure 5.4. SEM images of straight and bent NiTi tubes. (a) NiTi tube mineralized directly with calcium phosphate (no polymer), (b) NiTi tube coated with 40 layers of polyelectrolyte and subsequently mineralized, (c) the tube shown in (a) bent to 37º, (d) the tube shown in (b) bent to an angle of 37º. Inset: photograph of a NiTi tube bent to 37º in a homebuilt testing device.

2. Titanium wires. For testing the applicability of our process to other materials, we have also investigated the film formation on Ti wires. Figure 5.5 shows a representative Raman spectrum of a Ti wire coated with 20 layers of polyelectrolyte after mineralization with calcium phosphate. The bands at 483 and 961 cm^{-1} can be assigned to PO_4^{3-} valence vibrations (ν_2 and ν_1, respectively). The band at 1056 cm^{-1} can be assigned to PO_4^{3-} antisymmetric stretch vibrations of either HAP or OCP.[61,64,65] A broad band at ca. 2890 cm^{-1} can be assigned to CH vibrations. Raman spectroscopy therefore provides evidence for calcium phosphate deposition on the Ti wires. The signal intensity, however, of these samples is much lower than in the case of the NiTi samples. We surmise that this is due to the much rougher sample surface compared to the NiTi samples discussed above (see SEM data below), which makes the detection of the signals from the organic less straightforward, but qualitatively similar to the NiTi samples shown above.

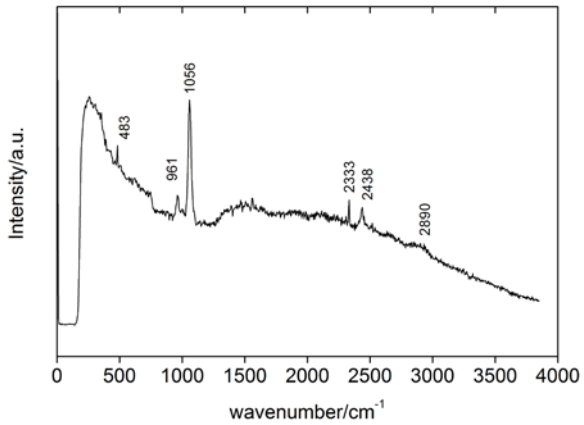

Figure 5.5. Raman spectrum of a Ti wire coated with 20 layers of polyelectrolyte and mineralized with calcium phosphate.

Figure 5.6 shows SEM images of representative Ti wire surfaces. SEM shows that the Ti surfaces are much rougher than the NiTi surfaces. Nevertheless, SEM also shows differences between the individual samples. While the bare Ti wire shows a number of holes and edges, the polymer coating leads to a smoothening effect in the sense that the holes appear partly covered with a polymer film. However, the polymer layer is too thin to lead to a completely smooth surface.

Upon mineralization of the bare Ti wire, there is no obvious change in the SEM images, although in some cases SEM shows particles in the micrometer range that are presumed to be calcium phosphate particles on the surface. This assignment is further supported by energy dispersive X-ray spectroscopy (EDS), which detects both intense calcium and phosphorus signals on the large crystals and less intense signals on the rest of the material, suggesting the formation of calcium phosphate on the entire surface.

Mineralization of the polymer coated Ti wires again leads to surfaces with a slightly smoother surface than without the polymer multilayers. Moreover, SEM detects large calcium phosphate particles with sizes from ca. 1 micron up to over 10 microns on the Ti surface. EDS again confirms the presence of both calcium and phosphorus. This clearly shows that the presence of the polymer multilayer has an advantageous effect on calcium phosphate formation on Ti. Interestingly, the size of the particles grown on the multilayers on Ti is much larger than the calcium phosphate grown on the multilayers on NiTi.

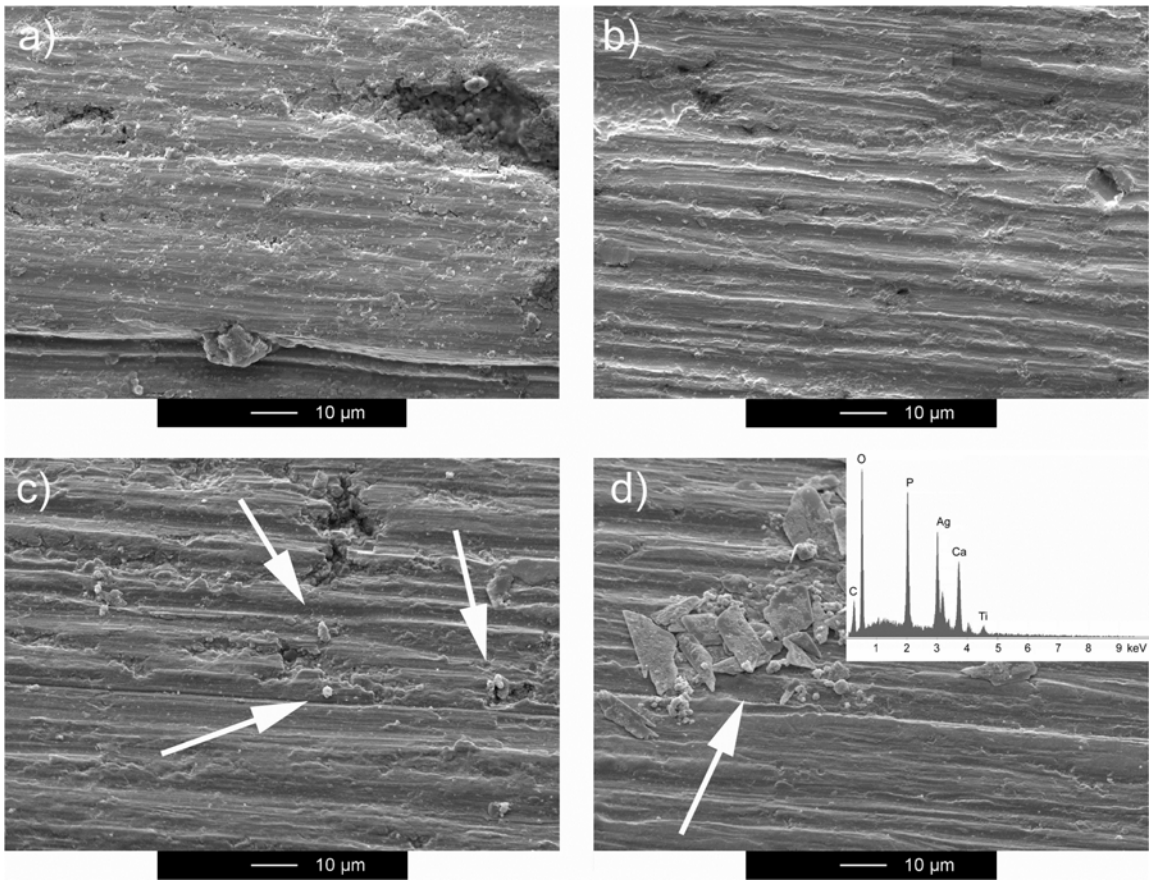

Figure 5.6. SEM images of (a) bare Ti wire, (b) polyelectrolyte coated Ti wire, (c) mineralized wire (no polymer), and (d) polymer-coated and mineralized Ti wire surface. Arrows in (c, d) point to select calcium phosphate particles. Inset is an EDS spectrum recorded on a large particle.

Table 5.2 shows the contact angles for some samples. Similar to the NiTi samples, there is a strong influence of the surface coating on the contact angle. Interestingly, however, already the coating with only Calcium phosphate (no polymer) leads to a dramatic decrease of the contact angle to ca. 37º (no relation to the bending angle of 37° described above), which is lower than any value observed in NiTi samples. Moreover, the effect is even more pronounced for the polymer multilayer/calcium phosphate hybrid coating. Here, the contact angle is ca. 21º indicating a very hydrophilic surface. Again, contact angle measurements suggest that calcium phosphate is an integral component of the surface coating, which is necessary for the fabrication of hydrophilic coatings, although the contributions of the polymer and the calcium phosphate are not the same on NiTi and Ti.

Table 5.2. Contact angles for Ti wires and various coatings.

Sample	Contact angle/°
Blank (no coating)	97.8 ± 3.7
20 layers of polyelectrolyte	95.4 ± 3.0
Calcium phosphate	36.7 ± 0.6
20 layers/Calcium phosphate	21.1 ± 0.8

Discussion

NiTi and titanium are important implant materials and their surface functionalization is therefore of prime interest to the biomaterials community. Our data show that both NiTi and Ti can be rendered more hydrophilic if a hybrid coating of a polymer multilayer and calcium phosphate is applied. The main point of this study is that this can be achieved without complicated and time-consuming pre-treatments. The only pretreatment necessary is a rinsing step with water. Such a simple process, which increases the hydrophilicity, is particularly interesting for NiTi as there are only a few procedures for the chemical modification of NiTi surfaces via the LbL process. The advantage of our approach is that no additional processing step is necessary and that the polymer multilayer can be directly deposited on the electropolished NiTi surface. This is in contrast to earlier reports, where surfaces have been etched or pretreated with a poly(ethylene imine) (PEI) layer.[36,37,39,66,67] PEI, however, is unfavorable because of its cytotoxicity,[36,37] although it has been shown recently that crosslinked PEI is presumably much less toxic.[67]

The current study shows that a combination of LbL deposition and mineralization with calcium phosphate yields NiTi and Ti surfaces with potentially interesting properties. Raman spectroscopy (Figures 5.1 and 5.5), SEM (Figures 5.2, 5.4, and 5.6), EDS (Figure 5.6), and AFM (Figure 5.3) show that the polymer multilayers form on both NiTi and Ti surfaces. Raman and EDS also show that the mineralization leads to the deposition of calcium phosphate. Raman spectra suggest that the mineral phase is hydroxyapatite (HAP) or octacalcium phosphate (OCP), as a number of characteristic bands of either of these crystal phases are observed.

The deposition of calcium phosphate on polyelectrolyte multilayers has been studied in the past,[40,68] but some of the data have been conflicting. While some studies show that the nucleation efficiency is enhanced and nanoscale calcium phosphate is deposited,[68] other studies suggest that the calcium phosphate growth is inhibited by the polymer film.[2] Our data

also suggest that there are differences in calcium phosphate deposition between NiTi and Ti. In the former case, small particles are obtained, while in the latter case rather large crystals form. This demonstrates that more studies into mineral deposition on polyelectrolyte multilayers are necessary, in particular, because the large calcium phosphate crystals observed on the Ti surfaces, may be dangerous if released and transported into the blood stream.

Contact angle measurements (Tables 5.1 and 5.2) show that the hydrophilicity dramatically increases if a calcium phosphate layer is the top layer of the coating. However, the partial contributions to the low contact angles are quite different between NiTi and Ti. NiTi surfaces show a moderate decrease of the contact angles with the polymer coating, which decreases by another 10º after mineralization. In contrast, the coatings on Ti show much stronger, but less coherent effects. While the pure polymer multilayer barely reduces the contact angle, both a pure calcium phosphate and a polymer/calcium phosphate hybrid coating lead to a much more dramatic reduction than in NiTi. This suggests that there are synergistic effects stemming from the interplay not only of the polymer and the calcium phosphate, but also from the chemistry, structure, and hydrophilicity of the NiTi or Ti substrate.

Our process is therefore an alternative to other approaches for reducing contact angles. For example, it has been shown that sterilisation, dry and steam autoclaving, and etching only show a small effect on the contact angle of LbL coatings. In contrast, plasma treatment reduces the contact angle to 16 to 18°,[69] which is much lower than electropolished NiTi (67°) or the NiTi used in our study, that is, simply rinsed with water (> 100°). Finally, inclusion of an additional hydrophilic polymer into the multilayer also lowers the contact angle.[66]

In our study, the different HAP or OCP particle sizes could additionally affect the contact angle: on NiTi, the calcium phosphate particles are ca. 100 nm, on Ti they are less evenly distributed but on the order of 10 microns. As a result, our data show that both NiTi and Ti can be efficiently modified with polymer/inorganic hybrid surface films, which appear to have advantageous properties. The reduction of the contact angle in particular suggests that such surfaces could favor faster endothelialization of the functionalized stents, a major challenge for implant manufacturers. Moreover, the calcium phosphate particles on NiTi do not exceed a size of ca. 100 nanometer, which should lead to a low thrombogenicity.

Low thrombogenicity and reduced platelet adhesion has also been reported for hyaluronan/chitosan films containing sodium nitroprusside and for heparin/hyluronan films.[9,35,39] Moreover, calcium phosphate has been deposited on several LbL coatings and in all cases a reduced thrombogenicity has been observed.[36,40,70] As a result, we combine the advantages of (antibacterial) chitosan, (anticoagulant) heparin, and calcium phosphate with

sizes below 100 nm in our coatings. The combination leads to mechanically stable, relatively hydrophilic implant coatings, which presumably also reduce thrombogenicity.

Conclusion

The study shows that both NiTi and Ti substrates can be efficiently coated with polyelectrolyte multilayers, similar to earlier studies.[36,37,39,66] The particular finding of this studyis that the polymer multilayer can directly be deposited on the NiTi surface, with no pretreatment needed, even if the NiTi stent has been stored at ambient conditions for quite a while. Furthermore, low contact angles, that is, hydrophilic surfaces, can only be obtained by using a procedure leading to a composite surface of polymer and calcium phosphate, most likely hydroxyapatite. Neither of the individual components (polymer multilayer or calcium phosphate) are able to individually achieve comparable contact angles. As a result, the report suggests that composite films, which are mechanically robust and also withstand bending, could be attractive coatings for cardiovascular implants. The concept is particularly appealing because we combine the advantages of the combination of several components, leading to mechanically stable, relatively hydrophilic implant coatings, which presumably also reduce thrombogenicity.

Acknowledgment. We thank D. Mathys, M. Düggelin, and E. Bieler for help with SEM, A. Reinecke for help with Raman microscopy, the Swiss National Science Foundation, Holcim Foundation, ERA Chemistry, the MPI of Colloids and Interfaces (Colloid Chemistry Department), the University of Potsdam, and ADMEDES Schüssler for financial support. S.S. acknowledges the Freiwillige Akademische Gesellschaft Basel for a PhD fellowship.

Keywords: implant, polyelectrolytes, layer-by-layer deposition (LbL), Nitinol (NiTi), stent

S. Schweizer, T. Schuster. M. Junginger, G. Siekmeyer, A. Taubert, ***Macromolecular Materials and Engineering****,* DOI: 10.1002/mame.200900347.

5.3 Embedding of fluorophores into the heparin/chitosan multilayer

Multilayers of chitosan and heparin coated via the LbL method were also deposited on glass substrates for further investigation. In the polyelectrolyte multilayer, fluorophores like oxonol V (green) and rhodamine 6G (RhG6, red) were incorporated during the LbL process. For this, the substrate was dipped alternately into a positively charged solution containing both chitosan and rhodamine 6G and a negatively charged solution of heparin and oxonol V. Monitoring under the fluorescence confocal microscope (FCM) proves that the fluorescence dyes are indeed deposited in alternating layers, Figure 5.7.

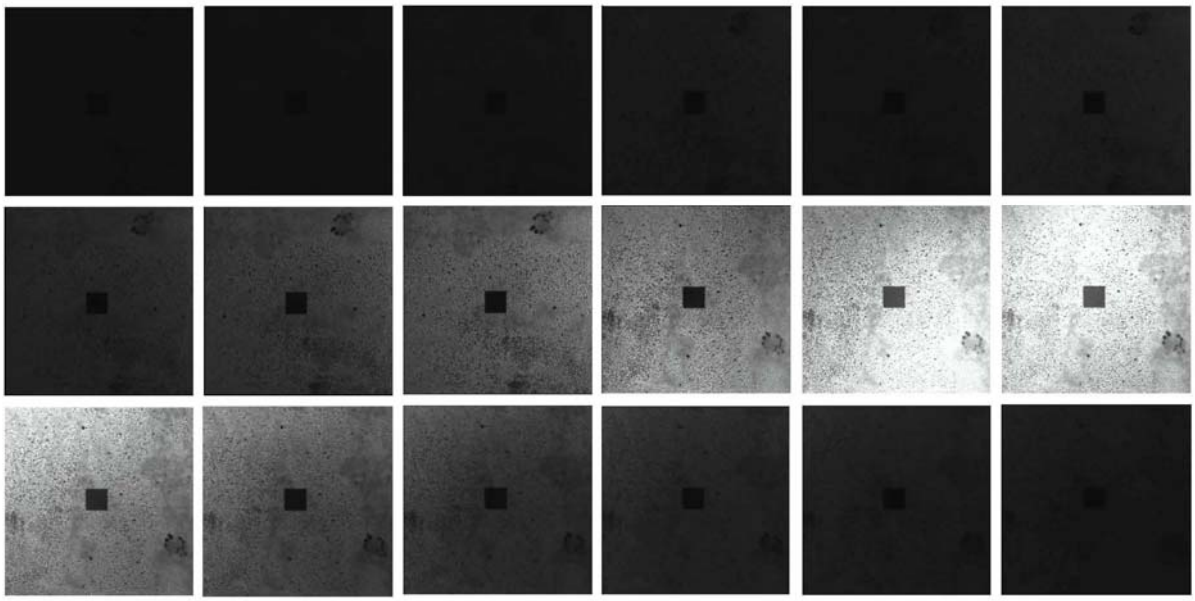

Figure 5.7: FCM intersections of the heparin/chitosan multilayer on glass substrates. Fluorophores appear in different depths which suppose an alternating deposition. The dark square occurs from the damage of fluorophores from higher magnification.

Heparin and chitosan are reasonably hydrophilic and may thus swell in aqueous solution.[35,71] Hence, also the multilayer may swell and smaller molecules present in the multilayer, such as drugs, growth factors, etc. may be released from the multilayer and become part of a long term therapy measure.[11,27,71,72] In the current study, the fluorescence dyes were used as simple model compounds for low molecular weight compounds. Their release can easily be monitored via UV/Vis spectroscopy and enables a first assessment of the release behavior of an LbL multilayer based on heparin and chitosan.

Nitinol stents, coated with the chitosan/heparin multilayer and rhodamine 6G, were kept in separate tubes, filled with water, to observe the release of the fluorophore from the stent surface into solution. The absorption of those solutions was measured at 530 nm, the absorption maximum of rhodamine 6G.

Figure 5.8 shows the results for three Nitinol stents. On stent 1 only a rhodamine 6G layer was deposited. Stents 2 and 3 were coated with a 20 layer film (10 layers of each polymer). In stent 2 one additional rhodamine layer (after 8 layers) and in stent 3 two additional layers of rhodamine (after 12 polyelectrolyte layers) were included in the middle of the multilayer.

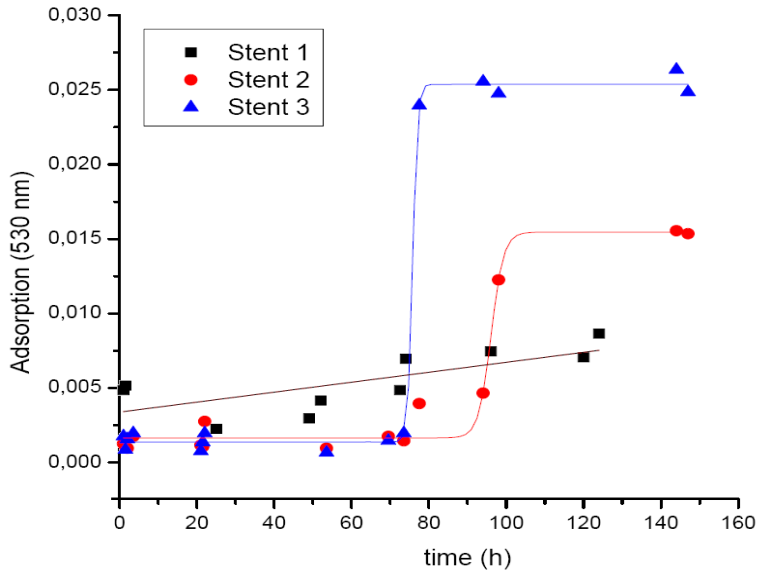

Figure 5.8: UV/Vis absorbance measurements of the stents 1-3. Stent 1: only Rh6G, stent 2: Rh6G after eight layers of polymer, stent 3: two layers of Rh6G after twelve polymer layers.

Stent 1, with only rhodamine on the Nitinol surface, shows a roughly linear release of the fluorophore. Stent 2 and stent 3 both show no release during the first days. Stent 3 then jumps to a marked increase of absorption, followed by another constant behavior. Stent 2 also shows this characteristics, but in a milder and delayed form. The fast increase in absorption can be explained by the swelling of the multilayer and the abrupt possibility to release. The milder progression of stent 2 results from the less rhodamine deposited on the Nitinol surface. Due to the fact that the rhodamine 6G on stent 2 is deposited after 8 polyelectrolyte layers and 12 additional chitosan and heparin layers are on the fluorophore, the release of the rhodamine 6G starts later compared to stent 3 where the fluorophore is deposited after 12 polyelectrolyte layers and therefore nearer to the surface.

Figure 5.9 shows the measured results for four additional stents. Their surfaces were treated as previously described with heparin/chitosan multilayer and rhodamine 6G embedding. Again all stents, except stent 7, were coated by multilayers of about 10 layers of each polyelectrolytes, resulting in a 20 layered multilayer. Stent 4 had additionally included one layer of rhodamine 6G near the Nitinol surface. Stent 5 as well had one additional layer of rhodamine 6G included, but near the multilayer/air surface. Stent 6 had three layers of rhodamine 6G included, distributed regularly in the multilayer. On stent 7, rhodamine 6G but no polyelectrolytes were deposited. In table 5.3, the deposition onto the described stents is summarized.

Table 5.3. Summary of all stents coated with chitosan/heparin and rhodamine 6G for release experiments.

	Number of polyelectrolyte layers	Number of rhodamine 6G layers	Location of rhodamine in the multilayer (in words)	Location of rhodamine after how many polyelectrolyte layers
Stent 1	-	1	Directly on the stent, on the bare nitinol	-
Stent 2	20	1	In the middle of the multilayer	after 8 polyelectrolyte layers
Stent 3	20	2	In the middle of the multilayer	after 12 polyelectrolyte layers
Stent 4	20	1	Near the stent	after 4 polyelectrolyte layers
Stent 5	20	1	Near the surface	after 16 polyelectrolyte layers
Stent 6	20	3	Distributed within the multilayer	after 8, 12 & 16 polyelectrolyte layers
Stent 7	-	1	Directly on the stent, on the bare nitinol	

Unfortunately, the results for these release measurements were ambiguous. The tendency for increasing release of rhodamine 6G into the solution during the observed time is certainly visible. This is true for all the observed samples, as the absorption of their corresponding solution is higher at the end of the observed period than at the first day for all samples. However, the measurements should as well correlate with the specific functional deposition of the stent, which seems not to apply here.

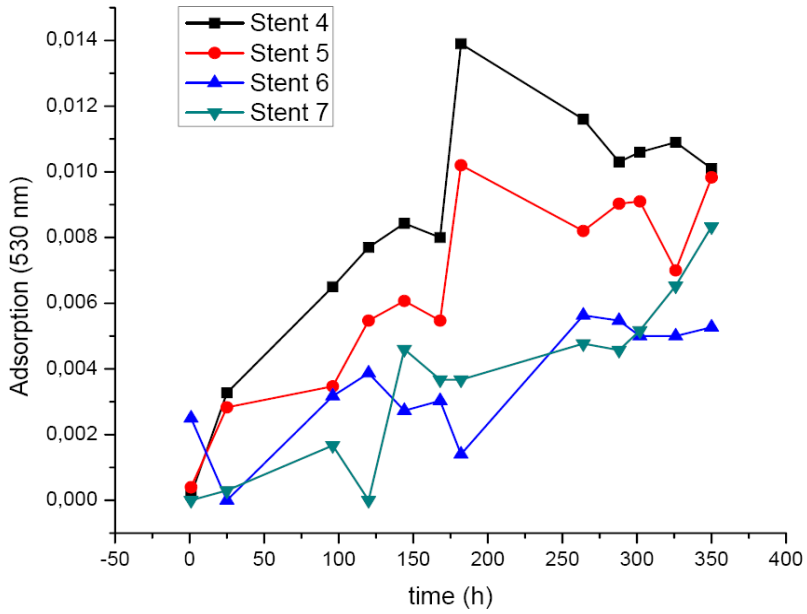

Figure 5.9: UV/Vis absorbance measurements of the stents 4-7.

Stent 4 shows the biggest release of rhodamine 6G, whereas stent 6 with three layers of rhodamine 6G has a final absorption only half as that of stent 4 with one rhodamine layer. The same interpretation problem exist for stent 5, where the rhodamine layer is nearer at the surface and therefore at the water solution than in stent 4. But neither a faster, nor a higher release can be recognized. As a consequence of these conflicting and poorly reproducible results, the idea to control and predict the release of smaller molecules out of the multilayer was abandoned.

5.4 Characterisation of heparin/chitosan multilayer and the following CaP mineralization

To control if the polyelectrolytes were deposited, scanning electron microscopy (SEM) was used. With SEM, samples can be imaged and with energy dispersive X-ray spectroscopy (EDS), a tool that can be mounted on SEMs, the surfaces can be chemically characterized. Typical acceleration voltages for SEMs are between 1 and 20 kV. For EDS, an acceleration voltage of at least 10 kV is needed to excite the samples.[73] However, electrons of this energy penetrate deep into the sample and the contribution of the surface to the detected signal becomes very weak. Moreover, with the primary electron beam of 10 kV, the surface also can also suffer significant damage, mostly from charging and ballistic impact, which is observed as black features in the images.

In the current study, both charging and damage of polymer multilayers was observed. This observation is confirmed by secondary electron imaging, which shows bubbles and movement in the surface. These findings indicate that there is an organic surface, which is damaged by irradiating the surface with the electron beam. In contrast, no bubbles and blisters can be observed without the multilayer coating.

EDS spectra have remained ambiguous. While the polymer-coated stants show a carbon signal, also the as-received stents show a carbon signal, which is most likely due to some adsorbed organic molecules, that have been taken up fronm the air during storage and transport. Calcium and phosphorus could barely be observed on areas with a nanoparticulate coating. Only the large crystals observed in the SEM provided clear evidence for the presence of calcium phosphate. For a more accurate analysis, a surface sensitive technique such as XPS or grazing incidence X-ray diffraction would have been necessary.

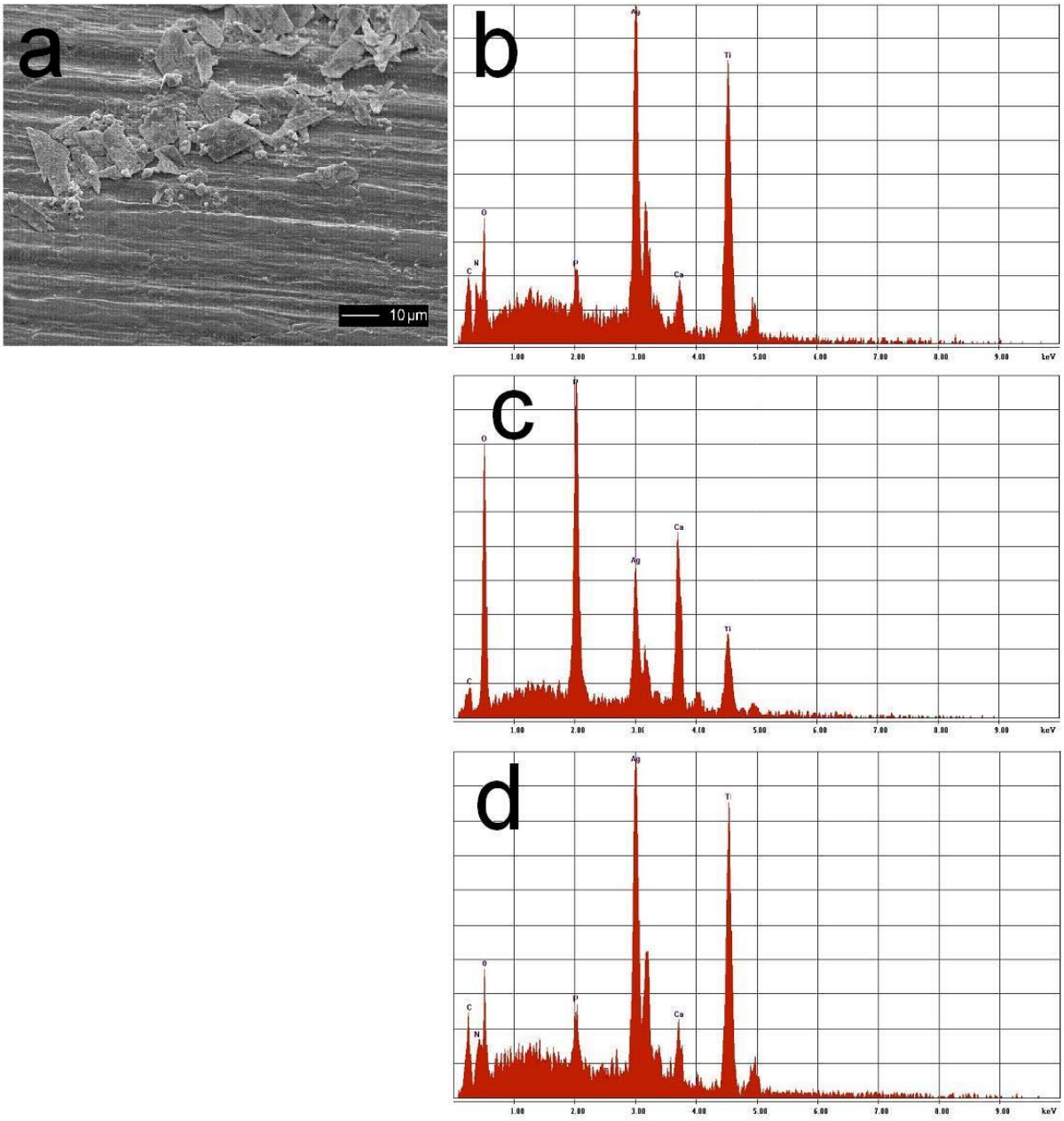

Figure 5.10: SEM image and EDS spectra of a titanium wire coated by 20 layers of electrolyte and CaP. Image **a** shows the surface of the titanium wire. Spectrum **b** was measured as overview on a surface area of about 1000 µm^2. Spectrum **c** characterizes one spot at a crystal. Spectrum **d** shows one spot beside the crystals. The silver signal results from the sputtering process resulting in a conductive sample.

5.5 Experimental section

5.5.1 LbL deposition on supporting material

5.5.1.1 Materials

Chitosan from crab shell with a deacetylation degree > 85%, titanium wire with a diameter of 2 mm (both Sigma-Aldrich), heparin sodium salt from porcine intestinal mucosa, calcium nitrate tetrahydrate (both Fluka), and ammonium hydrogen phosphate (ChemPur) were used as received. NiTi stents and tubes were obtained from ADMEDES Schüssler. Bidistilled water was used for all solutions and rinsing steps.

5.5.1.2 Multilayer deposition and embedding of fluorophores

Under intense stirring, Chitosan was dissolved in aqueous HCl with a pH below 2. Upon complete dissolution of the chitosan, the solution pH was adjusted with 1M KOH to pH 5. Heparin was dissolved in pure water and upon complete dissolution, the pH was adjusted to 8.5 with 1M KOH. Solutions of rhodamine 6G and oxonol V were prepared by dilution series to yield final concentrations of 10 nM. After the first unsuccessful fluorescence microscopy measurements, the concentration of rhodamine 6G was set to 10^{-4} mol/l. Samples for the UV/Vis measurements were coated from chitosan and heparin solutions in addition of a rhodamine containing solution where rhodamine 6G was diluted in water to yield a concentration of 0.1 mol/l.

After extensive rinsing with pure deionized water, bare NiTi, Ti, and glass substrates were coated by alternatively immersing them in a chitosan and heparin solution of 1 mg/mL, and rhodamine and oxonol solutions, respectively, for 20 to 30 minutes. After rinsing extensively with water, the immersion in the other polymer/fluorophore solution followed. At room temperature, this procedure was repeated as long as needed to obtain the desired number of polymer or dye layers. The first polyelectrolyte layer deposited was always positively charged, that is, chitosan or rhodamine 6G.

Samples for the UV/Vis spectrometry were kept in stirred water at 40° C to mimic body temperature and provide good diffusion in the solution.

5.5.2 CaP mineralization

For mineralization, $Ca(NO_3)_2$*4 H_2O and $(NH_4)_2HPO_4$ were dissolved in water to yield solutions with a concentration of 0.7 M and 0.25 M, respectively. After mixing the solutions, the pH of the resulting suspension was adjusted to pH 8.1 with 1M KOH. Subsequently, the polymer multilayer-coated substrates were immersed into the suspension and shaken for a week at room temperature. The pH at the end of the mineralization was about 7. After rinsing with water and THF, all substrates were dried in air.

5.6 References

(1) Decher, G. *Science (Washington, D. C.)* **1997**, *277*, 1232-1237.

(2) Ngankam, P. A.; Lavalle, P.; Voegel, J. C.; Szyk, L.; Decher, G.; Schaaf, P.; Cuisinier, F. J. G. *Journal of the American Chemical Society* **2000**, *122*, 8998-9005.

(3) Levine, B. *Advanced Engineering Materials* **2008**, *10*, 788-792.

(4) Robertson, S. W.; Imbeni, V.; Wenk, H. R.; Ritchie, R. O. *J Biomed Mater Res A* **2005**, *72*, 190-9.

(5) Itin, V. I.; Gyunter, V. E.; Shabalovskaya, S. A.; Sachdeva, R. L. C. *Materials Characterization* **1994**, *32*, 179-87.

(6) Tepe, G.; Schmehl, J.; P Wendel, H.; Schaffner, S.; Heller, S.; Gianotti, M.; Claussen, C. D.; Duda, S. H. *Biomaterials* **2005**, *27*, 643-650.

(7) Thierry, B.; Merhi, Y.; Bilodeau, L.; Trepanier, C.; Tabrizian, M. *Biomaterials* **2002**, *23*, 2997-3005.

(8) Pires, N. M. M.; Van der Hoeven, B. L.; De Vries, M. R.; Havekes, L. M.; Van Vlijmen, B. J.; Hennink, W. E.; Quax, P. H. A.; Jukema, J. W. *Biomaterials* **2005**, *26*, 5386-5394.

(9) Sydow-Plum, G.; Haidar, Z. S.; Merhi, Y.; Tabrizian, M. *Materials* **2008**, *1(1)*, 25-43.

(10) Steigerwald, K.; Merl, S.; Kastrati, A.; Wieczorek, A.; Vorpahl, M.; Mannhold, R.; Vogeser, M.; Hausleiter, J.; Joner, M.; Schoemig, A.; Wessely, R. *Biomaterials* **2008**, *30*, 632-637.

(11) Bognar, E.; Ring, G.; Balazs, T.; Dobranszky, J. *Materials Science Forum* **2008**, *589*, 361-366.

(12) Kraitzer, A.; Kloog, Y.; Zilberman, M. *Journal of Biomedical Materials Research, Part B: Applied Biomaterials* **2008**, *85B*, 583-603.

(13) van der Hoeven Barend, L.; Pires Nuno, M. M.; Warda Hazem, M.; Oemrawsingh Pranobe, V.; van Vlijmen Bart, J. M.; Quax Paul, H. A.; Schalij Martin, J.; van der Wall Ernst, E.; Jukema, J. W. *International journal of cardiology* **2005**, *99*, 9-17.

(14) Schwartz, R. S.; Chronos, N. A.; Virmani, R. *Journal of the American College of Cardiology* **2004**, *44*, 1373-1385.

(15) Iakovou, I.; Schmidt, T.; Bonizzoni, E.; Ge, L.; Sangiorgi, G. M.; Stankovic, G.; Airoldi, F.; Chieffo, A.; Montorfano, M.; Carlino, M.; Michev, I.; Corvaja, N.; Briguori, C.; Gerckens, U.; Grube, E.; Colombo, A. *JAMA, the Journal of the American Medical Association* **2005**, *293*, 2126-2130.

(16) Ong, A. T. L.; McFadden, E. P.; Regar, E.; de Jaegere, P. P. T.; van Domburg, R. T.; Serruys, P. W. *Journal of the American College of Cardiology* **2005**, *45*, 2088-2092.

(17) Takahashi, S.; Kaneda, H.; Tanaka, S.; Miyashita, Y.; Shiono, T.; Taketani, Y.; Domae, H.; Matsumi, J.; Mizuno, S.; Minami, Y.; Sugitatsu, K.; Saito, S. *Circulation Journal* **2007**, 226-8.

(18) McFadden Eugene, P.; Stabile, E.; Regar, E.; Cheneau, E.; Ong Andrew, T. L.; Kinnaird, T.; Suddath William, O.; Weissman Neil, J.; Torguson, R.; Kent Kenneth, M.; Pichard August, D.; Satler Lowell, F.; Waksman, R.; Serruys Patrick, W. *Lancet* **2004**, 1519-21.

(19) Werner, C.; Maitz, M. F.; Sperling, C. *Journal of Materials Chemistry* **2007**, *17*, 3376-3384.

(20) Rittersma Saskia, Z. H.; van der Wal Allard, C.; Koch Karel, T.; Piek Jan, J.; Henriques Jose, P. S.; Mulder Karla, J.; Ploegmakers Johanna, P. H. M.; Meesterman, M.; de Winter Robbert, J. *Circulation* **2005**, *111*, 1160-5.

(21) Ong, A. T. L.; Aoki, J.; Kutryk, M. J.; Serruys, P. W. *Arch Mal Coeur Vaiss* **2005**, *98*, 123-6.

(22) Schneider, D. B.; Dichek, D. A. *Circulation* **1997**, *95*, 308-10.

(23) Kong, D.; Melo, L. G.; Mangi, A. A.; Zhang, L.; Lopez-Ilasaca, M.; Perrella, M. A.; Liew, C. C.; Pratt, R. E.; Dzau, V. J. *Circulation* **2004**, *109*, 1769-1775.

(24) Werner, N.; Nickenig, G. *Journal of cellular and molecular medicine* **2006**, *10*, 318-32.

(25) Cook, S.; Wenaweser, P.; Togni, M.; Billinger, M.; Morger, C.; Seiler, C.; Vogel, R.; Hess, O.; Meier, B.; Windecker, S. *Circulation* **2007**, *115*, 2426-2434.

(26) Mintz Gary, S. *Circulation* **2007**, *115*, 2379-81.

(27) Rettig, R.; Kunze, J.; Stoever, M.; Wintermantel, E.; Virtanen, S. *Journal of Materials Science: Materials in Medicine* **2007**, *18*, 1377-1387.

(28) Stoever, M.; Renke-Gluszko, M.; Schratzenstaller, T.; Will, J.; Klink, N.; Behnisch, B.; Kastrati, A.; Wessely, R.; Hausleiter, J.; Schoemig, A.; Wintermantel, E. *Journal of Materials Science* **2006**, *41*, 5569-5575.

(29) Wu, S. L.; Liu, X. M.; Chung, C. Y.; Chu, P. K.; Chan, Y. L.; Yeung, K. W. K.; Chu, C. L. *Surface Review and Letters* **2008**, *15*, 97-104.

(30) Yang, X.; Zhu, S.; Cui, Z.; Yao, K. *Gongneng Cailiao* **2001**, *32*, 154-155.

(31) Demri, B.; Hage-Ali, M.; Moritz, M.; Muster, D. *Biomaterials* **1997**, *18*, 305-310.

(32) Shishkovsky, I. V.; Volova, L. T.; Kuznetsov, M. V.; Morozov, Y. G.; Parkin, I. P. *Journal of Materials Chemistry* **2008**, *18*, 1309-1317.

(33) Thierry, B.; Tabrizian, M.; Trepanier, C.; Savadogo, O.; Yahia, L. H. *Journal of Biomedical Materials Research* **2000**, *51*, 685-693.

(34) Tenke, P.; Riedl, C. R.; Jones, G. L.; Williams, G. J.; Stickler, D.; Nagy, E. *International Journal of Antimicrobial Agents* **2004**, *23*, S67-S74.

(35) Thierry, B.; Merhi, Y.; Silver, J.; Tabrizian, M. *Journal of Biomedical Materials Research, Part A* **2005**, *75A*, 556-566.

(36) Shabalovskaya, S.; Anderegg, J.; Van Humbeeck, J. *Acta Biomaterialia* **2008**, *4*, 447-467.

(37) Brunot, C.; Ponsonnet, L.; Lagneau, C.; Farge, P.; Picart, C.; Grosgogeat, B. *Biomaterials* **2006**, *28*, 632-640.

(38) McPherson, T. B.; Shim, H. S.; Park, K. *Journal of Biomedical Materials Research* **1997**, *38*, 289-302.

(39) Thierry, B.; Winnik, F. M.; Merhi, Y.; Silver, J.; Tabrizian, M. *Biomacromolecules* **2003**, *4*, 1564-1571.

(40) Chen, M. F.; Yang, X. J.; Hu, R. X.; Cui, Z. D.; Man, H. C. *Materials Science & Engineering* **2004**, *C24*, 497-502.

(41) Fishbein, I.; Alferiev, I. S.; Nyanguile, O.; Gaster, R.; Vohs, J. M.; Wong, G. S.; Felderman, H.; Chen, I. W.; Choi, H.; Wilensky, R. L.; Levy, R. J. *Proceedings of the National Academy of Sciences of the United States of America* **2006**, *103*, 159-164.

(42) Van Der Giessen, W. J.; Lincoff, A. M.; Schwartz, R. S.; Van Beusekom, H. M. M.; Serruys, P. W.; Holmes, D. R., Jr.; Ellis, S. G.; Topol, E. J. *Circulation* **1996**, *94*, 1690-1697.

(43) Lahann, J. *Abstracts of Papers, 229th ACS National Meeting, San Diego, CA, United States, March 13-17, 2005* **2005**, PMSE-021.

(44) Hale, P.; Turgeon, S.; Horny, P.; Lewis, F.; Brack, N.; Van Riessen, G.; Pigram, P.; Mantovani, D. *Langmuir* **2008**, *24*, 7897-7905.

(45) Orlando, F.; Ghiselli, R.; Cirioni, O.; Minardi, D.; Tomasinsig, L.; Mocchegiani, F.; Silvestri, C.; Skerlavaj, B.; Riva, A.; Muzzonigro, G.; Saba, V.; Scalise, G.; Zanetti, M.; Giacometti, A. *Peptides (Amsterdam, Netherlands)* **2008**, *29*, 1118-1123.

(46) Lin, C.-H.; Lin, J.-C.; Chen, C.-Y.; Cheng, C.-Y.; Lin, X.-Z.; Wu, J.-J. *Journal of Applied Polymer Science* **2005**, *97*, 893-902.

(47) Huang, N.; Yang, P.; Leng, Y. X.; Wang, J.; Sun, H.; Chen, J. Y.; Wan, G. J. *Surface and Coatings Technology* **2004**, *186*, 218-226.

(48) Dinu, C. Z.; Dinca, V. C.; Soare, S.; Moldovan, A.; Smarandache, D.; Scarisoareanu, N.; Barbalat, A.; Birjega, R.; Dinescu, M.; DiStefano, V. F. *Applied Surface Science* **2007**, *253*, 7719-7723.

(49) Ariga, K.; Hill, J. P.; Ji, Q. *Physical Chemistry Chemical Physics* **2007**, *9*, 2319-2340.

(50) Ariga, K.; Hill, J. P.; Lee, M. V.; Vinu, A.; Charvet, R.; Acharya, S. *Science and Technology of Advanced Materials* **2008**, *9*, No pp given.

(51) De Geest, B. G.; Sanders, N. N.; Sukhorukov, G. B.; Demeester, J.; De Smedt, S. C. *Chemical Society reviews* **2007**, *36*, 636-49.

(52) Meng, S.; Liu, Z.; Shen, L.; Guo, Z.; Chou, L. L.; Zhong, W.; Du, Q.; Ge, J. *Biomaterials* **2009**, *30*, 2276.

(53) Fu, J.; Ji, J.; Yuan, W.; Shen, J. *Biomaterials* **2005**, *26*, 6684.

(54) Crespilho, F. N.; Zucolotto, V.; Oliveira, O. N., Jr.; Nart, F. C. *International Journal of Electrochemical Science* **2006**, *1*, 194-214.

(55) Chen, W.; McCarthy, T. J. *Macromolecules* **1997**, *30*, 78-86.

(56) Quinones, R.; Gawalt, E. S. *Langmuir* **2007**, *23*, 10123-10130.

(57) Jiang, X.; Chen, Z.; Lv, D.; Wu, Q.; Lin, X. *Macromolecular Chemistry and Physics* **2008**, *209*, 175-183.

(58) Schoeler, B.; Delorme, N.; Doench, I.; Sukhorukov, G. B.; Fery, A.; Glinel, K. *Biomacromolecules* **2006**, *7*, 2065-2071.

(59) Garza, J. M.; Jessel, N.; Ladam, G.; Dupray, V.; Muller, S.; Stoltz, J.-F.; Schaaf, P.; Voegel, J.-C.; Lavalle, P. *Langmuir* **2005**, *21*, 12372-12377.

(60) Song, Z.; Yin, J.; Luo, K.; Zheng, Y.; Yang, Y.; Li, Q.; Yan, S.; Chen, X. *Macromolecular Bioscience* **DOI: 10.1002/mabi.200800164**.

(61) Sauer, G. R.; Zunic, W. B.; Durig, J. R.; Wuthier, R. E. *Calcified Tissue International* **1994**, *54*, 414-20.

(62) Schweizer, S.; Taubert, A. *Macromolecular Bioscience* **2007**, *7*, 1085-1099.

(63) Rautaray, D.; Sastry, M. *Biotechnol Prog* **2005**, *21*, 1759-67.

(64) Lin-Vien, D.; Colthup, N. B.; Fateley, W. G.; Grassetti, J. G. *The Handbook of Infrared and Raman Characteristics Frequencies of Organic Molecules*, 1991.

(65) Frost, R. L.; Cejka, J.; Ayoko, G. A.; Weier, M. *Spectrochimica Acta, Part A: Molecular and Biomolecular Spectroscopy* **2007**, *66A*, 979-984.

(66) Liu, M.; Yue, X.; Dai, Z.; Xing, L.; Ma, F.; Ren, N. *Langmuir* **2007**, *23*, 9378-9385.

(67) Shkilnyy, A.; Hiebl, B.; Neffe, A. T.; Friedrich, A.; Hartmann, J.; Taubert, A. *Macromolecular Bioscience* **DOI: 10.1002/mabi.200800266**.

(68) Ball, V.; Michel, M.; Boulmedais, F.; Hemmerle, J.; Haikel, Y.; Schaaf, P.; Voegel, J. C. *Crystal Growth & Design* **2006**, *6*, 327-334.

(69) Thierry, B.; Tabrizian, M.; Savadogo, O.; Yahia, L. H. *Journal of Biomedical Materials Research* **2000**, *49*, 88-98.

(70) Gu, Y. W.; Tay, B. Y.; Lim, C. S.; Yong, M. S. *Biomaterials* **2005**, *26*, 6916-6923.

(71) Huang, L.-Y.; Yang, M.-C. *Colloids and Surfaces, B: Biointerfaces* **2008**, *61*, 43-52.

(72) Deconinck, E.; Sohier, J.; De Scheerder, I.; Van Den Mooter, G. *Journal of Pharmaceutical Sciences* **2008**, *97*, 5047-5060.

(73) *http://pages.unibas.ch/zmb/rem.html*.

6 Summary

The goal of the work presented here was (i) the development of novel polymer/calcium phosphate composite materials that could find application in implantology and (ii) the development of a polymer/calcium phosphate hybrid coating of an actual implant material, nitinol, with the goal to improve the endothelialization and the biocompatibility of the metallic nitinol material.

Commercially available polyesters, poly(caprolactone) (PCL), poly(hydroxyl butyrate) (PHB), and poly(hydroxyl butyrate-*co*-hydroxyl valerate) (PHB-HV) were used to establish the electrospinning process. To investigate the effects of some of the key process parameters, electrospinning of PCL at different conditions was conducted. The parameters studied were needle-collector distance, applied voltage, and flow rate of the polymer solution. All these parameters have an essential influence on the resulting fiber morphology of the scaffolds:

- With decreasing distance between the needle tip and grounded plate, more uniform and beadless nanofibers were obtained in PCL samples.
- The average PCL fiber diameter increases with increasing voltage, but becomes more uniform.
- A slow flow rate is preferred for PCL solutions in chloroform, but it has to be fast enough to avoid excessive bead formation.
- The most reproducible and uniform fiber mats from PCL in chloroform with a concentration of 7 % wt resulted from a flow rate of 0.5 ml/ h, a distance of 10 cm between the needle and the collector and an applied voltage of 25 kV at our home-made electrospinning apparatus.

Electrospinning of PHB and PHB-HV always leads in uniformly distributed fibers. The HV fraction appears to affect the fiber diameter, as a low (0%) and high (20%) HV fractions the fiber diameters are larger than at intermediate (6%) HV fractions.

Mineralization experiments of the electrospun fiber mats show that after 10 days in simulated body fluid (SBF), the fibers are only slightly coated with CaP. Because functional groups can influence CaP nucleation and growth, incorporation of different functionalities were deemed an appropriate measure to enhance nucleation and growth of calcium phosphate of the polymer fibers. Instead of an additional functional coating of the electrospun polyester,

this thesis describes chemical modification of the polyester by addition of functional groups. Polyesters with double bonds in side chains were synthesized and functionalized with thioglucose tetraacetate via the “thiol-ene click” chemistry. In this reaction, a thiol attach to the double bonds (-ene) of the polyester by exposure to UV light. With this approach, variation in functionalization can easily be achieved by using different thiols. The resulting polyester was then spun to fiber scaffolds by electrospinning. Afterwards the scaffolds were mineralized with CaP.

In summary, the first part describes the successful electrospinning of commercial and custom-made polyesters and their mineralization with calcium phosphate. The study is also one of the first systematic investigation of electrospinning parameters of PCL and PHB-HV with respect to the hydroxyvalerate amount in the copolymer.

In a second project, the concept of polymer/calcium phosphate hybrids has been extended to an actual implant material, the coating of nitinol, a nickel titatium alloy used in implantology. Nitinol (NiTi) and titanium can easily be modified via layer-by-layer (LbL) deposition of positively charged chitosan and negatively charged heparin without any previous treatments. Moreover, mineralization of the polymer multilayers with calcium phosphate leads to surfaces with low contact angles around 70° and 20º for NiTi and Ti, respectively, suggesting that polymer multilayer/calcium phosphate hybrid coatings could be useful for improving implant surfaces.

The particular finding of this thesis is that the polymer multilayer can directly be deposited on the NiTi surface, with no pretreatment needed, even if the NiTi stent has been stored at ambient conditions for quite a while.

The mechanical stability of the coating was tested with a bending device. The possible point of rupture was imaged under bending of 37° using SEM. No cracks could be observed, which indicates that the films are stable enough to survive the friction forces that act on the coated nitinol during bending and allow possible application for implantation. First animal experiments have proven highly successful and a further development of the approach is underway.(G. Siekmeyer, personal communication 2010)